1-1-2012

Angular momentum and galaxy formation revisited

Aaron J. Romanowsky
San Jose State University, aaron.romanowsky@sjsu.edu

S. M. Fall
Space Telescope Science Institute

ANGULAR MOMENTUM AND GALAXY FORMATION REVISITED

Aaron J. Romanowsky[1,3] and S. Michael Fall[2]
[1] University of California Observatories, 1156 High Street, Santa Cruz, CA 95064, USA
[2] Space Telescope Science Institute, 3700 San Martin Drive, Baltimore, MD 21218, USA

ABSTRACT

Motivated by a new wave of kinematical tracers in the outer regions of early-type galaxies (ellipticals and lenticulars), we re-examine the role of angular momentum in galaxies of all types. We present new methods for quantifying the specific angular momentum j, focusing mainly on the more challenging case of early-type galaxies, in order to derive firm empirical relations between stellar $j_\star$ and mass $M_\star$ (thus extending earlier work by Fall). We carry out detailed analyses of eight galaxies with kinematical data extending as far out as 10 effective radii, and find that data at two effective radii are generally sufficient to estimate total $j_\star$ reliably. Our results contravene suggestions that ellipticals could harbor large reservoirs of hidden $j_\star$ in their outer regions owing to angular momentum transport in major mergers. We then carry out a comprehensive analysis of extended kinematic data from the literature for a sample of ∼100 nearby bright galaxies of all types, placing them on a diagram of $j_\star$ versus $M_\star$. The ellipticals and spirals form two parallel $j_\star$–$M_\star$ tracks, with log-slopes of ∼0.6, which for the spirals are closely related to the Tully–Fisher relation, but for the ellipticals derives from a remarkable conspiracy between masses, sizes, and rotation velocities. The ellipticals contain less angular momentum on average than spirals of equal mass, with the quantitative disparity depending on the adopted K-band stellar mass-to-light ratios of the galaxies: it is a factor of ∼3–4 if mass-to-light ratio variations are neglected for simplicity, and ∼7 if they are included. We decompose the spirals into disks and bulges and find that these subcomponents follow $j_\star$–$M_\star$ trends similar to the overall ones for spirals and ellipticals. The lenticulars have an intermediate trend, and we propose that the morphological types of galaxies reflect disk and bulge subcomponents that follow separate, fundamental $j_\star$–$M_\star$ scaling relations. This provides a physical motivation for characterizing galaxies most basically with two parameters: mass and bulge-to-disk ratio. Next, in an approach complementary to numerical simulations, we construct idealized models of angular momentum content in a cosmological context, using estimates of dark matter halo spin and mass from theoretical and empirical studies. We find that the width of the halo spin distribution cannot account for the differences between spiral and elliptical $j_\star$, but that the observations are reproduced well if these galaxies simply retained different fractions of their initial j complement (∼60% and ∼10%, respectively). We consider various physical mechanisms for the simultaneous evolution of $j_\star$ and $M_\star$ (including outflows, stripping, collapse bias, and merging), emphasizing that the vector sum of all such processes must produce the observed $j_\star$–$M_\star$ relations. We suggest that a combination of early collapse and multiple mergers (major or minor) may account naturally for the trend for ellipticals. More generally, the observed variations in angular momentum represent simple but fundamental constraints for any model of galaxy formation.

Key words: galaxies: elliptical and lenticular, cD – galaxies: evolution – galaxies: fundamental parameters – galaxies: kinematics and dynamics – galaxies: spiral – galaxies: structure

Online-only material: color figures

1. INTRODUCTION

Many schemes for classifying galaxies have been presented over the years, focusing on somewhat ephemeral properties such as morphology and color. Alternatively, one may consider three fundamental physical parameters: mass M, energy E, and angular momentum J. Qualitatively, these are related to the amount of material in a galaxy, to the linear size, and to the rotation velocity.

An important advantage of these parameters is that they may be related back to the earlier states of galaxies without having to unravel all of the messy intervening details such as baryonic dissipation, star formation, and morphological transformation. As an example, the simple assumption that J is approximately conserved during the collapse of gas within hierarchically forming dark matter halos naturally explains the observed basic

scaling relations of disk galaxies (Fall & Efstathiou 1980; Dalcanton et al. 1997; Mo et al. 1998).

Here "conserved" means that the initial J is retained at a factor of ∼2 level, unlike E, which can be readily lost by factors of ∼10 through dissipative collapse and radiation. Note that the "weak" conservation of *total* J is less restrictive and more plausible than the "strong" conservation of the *internal* distribution of J with radius, which could be readily altered by secular processes within disks while still preserving total J (e.g., Kormendy & Kennicutt 2004; see Fall 2002 and Freeman & Bland-Hawthorn 2002 for further discussion).

In this vein, Fall (1983, hereafter F83) introduced a general diagram of $j_\star$ versus stellar mass $M_\star$, where $j_\star \equiv J_\star/M_\star$ is the stellar specific angular momentum. This diagram has the important advantages that it deals with conservable physical quantities and that the axes represent independent variables. The $M_\star$ axis embodies a mass scale, while the $j_\star$ axis represents a length scale times a rotation velocity scale. On the contrary, the standard relations between $M_\star$ and circular velocity

---

[3] Current address: Department of Physics and Astronomy, San José State University, One Washington Square, San Jose, CA 95192, USA.
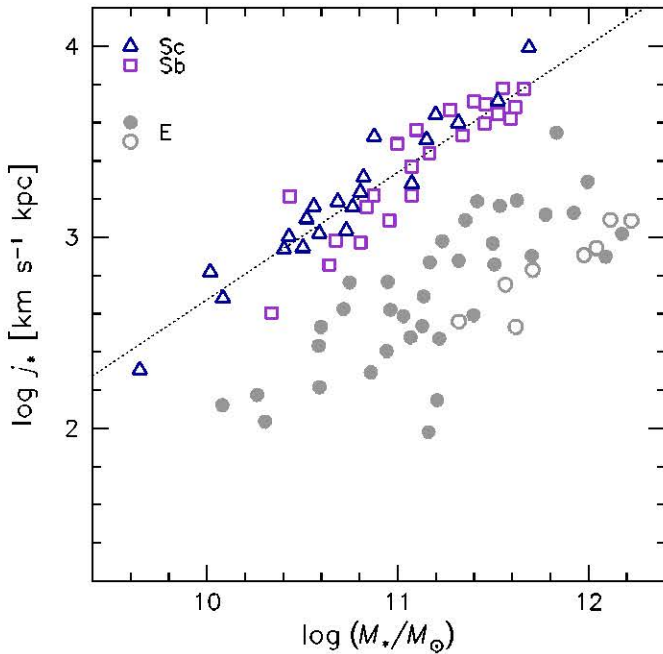
Figure 1. Total intrinsic stellar specific angular momentum of galaxies plotted against their total stellar mass, reproduced from Fall (1983), with corrections from a Hubble constant of $h = 0.5$–0.7. The symbols show galaxy types according to the legend at the upper left; for the ellipticals (E), open circles show galaxies with an upper-limit estimate of $j_\star$. The dotted line shows a trend of $j_\star \propto M_\star^{2/3}$. The logarithms plotted here and used throughout the paper are in base 10. These $j_\star$–$M_\star$ scaling relations are the focus of this paper, and will eventually be updated in Figure 14.

(A color version of this figure is available in the online journal.)

v_c (e.g., Tully & Fisher 1977; Dutton et al. 2010; Trujillo-Gomez et al. 2011) involve correlated variables, since v_c may be directly connected to $M_\star$. Another related parameter is the spin (λ), which is useful for characterizing dark matter halo rotation, and which we will discuss later in this paper.

The simple $j_\star$–$M_\star$ diagram is still charged with useful information for understanding galaxies, and to orient the remainder of our discussion, we begin by reproducing the original version from F83 here in Figure 1. The only change is to rescale the data for a Hubble constant of $h = 0.7$ rather than $h = 0.5$. These data were for late-type spirals (Sb and Sc) based on extended optical rotation curves, and for elliptical galaxies based on observations from their inner half-light radii, as feasible in that era.

The first key feature to note from Figure 1 is that the spirals follow a fairly tight scaling relation of $j_\star \propto M_\star^\alpha$, where $\alpha \sim 0.7$ (see also Takase & Kinoshita 1967; Heidemann 1969; Freeman 1970; Nordsieck 1973), which is a phenomenology that is now understood to provide a remarkable link between visible galaxies and their invisible dark matter halos. F83 provided a simple theoretical framework in which the gaseous baryons of galaxies are initially mixed with the dark matter and share in the same j. The baryons then cool and decouple from the dark matter, collapsing into star-forming disks. If the baryonic j is approximately conserved in this process, both the *zero point* and the *slope* of the observed spiral-galaxy $j_\star$–$M_\star$ relation are reproduced.

The formation of disk galaxies can thus be explained at a basic level through this long-standing picture of (weak) j conservation. To provide further understanding, hydrodynamical simulations of galaxy formation have been pursued for decades, with the $j_\star$–$M_\star$ observational diagram from F83 as a key benchmark for

theory. Attaining that benchmark has turned out to be a major challenge, with early studies finding catastrophic j loss (e.g., Katz & Gunn 1991; Navarro & Benz 1991; Navarro et al. 1995; Navarro & Steinmetz 1997).

This angular momentum "catastrophe" can be attributed partially to numerical limitations, and partially to uncertainties in modeling baryonic processes such as feedback following star formation, as reviewed by Fall (2002). Over the years, the simulations have improved and can now come close to reproducing the $j_\star$–$M_\star$ observations (e.g., Governato et al. 2007; Agertz et al. 2011; Guedes et al. 2011), although much work still remains in understanding both the numerics and the physics.

Besides the angular momentum benchmark from F83 which has become a standard ingredient in modeling the formation of disk galaxies, there is another aspect of the original $j_\star$–$M_\star$ diagram that has received relatively little attention: the inclusion of elliptical galaxies along with the spirals. The diagram thereby provides a fundamental diagnostic of scaling relations for *all* galaxies, which is important because there is still not a full explanation for such a basic property as the Hubble (1926) sequence of galaxy morphologies.

Star formation considerations aside, there is an obvious *dynamical* distinction between galaxy disks and spheroids, which are characterized by cold, ordered rotation versus random motions with fairly low net rotation, respectively. Differences in the conservation and distribution of j may very well be pivotal to explaining these differences and to governing the fates of galaxies.

As shown in Figure 1, F83 found that ellipticals followed a $j_\star$–$M_\star$ trend roughly parallel to the spirals, but lower by a factor of ~ 6, and with more apparent scatter (see also Bertola & Capaccioli 1975). There are several potential explanations for such a difference between spirals and ellipticals, but the most plausible one is traced to a violent, clumpy genesis for spheroids. For example, mergers could naturally redistribute angular momentum from the central regions of a galaxy to its outer parts by dynamical friction (e.g., Aarseth & Fall 1980; Gerhard 1981; Barnes & Efstathiou 1987; Zurek et al. 1988; Barnes 1992; Hernquist 1992; Navarro & White 1994; Heyl et al. 1996; D'Onghia & Navarro 2007; Zavala et al. 2008). Thus, j should be basically conserved but inconveniently locked up in unobservable components such as the dark halo and the faint outer stars.

With this theoretical sketch in hand, the $j_\star$ disparity between spirals and ellipticals has received little further attention over the years. However, the scenario of angular momentum redistribution has not yet been directly tested by observations—a situation that may now finally be remedied via the advent of new techniques for optical spectroscopy in galaxy halos (with preliminary results along these lines reported in Romanowsky et al. 2004).

In this paper we re-open various questions about angular momentum in all types of bright galaxies, following and extending the treatment of F83. Are the $j_\star$–$M_\star$ slopes, zero points, and scatter in Figure 1 supported upon re-examination? Does the "missing" $j_\star$ in ellipticals emerge in large-radius data? Can the $j_\star$ variations be associated with the natural dispersion in spin expected for standard dark matter halos, or is it necessary to invoke additional baryonic j evolution?

F83 also proposed that the Hubble sequence may be understood as a systematic variation in $j_\star$ at a fixed $M_\star$ (or equivalently, variation in $M_\star$ at fixed $j_\star$), but could not test this idea owing to the lack of adequate data for the crucial,
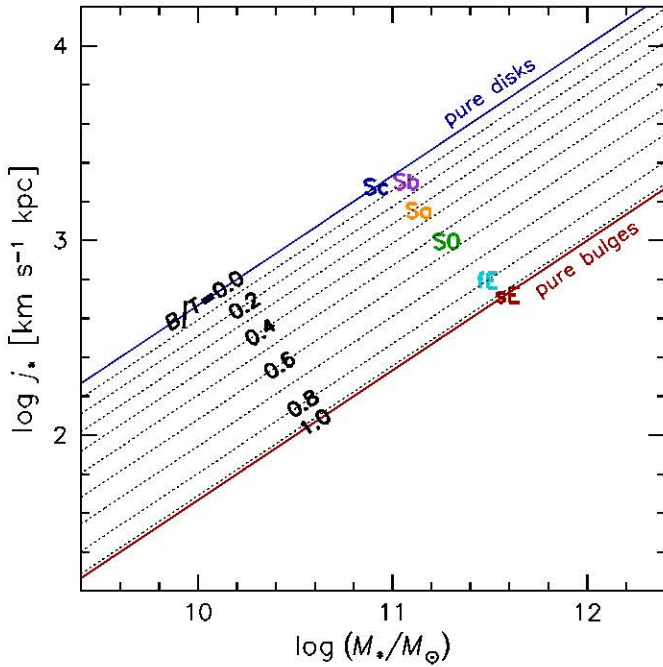
Figure 2. Physically motivated classification diagram of galaxies, using the parameter space of stellar mass and specific angular momentum. The solid blue and red lines show parallel scaling relations for disks and bulges, which are based loosely on our observational results to be presented in Section 5. Approximate positions are also shown for different galaxy types: Sc, Sb, Sa, S0, fE, and sE (the latter two being fast- and slow-rotating ellipticals).

(A color version of this figure is available in the online journal.)

intermediate cases of Sa and S0 galaxies. Here we will pursue this theme and advance a framework where every galaxy can be considered basically as a linear combination of a disk and a bulge, with each of these components following a characteristic $j_\star$–$M_\star$ scaling relation. In this idealized model, the $j_\star$–$M_\star$ parameter space maps uniquely to a space of $M_\star$ and bulge fraction B/T.

Figure 2 provides a schematic overview of this framework, showing decompositions of the Hubble sequence in $j_\star$–$M_\star$ parameter space. One of our goals in this paper will be to include observational results for Sa and S0 galaxies in this diagram for the first time, to see if such systems fill in the gap (if any) between earlier and later types, and if bulges and disks are homologous enough to explain the $j_\star$–$M_\star$ trends as primarily reflecting a B/T sequence.

The $j_\star$–$M_\star$ diagram does not simply provide a basic *description* of galaxies and their subcomponents, but also permits a novel approach to modeling the *evolution* of galaxies which is complementary to numerical simulations. As mentioned previously, there are simple models for the formation of disk galaxies that relate their $j_\star$ and $M_\star$ values to the initial conditions of their host halos. More generally, *any* stage in the evolution of a galaxy will involve a vector of change in the j–M diagram that is not arbitrary, since in real physical processes, changes in j and M will be linked in characteristic ways. Therefore, the empirical offsets between the $j_\star$–$M_\star$ sequences of different galaxy types, and of their subcomponents including bulges, disks, and dark matter halos, can reveal the evolutionary connections among them.

We set out to explore the preceding questions and issues as follows. In Section 2 we present a methodology for careful estimation of $j_\star$ in various types of galaxies and observations,

with most of the details of its derivation given in Appendix A. Section 3 uses detailed models of a handful of real galaxies to examine a simplified procedure for $j_\star$ estimation. Our updated analysis of the observed $j_\star$ trends in a large sample of galaxies follows, with the observational ingredients and their inter-correlations described in Section 4, and the full results presented in Section 5 including a definitive confirmation of the large offset between spirals and ellipticals. These empirical $j_\star$ trends can be considered as fundamental, enduring tools for constraining theories of galaxy evolution. In Section 6 we go on to connect the observations to generalized theoretical predictions for angular momentum in a modern cosmological context. We summarize in Section 7.

In addition, Appendix A is an important part of this paper, providing an extended presentation of new content relating to the derivation of $j_\star$, which has been split off from the main text for the sake of readability. Appendices B–D provide data tables of $j_\star$ and other properties of observed galaxies, along with detailed discussion of the observations and data analysis for a subsample of these galaxies.

The reader looking for immediate answers to the questions above may wish to skip ahead to the results of Section 5.2 and onward.

2. BASIC FORMULAE: DISKS AND SPHEROIDS

The foundation for this paper is a revised, general observational analysis of specific stellar angular momentum $j_\star$ for bright galaxies in the nearby universe. This quantity is most generally calculated by the following expression:

$$\mathbf{j}_t \equiv \frac{\mathbf{J}_t}{M_\star} = \frac{\int_\mathbf{r} \mathbf{r} \times \bar{\mathbf{v}} \rho \, d^3\mathbf{r}}{\int_\mathbf{r} \rho \, d^3\mathbf{r}}, \tag{1}$$

where the subscript "t" denotes the "true" angular momentum in three-dimensional space, $\mathbf{r}$ and $\bar{\mathbf{v}}(\mathbf{r})$ are the position and mean-velocity vectors (with respect to the center of mass of the galaxy), and $\rho(\mathbf{r})$ is the three-dimensional density of the population under study (generally assumed to be stars in this project).

For spiral galaxies, we approximate the density distribution as an axisymmetric, infinitely thin disk with an exponential surface density profile. Also assuming a radially constant rotation curve, Equation (1) yields the simple expression

$$j_t = 2 \, v_c \, R_d \,, \tag{2}$$

where v_c is the intrinsic circular rotation velocity and R_d is the intrinsic exponential-disk scale length. These deprojected quantities are relatively easy to infer from observations because it is straightforward to estimate disk galaxy inclinations. Equation (2) is widely used in the literature (including in F83), but we will demonstrate explicitly that it provides an excellent approximation to real galaxies whose rotation curves vary with radius.

For more general cases including elliptical galaxies,[4] there is no established recipe equivalent to Equation (2). For multiple

---

[4] We use the term "spheroid" to mean a pressure-dominated stellar system (which may also rotate). A "bulge" is the spheroidal component of a spiral galaxy. An "elliptical" is a galaxy with only a spheroidal component, although many galaxies commonly classified as ellipticals probably have embedded disk-like components, similar to those in lenticulars but less obvious. We consider jointly the ellipticals and lenticulars under the general rubric of "early-type" galaxies.
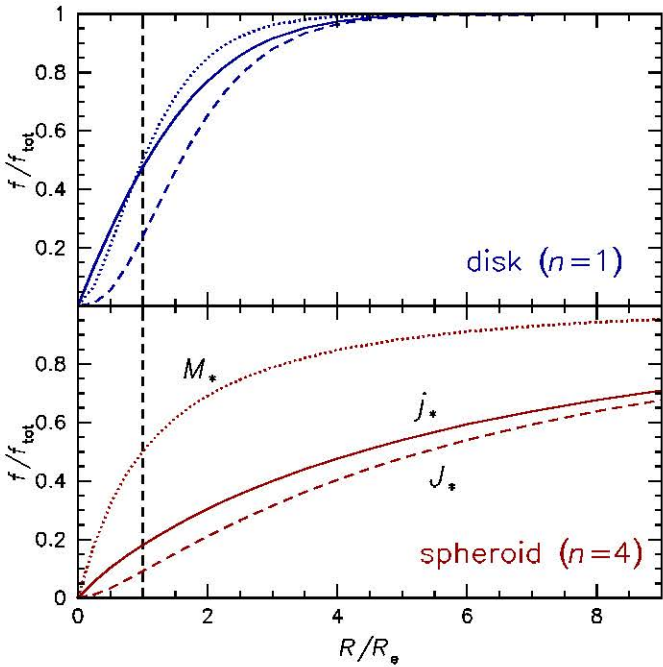
Figure 3. Fraction of enclosed cumulative quantities vs. cylindrical galactocentric radius (normalized by the effective radius R_e) for model galaxies with an exponential profile ($n = 1$ disk, top) and a de Vaucouleurs profile ($n = 4$ spheroid, bottom). A constant, cylindrical rotation field is assumed. The quantities are projected stellar mass $M_\star$ (dotted curve), angular momentum $J_\star$ (dashed), and specific angular momentum $j_\star$ (solid). The latter quantity is computed using the cumulative values of both $J_\star$ and $M_\star$ within the radius R. The vertical dashed line marks $1\,R_e$. To capture half of $j_\star$, the observations must extend to $\sim 1\,R_e$ in a disk galaxy, and to $\sim(4\text{–}5)\,R_e$ in a spheroid.

(A color version of this figure is available in the online journal.)

reasons, estimating j_t for these galaxies is much harder than for spirals. Not only are their inclinations and intrinsic shapes uncertain, but also large-radius rotation measurements are both more difficult and more critical.

We illustrate the last point with some basic galaxy models. Adopting the simple assumption of an axisymmetric system with cylindrical rotation that is constant with respect to the intrinsic radius R, we consider both a disk galaxy with an exponential surface density profile, and an elliptical galaxy with a standard de Vaucouleurs (1948) $R^{1/4}$ profile. Although ellipticals are in general triaxial systems, the axisymmetric model is sufficiently accurate for our purposes.

Figure 3 then shows the cumulative distribution of angular momentum (both total and specific) with radius. For the disk galaxy, the specific angular momentum reaches roughly half of its total value at the effective radius R_e that encloses half of the stellar light. This implies that observational estimates of j_t will be relatively easy for disk galaxies.

For the elliptical galaxy on the other hand, the halfway mark for j_t is reached at $4.5\,R_e$. This is because ellipticals contain a fairly large fraction of their light in their outer regions where the radius lever arm in $\mathbf{r} \times \bar{\mathbf{v}}$ is large. The implication is that observations of elliptical galaxies need to extend to much larger radii than for spirals, in order to be confident of capturing the total j_t.

Typical stellar kinematics observations in 1983 extended to $\sim 1\,R_e$, and even today, only a small handful of galaxies have been observed kinematically out to $\sim 5\,R_e$, which means the positions of the ellipticals in the original $j_\star$–$M_\star$ diagram (Figure 1) were highly uncertain, and continue to be challenging

to determine with surety. Fortunately, after a great deal of experimentation, which we will discuss below, we find that there is a heuristic approach where observations around $\sim 2\,R_e$ can be used to estimate the total j_t of ellipticals with reasonable accuracy.

Returning to a general framework for estimating j_t from observations, there is not only the challenge of extending the data to large radii, but also of having only three of the six phase-space quantities in Equation (1) accessible (i.e., the projected positions and line-of-sight velocity). Even the projection of $\mathbf{j}_t$ on the sky involves unobservable velocity components tangential to the line of sight, and requires additional modeling assumptions.

To cope with these issues, we will model the observed rotation and luminosity profiles of galaxies and convert these to j_t estimates using approximate deprojection factors. Although these factors are based on highly simplified models, the dominant source of uncertainty is still the limited extent of the data to large radii.

We derive in Appendix A two alternative expressions for estimating j_t from observations, both of them based again on the simplifying assumption of cylindrical rotation. The first expression starts with a detailed calculation of a "projected" specific angular momentum proxy that can be estimated directly from observations:

$$ j_p = \frac{\int v_{\rm rot,p}(x)\, \Sigma(x)\, x^2 \, dx}{\int \Sigma(x)\, x \, dx}. \qquad (3) $$

Here $v_{\rm rot,p}(x)$ is the observed profile of rotation velocity along the projected semimajor axis x, and $\Sigma(x)$ is the surface density profile, again along the semimajor axis.

The quantity j_p is related to j_t through a "deprojection" factor C_i:

$$ j_t = C_i\, j_p. \qquad (4) $$

Therefore, the problem of estimating j_t separates into two parts: the calculation of j_p from observations, and the factor C_i which can be calibrated from theoretical models.

As we describe in Appendix A, this latter factor has some dependence on the detailed density–velocity structure of the galaxy, but is primarily a function of the inclination i relative to the line of sight. For thin-disk galaxies, it is simply $C_i = (\sin i)^{-1}$. With spheroidal galaxies, there is an additional dilution effect that comes from the line-of-sight intersecting the rotation field at non-tangent points. In principle, this effect is dependent on the detailed shape of the rotation profile, but we have found with simplified test models that such variations can be neglected in practice. We also find that as long as the major-axis radius x, rather than a circularized radius R, is used in Equation (3), then C_i is insensitive to galaxy flattening.

A general approximation to C_i as a function of inclination is provided by Equation (A29). It is normally difficult to determine i for spheroidal galaxies, and we will when needed adopt inclination-averaged values.

Equation (3) yields accurate results that are commensurate with the quality of modern observations, but involves numerical integration, and careful compilation of $\Sigma(x)$ and $v_{\rm rot,p}(x)$ profiles along with extrapolation beyond the bounds of the data.

We could in principle simplify the problem further by using parametric models for $v_{\rm rot,p}(x)$ and $\Sigma(x)$. Unfortunately, the diversity of observed rotation profiles (when non-spiral galaxies are considered) defies parameterization. We can at least adopt for the surface density the general Sérsic (1968) law which

accurately represents a wide range of galaxy types:

$$\Sigma(x) \propto \exp[-b_n(x/a_e)^{1/n}], \qquad (5)$$

where a_e is the effective radius along the semimajor axis, and the shape index n determines the steepness of the outer density profile (higher values are shallower: e.g., an exponential-disk profile has $n = 1$ and the de Vaucouleurs law for ellipticals has $n = 4$), while b_n is a numerical function of n (Equation (A27)).

We use this $\Sigma(x)$ simplification in practice when deriving j_p from a detailed $v_{rot,p}(x)$ profile in expression (3). We also generally base our $\Sigma(x)$ profiles on observations of stellar surface brightness profiles $I(x)$, assuming for simplicity that there are no variations of stellar mass-to-light ratio with radius (e.g., due to dust).

Our second method is a quick-and-dirty shortcut for estimating j_t, as needed to generate an initial overview of the trends for a large sample of galaxies. We simply calculate the following linear scalar expression (derived in Appendix A from Equation (3)):

$$\tilde{j}_p = k_n\, v_s\, a_e, \qquad (6)$$

where $\tilde{j}_p$ means an approximation for j_p, v_s is the *observed* rotation velocity at some arbitrary measurement location x_s, and $k_n \sim 1$–5 is a numerical coefficient that depends on the Sérsic index n of the galaxy (see Equation (A31)). As in Equation (4), $\tilde{j}_p$ is multiplied by C_i to provide an approximate $\tilde{j}_t$. Here the basic idea is that a galaxy can be represented by a characteristic observed rotation velocity scale v_s, a length scale a_e, and a factor k_n that relates to the moment of inertia (discussed further below).

The heuristic approximation that we make here is to select v_s at $x_s \sim 2a_e$ for all galaxies. We will show in the next section that this choice allows us to estimate j_p with an accuracy of $\sim\pm0.1$ dex, which is good enough to start making some interesting inferences about trends in j_t.

For $n = 4$ spheroids, the expression equivalent to Equation (2) for spirals is

$$\tilde{j}_t = 3.03\, v_s\, R_e, \qquad (7)$$

for a median, unknown inclination (Equation (A32)). An important concept with the more general expression (6) is that k_n increases strongly with n; for fixed galaxy size and rotation velocity, a more extended luminosity profile implies a higher j_p owing to the large fraction of mass residing at large radii. This also means that a spheroidal ($n \sim 4$) galaxy with the *same* observed rotation v_s and size a_e as a spiral has a *larger* specific angular momentum. Late-type and early-type galaxies near the L^* characteristic luminosity *do* have similar sizes for the same stellar mass (e.g., Shen et al. 2003). Therefore, we can already make the basic prediction that if j_p at a fixed mass is independent of morphology, then the early types should have v_s values relative to late types of $\sim k_1/k_4$, i.e., lower by a factor of ~ 2.

The $j_\star$ formalism that we have outlined here represents a modest extension of the simpler methods in F83. The improvements introduced here include allowance for a range of luminosity profiles (not only $n = 1$ and $n = 4$), and better treatment of elliptical galaxies where rotation at large radii is critically important. It also becomes more straightforward to understand the interplay between observations and uncertainties in the $j_\star$ estimates, as explored in the next section.

3. OBSERVATIONS: ANALYSIS METHODS

Before we move on to $j_\star$–$M_\star$ analyses of a large sample of galaxies, we examine a small sample in more detail. The goals here are to illustrate the nature of the available data, to demonstrate that the simplified Equations (2) and (6) are good approximations to a full treatment with Equation (3), and to understand some systematic effects in the $j_\star$ and $M_\star$ determinations.

Because this paper is concerned with the angular momentum bound up in the stellar components of galaxies, the preferred kinematic tracer comes from integrated-light absorption-line spectroscopy. In many cases, such data do not extend to large enough radii, so we make use of additional tracers as proxies for the field stars: cold and warm gas, planetary nebulae (PNe), and metal-rich globular clusters (GCs).

We consider disk- and bulge-dominated galaxies in Sections 3.1 and 3.2, respectively. We evaluate our simplified $\tilde{j}_p$ estimate (6) in Section 3.3, describe our mass estimates in Section 3.4, and then consider systematic uncertainties in Section 3.5.

3.1. Disk-dominated Galaxies

The most straightforward galaxies for estimating angular momentum are the gas-rich spirals, since the stellar rotation profile, which cannot always be measured directly, follows the gas rotation profile to a good approximation. Also, the observed rotation can easily be corrected for projection effects in order to recover the intrinsic value (see Appendix A.2). The detailed analysis below is overkill for these galaxies, whose j_t can be readily estimated through Equation (2), but we wish to illustrate how our more general treatment works for them, before moving on to the spheroids.

We consider two real galaxies: NGC 3054 and NGC 3200, which are well-studied disk-dominated spirals from the classic optical rotation curve analyses of Rubin et al. (1982). These cases are chosen to bracket the typical range of inner rotation profile shapes for spirals (slowly and rapidly rising, respectively).

We take the long-slit major-axis ionized-gas kinematics data from Pizzella et al. (2004), shown in Figure 4 after a modest amount of re-binning. These rotation profiles have high-frequency bumps and wiggles that are presumably caused by local perturbations such as spiral arms. Fortunately, these features tend to average out when calculating a cumulative j and are not important in this context.

To calculate the projected specific angular momentum j_p, we carry out a piecewise integration of Equation (3), using the major-axis rotation-velocity data $v_{rot,p}(x)$ up to $\sim 2a_e$, along with simple power-law extrapolations at larger radii, as shown in Figure 4. For $\Sigma(x)$, we use an exponential model ($n = 1$ in Equation (5)), with the disk scale lengths R_d taken from r-band photometry as we will discuss in the next section. Note that $a_e = 1.68 R_d$ for a pure exponential disk.

The resulting cumulative $j_p(\leqslant x)$ profiles with radius for these galaxies are shown in Figure 5. Here it would be trivial to convert $j_p(\leqslant x)$ immediately to $j_t(\leqslant R)$ using the known inclinations of these galaxies, but our general strategy is to focus first on the direct modeling of the observations for all galaxies, and later apply the deprojection factors C_i, which involve different systematics.

It can be seen that j_p hardly changes outside $\sim 3a_e$, and that the large-radius extrapolations make very little difference: the
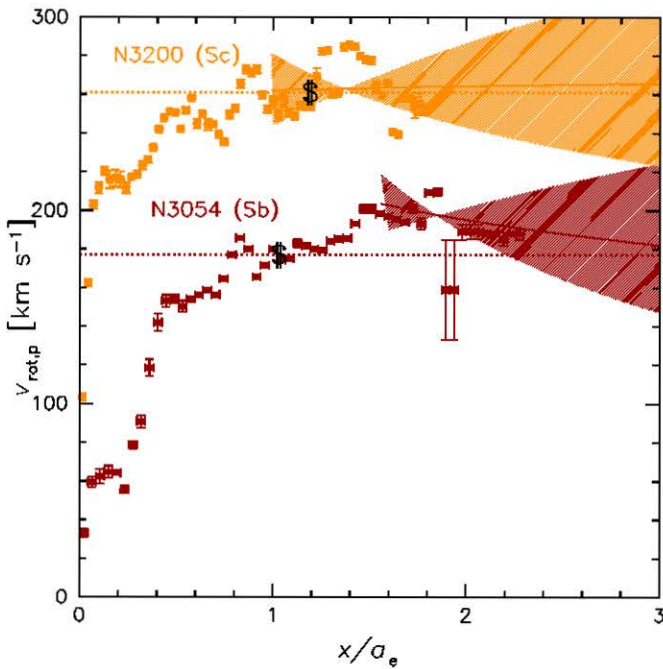
Figure 4. Observed rotation-velocity profiles of two spiral galaxies (NGC 3054 and NGC 3200) vs. semimajor-axis radius (renormalized by the effective radius). Each galaxy is labeled with its Hubble type. The data are ionized-gas velocities from Pizzella et al. (2004). The solid curves with shaded regions show power-law fits (with uncertainties) used to extrapolate the rotation velocity to larger radii. See the main text and Appendices A and B for further details. Dotted horizontal lines show the characteristic rotation velocity v_s for each galaxy; the approximate intersection with the corresponding rotation-velocity profile is marked with a $ symbol and defines the radius x_s (see Section 3.3).

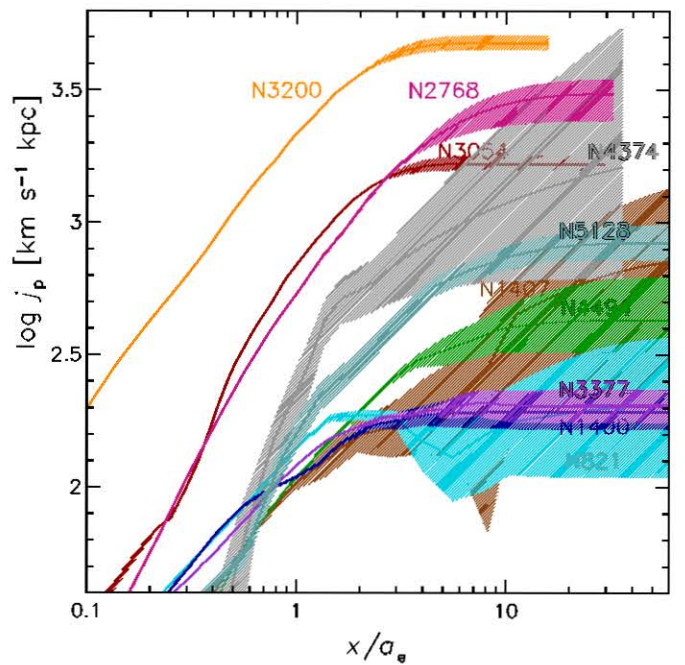(A color version of this figure is available in the online journal.)

Figure 5. Cumulative projected specific angular momentum, $j_p(< x)$, of several nearby galaxies as a function of semimajor-axis radius (with log axes), based on modeling of kinematic observations. Solid curves show the best-fit models, with shaded regions illustrating the uncertainties (including those due to extrapolations at large radii). See Table 3 for the distances and a_e values adopted. For most of the galaxies, j_p has nearly reached its asymptotic value by $x \sim 5a_e$.

(A color version of this figure is available in the online journal.)

regions outside $\sim$2–2.5a_e ($\sim$3–4R_d) contain only $\sim$8%–15% of the total luminosity, and contribute only $\sim$15%–25% of the total j_p (half of j_p is enclosed within $\sim$1.2a_e $\sim$ 2R_d; Figure 3). Given reasonable extrapolations of the data, the total j_p for these two galaxies, using our basic modeling assumptions, is constrained to $\sim$5% ($\sim$0.02 dex).

Thus the kinematics is not a major source of uncertainty for j_t estimation in disk-dominated galaxies. Additional complications that we have not considered here are deviations of the disk surface density profile from a simple constant mass-to-light ratio exponential model, and inclusion of a bulge (to be discussed later). We will examine more general systematic uncertainties in Section 3.5.

3.2. Bulge-dominated Galaxies

We now turn to the novel component of this paper, which is the careful treatment of j_t in early-type, bulge-dominated galaxies. Figure 3 demonstrated that traditional observations within 1a_e provide little assurance about the total angular momentum content of these systems, while even current cutting-edge observations out to $\sim$5a_e might in principle not be adequate.

Here we analyze a sample of eight real galaxies in detail in order to characterize the accuracy of j_t estimations. Seven of these galaxies were chosen because of the availability of high-quality extended kinematic data using integrated stellar-light spectroscopy from two recent papers (Coccato et al. 2009; Proctor et al. 2009). Both papers represent the first installments of systematic surveys of early-type galaxies in the local universe, and there is no obvious selection bias for

the seven galaxies. Five of them are "ordinary" near-L^* early types with central "fast-rotator" kinematics as is typical for such galaxies (Kormendy & Bender 1996; Emsellem et al. 2011). The other two (NGC 1407 and NGC 4374 = M84) are examples of round, bright "slow rotators" that are common in high-density environments (Cappellari et al. 2011b).

Five of these galaxies also have PN or GC kinematics data available (Coccato et al. 2009; Romanowsky et al. 2009), which we incorporate into our analysis in order to extend the range of galactocentric radii probed. We include an eighth galaxy in our sample, NGC 5128 (Cen A), because it has the most extended (PN) kinematics data of any early-type galaxy in the literature (Peng et al. 2004). It may also be the remnant of a recent major merger (e.g., Bekki & Peng 2006), which as discussed in Section 1 is expected to generally transfer angular momentum into the outer regions. Analysis of this galaxy thus provides a golden opportunity to search for the "missing" angular momentum, and to see if any clear j_t difference emerges with respect to the other galaxies in the sample.

The use of PNe and GCs to provide proxies for stellar kinematics may seem risky, given the considerable uncertainties that remain about the parent stellar populations of these tracers. However, in most galaxies studied to date, both the density and kinematical profiles of PN and metal-rich GC systems have been found to correspond well to those of the full stellar population in the regions of overlap (e.g., Coccato et al. 2009; McNeil et al. 2010; Das et al. 2011; McNeil-Moylan et al. 2012; Cortesi 2012; Pota et al. 2012). We have also verified that this is generally the case for the galaxies in our sample.

Further details of the observations as well as of the kinematical modeling are provided in Appendix B, along with the resulting rotation and angular momentum profiles. It should be
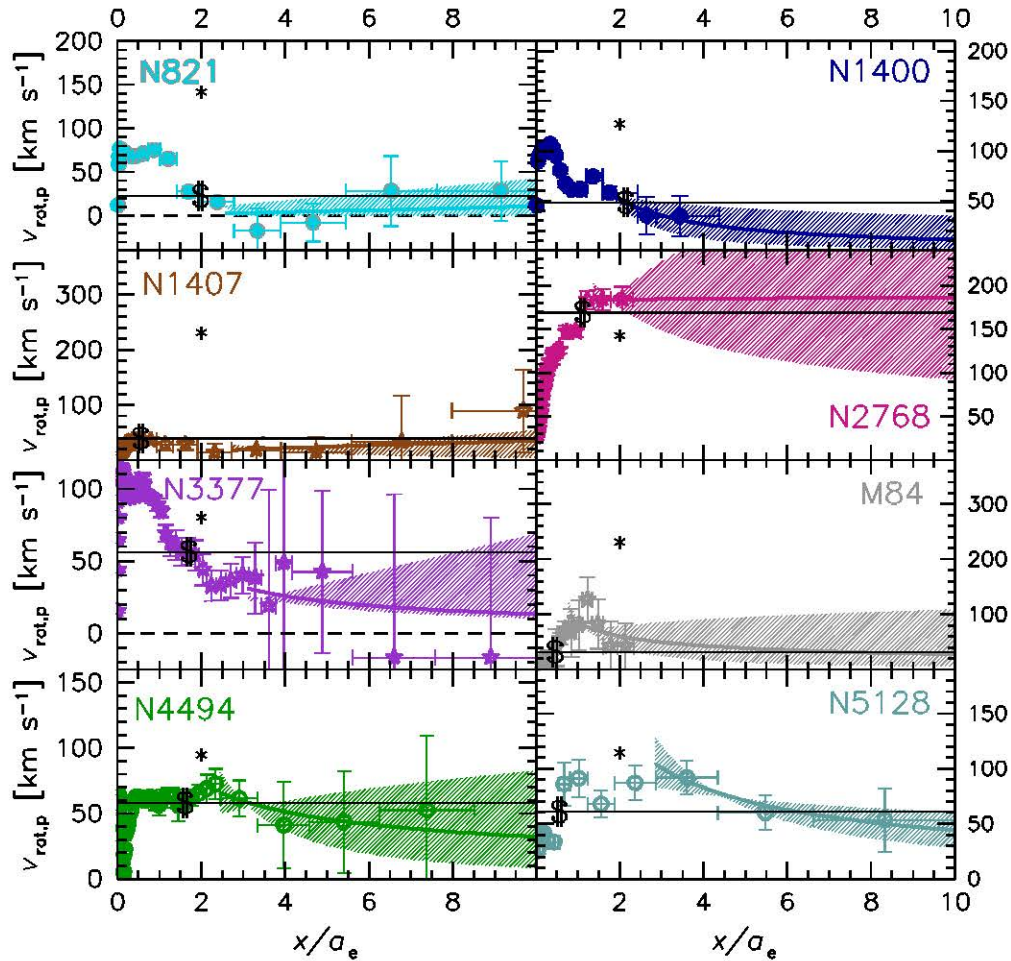
Figure 6. Rotation-velocity profiles for eight early-type galaxies. See Figure 4 for further details, including an explanation of the shaded uncertainty regions. For ease of inter-comparisons, the vertical axis of each panel has been scaled according to the velocity dispersion of the galaxy at $2a_e$, which is marked in each panel by a $*$ symbol. Note the dashed lines at zero rotation velocity in some cases. The galaxies show a diversity of rotation-velocity trends with radius.

(A color version of this figure is available in the online journal.)

emphasized that the careful, homogeneous construction of these profiles is laborious, which is why the current sample of galaxies that we consider in detail is relatively small.

The rotation-velocity profiles of these eight galaxies are summarized in Figure 6. Unlike the spirals (Figure 4), the early types show great diversity in the characteristic shapes of their profiles. Some are fairly constant with radius, others plummet rapidly from a central high value, and one continues increasing to the limits of the data. This diversity is *not* simply a matter of inclination, as can be seen by the divergent cases of NGC 821 and NGC 2768, which are both highly flattened and probably close to edge-on. We thus find that the central rotation properties of early-type galaxies cannot be used to reliably estimate the total angular momentum content, and there is probably no simple function that universally characterizes their full rotation-velocity profiles.

As with the spirals, we fit power laws to the outer regions of the rotation data in order to extrapolate to larger radii (see Appendix B for further details). We then use Equation (3) to calculate profiles of cumulative j_p with radius, which we plot in Figure 5. Even though the data do not reach the total asymptotic value for j_p, the requirement of a smooth power-law extrapolation for the rotation-velocity profile does in most cases strongly limit the total j_p, which is typically determined at the $\pm15\%$ level (±0.06 dex). The radius enclosing half of the total

j_p varies from galaxy to galaxy depending on the shape of its rotation-velocity profile: 0.7–$3a_e$ (for the two spirals, it is $1a_e$).

The exceptions to these findings are the two bright, round ellipticals NGC 1407 and NGC 4374. Figure 5 shows that much of the angular momentum in these galaxies is found at very large radii (half of j_p within $9a_e$ and $4a_e$, respectively), as expected from their fairly high Sérsic indices of $n \sim 4$–8 (the ordinary early types have $n \sim 2$–4). However, beyond the usual uncertainties introduced by extrapolating the rotation velocity, there are a couple of other practical considerations.

One issue is that although these particular galaxies have relatively well-studied surface brightness profiles, many such massive ellipticals do not, with their n and a_e values poorly known. This situation produces "double jeopardy" for angular momentum estimation, since both the luminosity and the rotation-velocity profiles at very large radii are important yet poorly constrained.

The other issue demonstrated with NGC 4374 is that its cumulative j_p has not yet converged at the (estimated total) virial radius of $\sim35a_e$, so it is not clear how its angular momentum should even be defined. This class of high-n galaxies is clearly problematic, and we will consider any j_t results on them to be tentative for now.

Figure 5 also reveals a first glimpse of the basic result of this paper. For most of the early types in the sample, there is
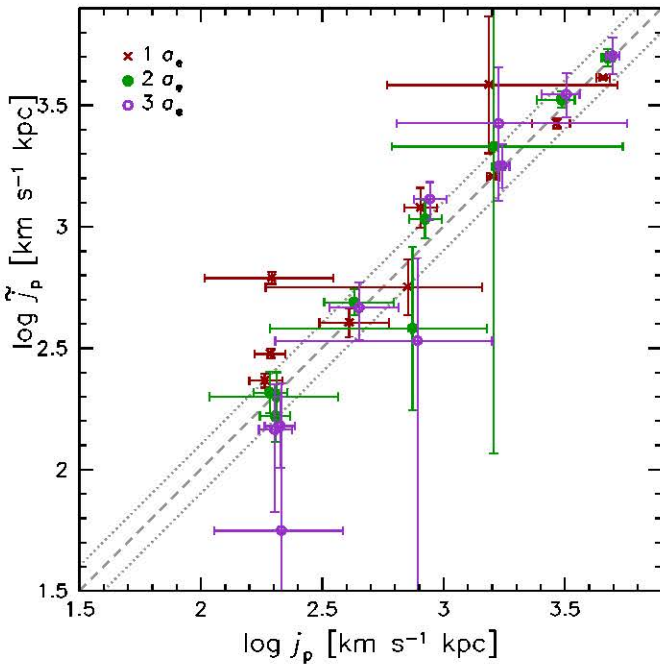
Figure 7. Comparison of a simple projected specific angular momentum estimate ($\tilde{j}_p$; Equation (6)) with the more accurate value (j_p). Results are shown for 10 different galaxies, each with a choice of three reference radii: $x_s/a_e =$ 1 (red crosses), 2 (green filled circles), and 3 (purple open circles). Some of the points are given a 0.02 dex horizontal offset for visibility. The dashed and dotted lines mark the one-to-one relation with a ±0.1 dex scatter. The optimal choice here for x_s is $2a_e$.

(A color version of this figure is available in the online journal.)

Figure 8. Logarithmic ratio between simple estimates of projected specific angular momentum (Equation (6)) and more accurate values (Equation (3)) vs. the rotation-measurement radius x_s in units of the effective radius. Each point indicates a sample ratio for an individual galaxy, with error bars indicating the kinematics-driven uncertainties in total j_p from the detailed models. Results are plotted for 10 galaxies: two spirals (orange profiles with open circles), six ordinary early types (blue profiles with filled circles), and two giant ellipticals (red profiles with filled squares). As in Figure 7, $x_s \sim 2a_e$ provides a good measurement location, resulting in minimal scatter and bias for the angular momentum estimates.

(A color version of this figure is available in the online journal.)

relatively little angular momentum hidden beyond $\sim$1–2a_e, and their total values of j_p are lower than those of the spirals. We will make more detailed comparisons later in this paper.
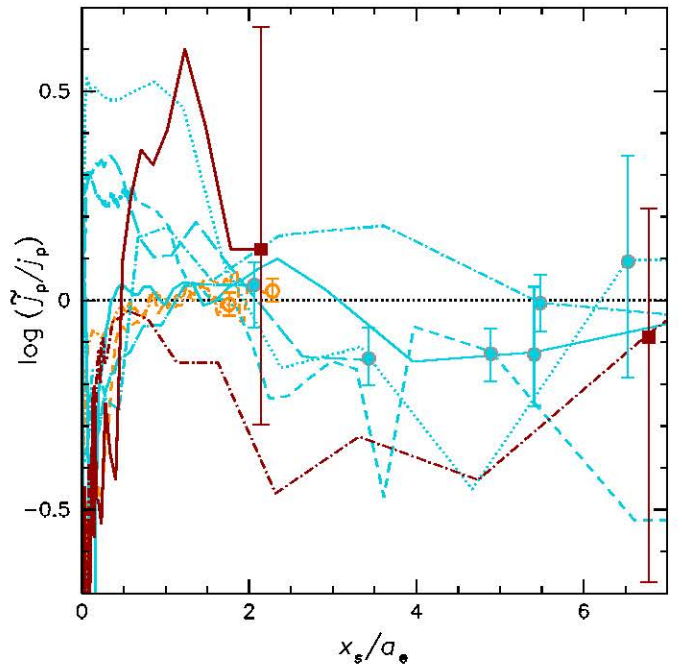
3.3. Simple J/M Approximations

We now arrive at a question that is critical for the wider survey of angular momentum in the rest of this paper: how accurate is the simplified Equation (6)? As a reminder, this $\tilde{j}_p$-estimator would replace the detailed calculations based on Equation (3) that we have carried out in the preceding subsections, but which are time consuming to carry out for a larger sample of galaxies, and are not even possible for cases without very extended kinematic data.

In Appendix A, we have motivated the construction of Equation (6) via toy models of galaxies, and calculated the corresponding coefficient k_n. We will now apply this formula to the set of 10 real galaxies just discussed (both late and early types), and find an optimum radial location x_s for measuring the characteristic rotation velocity v_s.

For each galaxy, it is straightforward to find the constant value of v_s which when substituted in Equation (3) yields the same j_p as with the nearly constant rotation-velocity profile. These results are listed in Table 3 and shown in Figures 4 and 6, where the intersection of v_s with the rotation-velocity profile determines the characteristic measurement radius x_s. As an example, for NGC 821, it is clear that $x_s \sim 2a_e$. For NGC 4494 on the other hand, a broad range of choices for x_s would work, owing to its nearly constant rotation-velocity profile.

Considering this issue in more detail, we calculate $\tilde{j}_p$ using Equation (6) with an arbitrary choice for x_s (which in turn determines a guess for v_s from the observed rotation velocity

at this radius). The results for $x_s/a_e = (1, 2, 3)$ are shown in Figure 7, plotted against j_p calculated in full from Equation (3). It can be seen that $x_s/a_e = 2$ provides a reasonably good match between $\tilde{j}_p$ and j_p for all of the galaxies in this sample. The other radius choices fare worse, owing to galaxies like NGC 821 that have rotation-velocity profiles with a distinct transition between the inner and outer regions near $2a_e$, and thus v_s measurement elsewhere would be biased.

Now to home in more finely on a choice for x_s, in Figure 8 we present the ratio of estimated and "correct" j_p, as a function of the chosen x_s, for each galaxy. Some of the galaxies permit a broad range of choices for x_s, while others do not. Especially noteworthy again are the galaxies like NGC 821 and NGC 3377 which have sharp drops in their rotation-velocity profiles, so v_s measured at small radii would overestimate j_p by factors of $\sim$2–3.

We do not find a strong correlation between n and optimal x_s as expected from the simple models we constructed in Appendix A.4; the dominant effect on x_s with the real galaxy sample is the scatter in the shapes of the rotation-velocity profiles. Future detailed analyses of a larger sample of galaxies may reveal systematic trends with n that motivate improved j_p estimation methods, but for now we stick with our simple $\tilde{j}_p$ approach.

Because the real galaxies so far do not show strongly rising outer rotation-velocity profiles, and if anything the reverse, $x_s \sim 2a_e$ appears to be a good overall choice for the rotation-velocity measurement radius. This minimizes the galaxy-to-galaxy scatter in the $\tilde{j}_p$ approximation ($\sim\pm0.1$ dex) and appears

to produce little systematic bias ($< \sim 0.1$ dex). Such "errors" are comparable to the uncertainties from carrying out the full j_p calculations, and are therefore acceptable for our purposes in this paper.

One caveat here is that this sample of galaxies is still small, and we cannot yet be sure of the universal validity of our approximation, e.g., for the larger sample of galaxies that we will study in the remainder of this paper. However, we will show that there is no apparent systematic bias, i.e., the overall scientific conclusions are consistent with the subset of detailed j_p profiles.

3.4. Stellar Mass Estimates

So far we have focused on estimating $j_\star$, but the other key component in constructing the $j_\star$–$M_\star$ diagram is of course the stellar mass $M_\star$. Assuming that we have a well-determined surface brightness profile $I(x)$ or total luminosity, we then need to know the stellar mass-to-light ratio $\Upsilon_\star$. We also assume that $\Upsilon_\star$ is constant throughout each galaxy, which means that its value is not relevant in our $j_\star$ calculations (only in $M_\star$ calculations).

Estimating $\Upsilon_\star$ in galaxies is a classic and not fully resolved problem. One standard approach is to use theoretical models for stellar populations in combination with observations of the stellar light (e.g., broadband colors or spectroscopic line indices). Although there are well-known degeneracies between the ages and metallicities inferred for the stars, fortunately $\Upsilon_\star$ can be estimated with more certainty (e.g., Tortora et al. 2009), modulo the initial mass function (IMF) of the stellar populations.

In this paper, our default assumption will be that all galaxies have the same value of $\Upsilon_\star$ in the near-infrared (NIR) K band. This band is only mildly affected by internal and foreground extinction, is thought to be relatively insensitive to variations in stellar populations, and has uniform photometry available from the Two Micron All Sky Survey (2MASS) survey (Skrutskie et al. 2006). We adopt a value of $\Upsilon_{\star,K} = 1.0$ based on both stellar populations modeling and dynamical analysis (Bell et al. 2003; Williams et al. 2009, Figure 9). According to these studies, $\Upsilon_{\star,K}$ varies only weakly among galaxies of different types (and colors).

This near-universality of $\Upsilon_{\star,K}$ is a convenient, simplifying assumption. However, just as this paper was being completed, we became aware of a growing consensus for larger variations in $\Upsilon_{\star,K}$ among galaxies with different star formation histories (e.g., Bell & de Jong 2001; Mouhcine & Lançon 2003; Vázquez & Leitherer 2005; Maraston 2005; Zibetti et al. 2009; Bershady et al. 2011; Westfall et al. 2011; Portinari & Into 2011). Our review of the recent literature suggests a most likely systematic variation in $\Upsilon_{\star,K}$ of a factor of ~ 2.5–3.5 (~ 0.4–0.55 dex) between the bluest spirals and reddest ellipticals in our sample.

We have not revised our analyses to reflect such variations in $\Upsilon_\star$, but we have included some brief comments on their expected impact throughout the paper. Fortunately our conclusions are not qualitatively changed, although there are some potential effects on the quantitative results. We note also that current stellar population models may not be definitive, as there are still substantial uncertainties associated with several factors, such as metallicity, star formation histories, dust extinction, and the thermally pulsing asymptotic giant branch phase. In this context, one may view the true situation as bracketed by our default uniform $\Upsilon_\star$ value and by a factor of ~ 3 variation in $\Upsilon_\star$.

The IMF is another potential wrinkle in this analysis. It affects the overall normalization of $\Upsilon_\star$ via the mass contributions of late-type dwarf stars or compact stellar remnants, which are
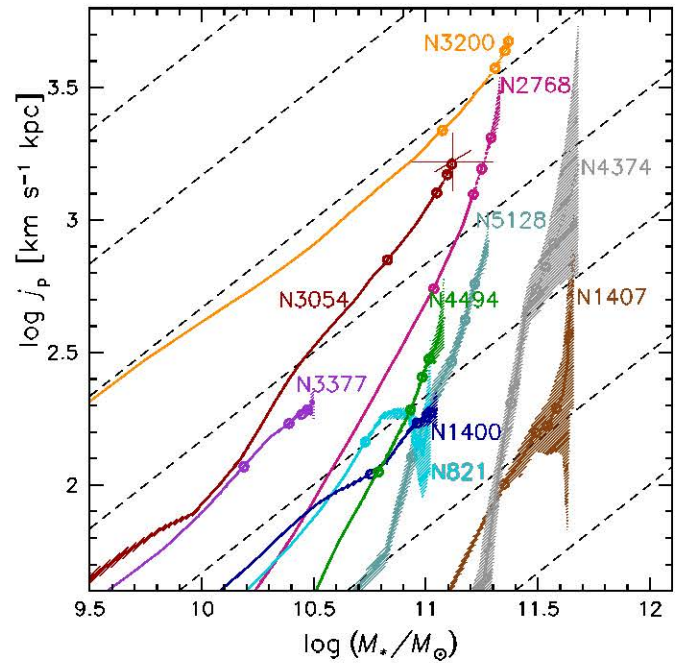
Figure 9. Cumulative projected specific angular momentum of nearby galaxies (as in Figure 5), now plotted vs. cumulative projected stellar mass. The curves are solid where constrained by the data, and dotted for extrapolations. Circles show intervals of $1a_e$ up to $4a_e$. Error bars at the end of the NGC 3054 curve illustrate the effects of systematic uncertainties (see the text for details): diagonal for the distance, vertical for scale length, and horizontal for $\Upsilon_\star$. Diagonal dashed lines show tracks of $j_p \propto M_\star^{2/3}$, which represent constant halo spin.

(A color version of this figure is available in the online journal.)

observationally difficult to tally. If all galaxies have the same IMF, then our analyses of the *relative* differences between galaxies in the $j_\star$–$M_\star$ plane will be secure. There are also recent, indirect claims for possible galaxy-to-galaxy IMF variations (e.g., Davé 2008; Treu et al. 2010; Tortora et al. 2010; van Dokkum & Conroy 2011; Dutton et al. 2012; Ferreras et al. 2012; Smith et al. 2012). However, even in this case we do not expect a major impact on our conclusions.

As an example, the recent analysis of Cappellari et al. (2012) implies that strong IMF variations tend to occur in only the most massive, and relatively rare, early-type galaxies, which would have $\log (M_\star/M_\odot) \gtrsim 11.3$ in our plots (based on a standard IMF midway between Kroupa 2001 and Salpeter 1955). Such galaxies might have masses larger than our estimates by factors of ~ 2, but given the relatively small numbers of such galaxies and the weak constraints on their $j_\star$ values, they will have little effect on our estimated $j_\star$–$M_\star$ trends.

Our calculations of $M_\star$ also require estimates of total luminosity, L_K. However, we do *not* simply adopt the total magnitudes provided by the 2MASS archive. These values are not reliable for early-type galaxies (e.g., Noordermeer & Verheijen 2007; Devereux et al. 2009; Williams et al. 2009; Schombert 2011), particularly the variety with extended high-n envelopes, where the 2MASS values could be too faint by as much as 1 mag.

Instead, we construct our own "aperture corrections." We adopt the 2MASS magnitudes within the 20th mag isophote, K_{20}, and use the best available optical photometry for each galaxy along with a Sérsic model fit to estimate the fraction of the galaxy light residing beyond K_{20}.

This procedure neglects any bandpass dependence in the light profiles $I(x)$, which are often more radially extended in bluer bands (e.g., de Vaucouleurs 1961; Peletier et al. 1990;

Roediger et al. 2011). Such differences imply $\Upsilon_\star$ variations with radius (Tortora et al. 2011), which is a reminder of the limitations of our constant-$\Upsilon_\star$ approximation. Given our reliance on optical profiles $I(x)$ to derive $\Sigma(x)$ and estimate j_p, as in Equation (3), for consistency we do need to use the optical data to extrapolate the K-band photometry in estimating $M_\star$. However, the scale lengths a_e of the stellar *mass* distributions are probably smaller on average than the a_e values that we use based on optical *luminosity* distributions, leading us to overestimate both j_p and $M_\star$. Improvement on this point could be made in the future by analysis of deep $I(x)$ data at NIR wavelengths. NIR spectroscopy would then also be needed for full consistency of both j_p and $M_\star$ estimates (e.g., Silge & Gebhardt 2003; Silva et al. 2008; Vanderbeke et al. 2011).

3.5. The $j_\star$–$M_\star$ Diagram

Here we focus on the $j_\star$–$M_\star$ plane, our ultimate destination in this paper, but for now considering the projected specific angular momentum j_p rather than the true j_t in order to isolate various effects that are disjoint from inclination uncertainties. Figure 9 shows our detailed galaxy sample where cumulative $j_p(< R) = J_p(< R)/M_\star(< R)$ is plotted not as a function of radius (as in Figure 5) but of *enclosed projected stellar mass*, $M_\star$.

For reference, we show dashed lines corresponding to $j_p \propto M_\star^\alpha$, with $\alpha = 2/3$. This value for α is motivated by previous observations (Section 1), and by theoretical predictions for j_t–$M_\star$, given constant values of an initial halo spin parameter λ, as we will see in Section 6.1. We are most concerned with the locations of galaxies relative to these tracks, and with any systematic effects that could shift the data in a direction *perpendicular* to them.

The shaded regions of the curves in Figure 9 indicate the uncertainties due to the kinematic data, including the extrapolations to large radii. For most of the galaxies, the asymptotic position in the j_p–$M_\star$ diagram is relatively well determined. The main exceptions are NGC 1407 and NGC 4374, which as discussed before are extended giant ellipticals whose total j_p is very difficult to determine. The early-type galaxy NGC 2768 is also a concern even though the formal j_p uncertainties are small, since there are large contributions to the total j_p estimate from the region of extrapolation.

An offset in total j_p between the late types and most of the early types as in Figure 5 is also apparent in Figure 9. However, the mass dimension brings the relative positions into sharper focus. For example, NGC 4374 and NGC 5128 have similar j_p values to NGC 3054, but also have larger stellar masses, which means that their inferred halo spins will be *lower* (considering distances perpendicular to the dashed tracks).

We next consider some systematic uncertainties that apply even if the rotation-velocity profiles are perfectly measured. First, there is a typical distance uncertainty of $\sim$10%. This affects j_p linearly and $M_\star$ quadratically, moving the position of the data by a very small amount nearly parallel to the λ tracks (see sample error bars marked for NGC 3054 in the figure).

Next we consider an uncertainty of $\sim$30% ($\sim$0.11 dex) in the scale lengths a_e, which translates into a similar uncertainty in j_p (see Equation (2)).[5] Also, in some cases the surface brightness profile is well constrained and the associated j_p uncertainty is very small (e.g., $\sim$5% or $\sim$0.02 dex in the case of the $n \sim 3$ elliptical NGC 4494).

Finally, there is the stellar mass-to-light ratio $\Upsilon_\star$, which as discussed in Section 3.4 may be uncertain by a factor of up to $\sim$3 ($\sim$0.5 dex), and which would affect $M_\star$ by the same amount. For spiral galaxies in particular, this is probably the dominant uncertainty in their inferred λ values, as we will see in Section 4.2. For the early types, the inclination is generally unknown and may be a significant source of uncertainty for estimating j_t, even when j_p is well constrained. We will return to this theme in Section 5.1.

4. OBSERVATIONS: SCALING RELATIONS AND DERIVATIONS OF J/M FOR THE FULL SAMPLE

Having carried out detailed analyses of $j_\star$ for a handful of galaxies in the previous section, we now derive $j_\star$ for a much larger galaxy sample, using simpler methods. Besides these derivations, in this section we also examine some basic scaling relations for galaxies, in order to understand the observational underpinnings of the $j_\star$–$M_\star$ results in the next section, and to verify that our results are consistent with some well-known properties of galaxies. We also introduce a novel, generalized version of the Tully–Fisher relation for galaxies of all types. Those who are keen to get straight to the angular momentum results may wish to skip to Section 5.2.

In order to populate the observational $j_\star$–$M_\star$ diagram, we will use the $\tilde{j}_p$ approximation of Equation (6) which we have found to be generally accurate at the $\sim$0.1 dex ($\sim$25%) level. The basic parameters that we then need for all of the galaxies are the total stellar mass ($M_\star$) and its scale length (R_d or a_e), the Sérsic index n, and the characteristic rotation velocity v_s.

The distances to the galaxies are estimated from redshifts and surface brightness fluctuations. As discussed in Section 3.4, $M_\star$ is derived from aperture-corrected 2MASS magnitudes m_K, assuming $\Upsilon_{\star,K} = 1.0$.

The other parameters are derived differently for the late-type and early-type samples, as we will discuss in Sections 4.1 and 4.2, respectively. Section 4.3 brings the data together in an examination of basic scaling relations, before proceeding to the final $j_\star$–$M_\star$ analyses of Section 5.

4.1. Late Types

Because spiral galaxies are dominated by their disk components, whose photometric and kinematic properties are relatively straightforward to measure, past studies of their angular momenta have generally treated them as pure disks, e.g., using Equation (2) to calculate j_t. However, this approximation may be inadequate for the spirals with relatively large bulges (Sa and some Sb), and it is one of the goals of this paper to consider these components.

With Equation (6) in mind, we could use values for the parameters n, a_e, and v_s that characterize the composite bulge–disk systems (e.g., with an overall n somewhat larger than 1). However, the required stellar photometry and kinematic data are not available for a large sample of galaxies. Instead, we analyze disk and bulge components separately, make some simple assumptions for the bulges to compensate for the missing data, and then combine the disks and bulges into global $j_\star$ analyses.

We focus on the classic spiral galaxy data set assembled by Kent (1986, 1987, 1988), comprising 64 galaxies from type Sa to Sm, at distances ranging from 1 to 100 Mpc. These data include r-band CCD photometry along with bulge–disk decompositions, and inclination-corrected gas-disk rotation curves from both optical emission lines (e.g., Rubin et al.

---

[5] In practice, the a_e uncertainty is correlated with an uncertainty in the galaxy luminosity and thus in $M_\star$, but this is a relatively weak effect.

1980, 1982, 1985) and H I radio emission (based on various sources in the literature). Most of Kent's sample comes from the Rubin et al. surveys, which selected for spiral galaxies with high inclinations, spanning a wide range of luminosities, scale lengths, and Hubble types, and without strong bars. Despite advances in observational resources in the intervening decades, we know of no comparable, publicly available sample that includes both rotation curves and photometry with detailed bulge–disk decompositions for a wide range of disk galaxy types.

We estimate the disk and bulge scale lengths (R_d and $a_{e,b}$) by modeling the non-parametric Kent decompositions with simple exponential and de Vaucouleurs profiles ($n = 1$ and $n = 4$, respectively). Our models thereby treat all bulges as "classical," with $n \sim 4$, neglecting some variations in their detailed properties, such as the $n \sim 1$–2 indices of "pseudo" bulges (Kormendy & Kennicutt 2004). The latter bulges tend to be much less massive, and make only minor contributions to the total $j_\star$ for spirals, which is insensitive to the details of the adopted bulge density and rotation profiles.[6]

For 34 of these sample galaxies (type Sb to Sc), independent decompositions were carried out on the *same data set* by Andredakis & Sanders (1994), using parametric fits to the raw surface brightness profiles. Our R_d values agree with theirs at the $\sim 10\%$ level, while the bulge results are highly variable, both between our analyses and theirs, and between different model fits by these authors. Most of these galaxies are very disk dominated ($B/T \lesssim 0.1$), so it is not surprising that the bulge parameters would be very uncertain. Fortunately the bulges in such cases turn out to be only very minor contributors to the total $j_\star$ of their host galaxies. Other parameters and their sources are listed in Table 4.

For v_s of the stellar disk components of these galaxies, we assume that they rotate with the same velocities as their gas disks. We derive v_c based on the rotation curves over the range (2–3) R_d, re-projecting this intrinsic value to the observed v_s according to the inclination ($v_s = v_c \sin i$).

The final and most challenging parameter to estimate is the characteristic rotation velocity v_s for the bulges. Direct estimates of bulge rotation-velocity profiles over a large range in radius require extensive spectroscopic data combined with careful bulge–disk kinematic decomposition. As far as we know, this has only been done for *one* spiral galaxy to date (Dorman et al. 2012). Thus we are much worse off with estimating $j_\star$ for spiral bulges than for early-type galaxies, and must make even stronger simplifying assumptions than in the original F83 analysis of ellipticals. Fortunately, because the spirals are disk dominated, we will find that their total $j_\star$ estimates are only mildly sensitive to the assumptions about bulge kinematics.

Our strategy for the bulge v_s values is to estimate these indirectly, based on other observables: the ellipticity $\epsilon \equiv 1 - q$ and the central velocity dispersion σ_0. These three parameters may be related together through the following model:

$$v_s = \left(\frac{v}{\sigma}\right)^* \sigma_0 \left(\frac{\epsilon}{1-\epsilon}\right)^{1/2}, \qquad (8)$$

where $(v/\sigma)^*$ is a parameter describing the relative dynamical importance of rotation and pressure. In an edge-on galaxy, $(v/\sigma)^* \simeq 1$ represents an oblate isotropic system where the
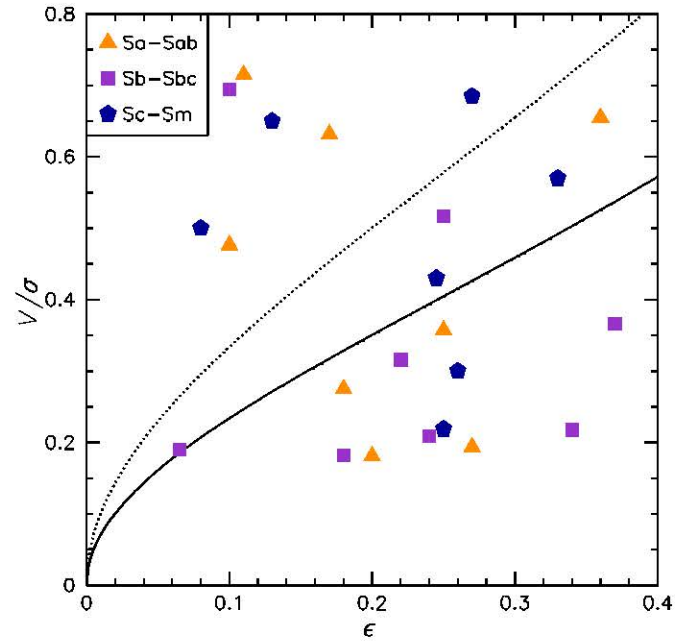
Figure 10. Relation between bulge rotation velocity and velocity dispersion as a function of ellipticity. The points show data for 26 spiral galaxies from the literature, with symbol shapes and colors corresponding to different Hubble types as in the legend. The curves show Equation (8) with $(v/\sigma)^* = 1$ and $(v/\sigma)^* = 0.7$ for the dotted and solid curves, respectively. We adopt $(v/\sigma)^* = 0.7$ as our default model.

(A color version of this figure is available in the online journal.)

observed ellipticity is supported by rotation, and this model also turns out to work well at other inclinations (Kormendy 1982).

The standard lore is that spiral bulges and low-luminosity ellipticals are near oblate isotropic, with typical $(v/\sigma)^* \sim 0.9$ (Kormendy & Illingworth 1982; Davies et al. 1983; Binney & Merrifield 1998; Binney & Tremaine 2008). However, some concerns about these conclusions were raised early on (Whitmore et al. 1984; Fillmore et al. 1986) and modern integral-field analysis of early types has revealed that their rotation velocities tend to be significantly *lower* than in the oblate isotropic model (Cappellari et al. 2007; Emsellem et al. 2011). The rotation of spiral bulges, on the other hand, has not seen systematic investigation in decades (some new work has just appeared in Fabricius et al. 2012), and here we attempt only a quick look at the implications of recent papers that have reported bulge kinematics for a handful of cases.

We take results on (v/σ) and ϵ from Laurikainen et al. (2007), Morelli et al. (2008), and MacArthur et al. (2009), and plot them in Figure 10. We see that the oblate isotropic model is *not* a good representation of most of the data, nor is any other simple value of $(v/\sigma)^*$. However, in order to have a simplified framework for bulge rotation, we characterize this data set as having $(v/\sigma)^* = 0.7 \pm 0.4$ (median and 68% scatter).

We therefore adopt the following procedure for estimating bulge $j_\star$. We use the observational values for ϵ and σ_0, and then estimate v_s using Equation (8) with $(v/\sigma)^* = 0.7$ representing a typical value for bulges. We test the impact of the latter assumption on the results by also using $(v/\sigma)^* = 0.3$ and 1.1 to bracket the possible range of average bulge rotation. We thereby explore the systematic uncertainty in bulge rotation but not the intrinsic scatter, keeping in mind also that this bulge model is based on the central regions and does not account for the uncertainties in extrapolating the rotation to large radii, as discussed in detail for the early-type galaxies.

---

[6] More extensive observations and modeling in the future could be used to establish the $j_\star$–$M_\star$ trends for morphologically different bulges, and thereby provide physically based information as to whether or not there are genuinely distinct sub-types.

The ϵ values are taken from the Kent derivations. We take the σ_0 measurements in most cases from HyperLeda (Paturel et al. 2003), and also from Corsini et al. (1999) and Pizzella et al. (2004). For some of the later-type galaxies, there are no σ_0 measurements available, and for these we use an empirical relation (which we infer from other galaxies in these studies) that σ_0 is approximately equal to the gas-disk rotation velocity. Such cases all have $B/T < 0.15$, so this approximation is not of major importance for the total $j_\star$ estimates, but any inferences for these particular bulges will be relatively uncertain.

We now have enough information to proceed with the specific angular momentum calculations for the spiral galaxies. Again, our basic approach is to estimate separately the bulge and disk angular momenta j_b and j_d. Given a bulge stellar mass fraction quantified as f_b, we can then estimate the total specific angular momentum by

$$j = f_b j_b + (1 - f_b) j_d. \tag{9}$$

In practice, we use the bulge-to-total r-band luminosity ratio B/T (from the series of Kent papers) as a proxy for f_b. Note that by neglecting variations in the stellar mass-to-light ratio $\Upsilon_\star$ (e.g., Yoshino & Ichikawa 2008), this approach may systematically underweight the contributions of the bulges (since they are thought to have higher $\Upsilon_\star$ than the disks).

To calculate the projected values of j_b and j_d, we use Equation (6). For the intrinsic values, we assume that both the bulge and the disk in a given galaxy have the same inclination i, which is estimated from the observed disk ellipticity. We then use the deprojection factor C_i to convert projected to intrinsic values (see Equation (4)). For the disk, this is a simple factor of $(\sin i)^{-1}$, and the calculation reduces to Equation (2). For the bulge, we calculate C_i from Equation (A29).

Using these procedures, we construct a catalog of spiral galaxies with characteristic masses, scale lengths, and rotation velocities for both their bulge and disk components. We report these values in Table 4, along with the total galactic specific angular momenta (bulge and disk combined), both projected and intrinsic. When we vary the assumed bulge rotation systematically across the bracketing range, the total $j_\star$ is changed by no more than ~0.03 dex (~7%) for the vast majority of the galaxies, and up to ~0.1 dex (~25%) for a few of the Sa–Sab galaxies. Therefore, the details of the bulge modeling are of only very mild importance to the overall $j_\star$ results for the spirals. These data will be used in later sections to examine various scaling relations for these galaxies and for their subcomponents.

4.2. Early Types

For the gas-poor early-type galaxies (lenticulars and ellipticals), the challenge is to assemble a large sample with all of the ingredients that we need to calculate $j_\star$ (i.e., v_s, a_e, n). The information is scarcest for v_s, and therefore we have scoured the literature for kinematic data sets extending to radii of at least ~$2a_e$, assembling a sample that, although not exhaustive, is unprecedented in its size and scope. The sources include integrated-starlight absorption-line spectroscopy, and velocities of GCs and PNe. To estimate approximate values for v_s, we simply read off the major-axis rotation velocity at $2a_e$ (as explained in Section 3.3). We thereby assemble a total sample of 40 early-type galaxies, including the eight galaxies that we modeled in detail in Section 3.

Table 5 provides a summary of our sample, along with the sources of kinematic data. Given that the data are drawn from a variety of literature sources with complex selection effects, it is important to check whether or not the sample is a fair representation of early types in the nearby universe. We have done so in Appendix C, using the ATLAS^{3D} volume-limited sample of nearby galaxies as a reference, and focusing on the masses $M_\star$ and central rotation parameters $(v/\sigma)^*$.

We find that the distribution of our sample galaxies in the $(v/\sigma)^*$–$M_\star$ parameter space is fairly similar to that of an unbiased sample over a similar mass range. The median galaxy mass in our sample is $\log(M_\star/M_\odot) = 10.8$, which is near the characteristic mass $M_\star^*$ of nearby galaxies (Guo et al. 2010). We thus conclude that our observational results should be representative of low-redshift ordinary early-type galaxies. The only caveat here is that our sample is biased toward ellipticals at the expense of lenticulars, which we must take into account later when drawing conclusions about the overall population of early-type galaxies.

An alternative scheme for classifying early types is as "fast rotators" (including almost all lenticulars) and "slow rotators," based on their central kinematics (Emsellem et al. 2007). The central rotation is known to correlate with many other galaxy properties (Davies et al. 1983; Kormendy & Bender 1996), and the fast and slow rotators have been interpreted as having different formation histories. Therefore, it is important that we investigate to what extent the *global* specific angular momentum $j_\star$ correlates with the central rotation classification. Our sample includes three slow rotators, which is consistent with the fraction of such galaxies in the nearby universe (Emsellem et al. 2011), and will provide a rough initial idea of any systematic differences between fast and slow rotators.

Returning to the remaining observational parameters, for each early-type density profile, we need both the Sérsic index n and the corresponding scale length a_e (which can differ significantly from the value obtained with a classic $n = 4$ fit, e.g., in the RC3 catalog of de Vaucouleurs et al. 1991). Unfortunately, there is no comprehensive source available for such measurements, and we resort to a medley of literature data.

For 34 of the galaxies in our sample, there are published Sérsic fits, and we take the (a_e, n) values according to the following priority: detailed photometric analysis in individual galaxy papers (e.g., Napolitano et al. 2009), the Kormendy et al. (2009) tabulation for Virgo galaxies, Hopkins et al. (2009a, 2009b), and D'Onofrio (2001).

For the remaining six galaxies, we have as a starting point the RC3 value for the effective radius. Then we use the well-established observation that there are strong correlations between early-type galaxy size and luminosity, and the Sérsic index n (e.g., Caon et al. 1993; Prugniel & Simien 1997; Graham & Guzmán 2003; Blanton et al. 2003; Kormendy et al. 2009). This allows us to estimate a most-probable n value for each galaxy (see Appendix C for details).

Note that if we were simply to approximate all of the early types as $n = 4$ spheroids, the k_n values in Equation (6) would be too high on average by ~30% (~0.15 dex, given a median index value of $n \sim 2.5$). This would translate to an equivalent systematic error on $j_\star$. We could adjust for this effect by adopting $n = 2.5$ in all cases, but n also has a systematic dependence on galaxy mass, and ignoring this fact would produce a spurious mass-dependent trend in $j_\star$ of ~50% (~0.2 dex) over the full range in mass.

In Table 5, we compile the observed parameters v_s, a_e, and n for our full early-type galaxy sample. We use these to calculate j_p approximately from Equation (6), and tabulate these values

Table 1
Uncertainty Budget

Galaxy Type	D	C_i	v_s	$\tilde{v}_s$	n, a_e	Bulge	$\Upsilon_\star$	Total
				$\Delta\lambda$ (dex)				
Sb–Sm	0.01	0.01	0.02	0.03	0.05	0.03	0.5	0.5
Sa–Sab	0.01	0.01	0.02	0.03	0.05	0.1	0.4	0.4
S0	0.01	0.05	0.06	0.1	0.15	0	0.25	0.3
fE	0.01	0.15	0.06	0.1	0.15	0	0.2	0.3
sE	0.01	0.12	0.35	0.35	0.2	0	0.4	0.5

Notes. The uncertainties on $j_\star$ and $M_\star$ have been converted into equivalent uncertainties on λ. The different galaxy types include fast- and slow-rotating ellipticals (fE and sE). The listed sources of potential error are distance (D), corrections for projection effects including inclination (C_i), the rotation velocity scale calculated in detail (v_s), the alternative approximate rotation velocity scale ($\tilde{v}_s$), the stellar density profile Sérsic index (n) and scale radius (a_e), the incorporation of bulge contributions, and the stellar mass-to-light ratio ($\Upsilon_\star$). For the latter, the error budget includes uncertainties in stellar population models, including potential IMF variations. The error bars in this case are asymmetric, in the sense that the λ values are most likely to be underestimated.

as well. For some of the very extended galaxies like NGC 4374, the total luminosity and angular momentum (via the factor k_n) are integrated out only to the estimated virial radius.

In order to convert projected j_p to intrinsic j_t for analysis in later sections, we must apply a deprojection factor C_i which depends on the inclination i. Unfortunately, the individual inclinations are not generally known, but neither are they completely random, because of an inclination bias in galaxy classification. As discussed in Appendix A.3, we therefore apply median deprojection factors of $C_{med} = 1.21$ (+0.08 dex) to the lenticulars, and $C_{med} = 1.65$ (+0.22 dex) to the ellipticals.

Since one of our eventual goals will be to quantify the intrinsic scatter in the observed $j_\star$–$M_\star$ relations, it is important to be clear about the error budget in our analyses. Again, the basic parameters that go into our $j_\star$ calculations are C_i, a_e, n, and v_s. For early-type galaxies with an assumed $n = 4$ profile, the typical uncertainties in a_e are $\sim$25% ($\sim$0.1 dex; Cappellari et al. 2011a). If we allow for a more general n, which for some galaxies is measured directly and in other cases is derived statistically (Appendix C), then we estimate a combined uncertainty on $j_\star$ from a_e and n of $\sim$40% ($\sim$0.15 dex). The uncertainty on v_s from our simplified measurement and extrapolation approach is $\sim$25% ($\sim$0.1 dex; Section 3.3).

Table 1 summarizes the uncertainties introduced by a number of different ingredients in the $j_\star$–$M_\star$ calculations. The separate uncertainties for $j_\star$ and $M_\star$ are mapped to the direction perpendicular to a $j_\star \propto M_\star^{2/3}$ trend, as discussed in Section 3.5. This net uncertainty is designated $\Delta\lambda$, owing to the connection with spin-based theoretical models.

The total uncertainty in λ for all types of galaxies is dominated by the estimate of $M_\star$ (via $\Upsilon_\star$) rather than of $j_\star$. As discussed in Section 3.4, one could in principle refine the $\Upsilon_\star$ estimates using stellar population models. This would decrease $M_\star$ for the latest-type spirals by a factor of $\sim$3 but leave $M_\star$ for ellipticals nearly the same. In this case, the systematic uncertainties in $\Upsilon_\star$ would likely still dominate the error budget in λ, particularly for the late-type galaxies.

This full $j_\star$–$M_\star$ data set is assembled from a generally unbiased $\sim M_\star^*$ galaxy sample that we can use to investigate differences in angular momentum not only between early types and spirals, but also between ellipticals and lenticulars, and between fast and slow rotators.
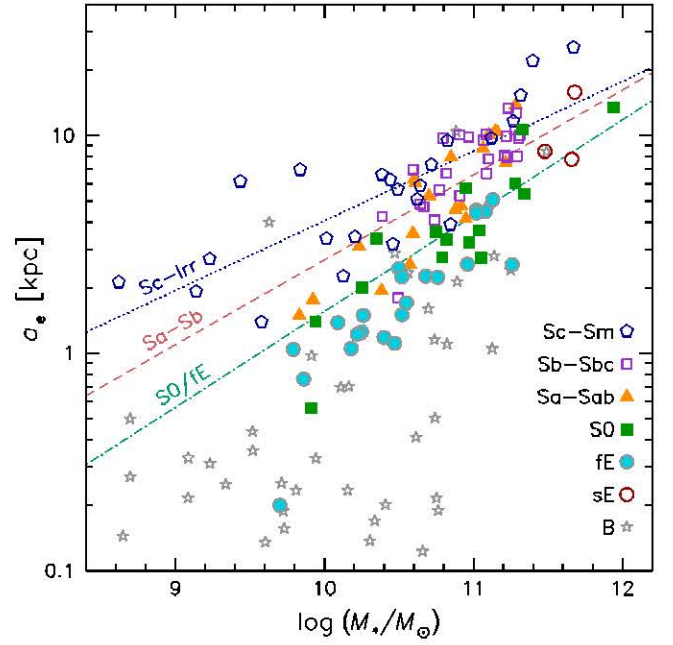
Figure 11. Relation between size and stellar mass for our galaxy sample. The former is the semimajor-axis effective radius, and the latter is based on K-band total luminosities with an adopted mass-to-light ratio of $\Upsilon_{\star,K} = 1$ in solar units. Different symbols denote different galaxy types as shown in the legend; for the spirals, the disk and bulge ("B") components are shown separately. The range of the plot is restricted in order to better see the main trends in the data; the bulge data extend to radii as small as $a_e \sim 0.01$ kpc (note also that the most compact elliptical shown is NGC 4486B, which is considered a rare, highly stripped galaxy). For comparison, diagonal lines show power-law model fits to the data from the ATLAS^{3D} survey (i.e., *independent* from our data set): lenticulars and fast-rotator ellipticals (dot-dashed), Sa–Sb spirals (dashed), and Sc–Irr spirals (dotted). For both data sets, the late-type galaxies are systematically larger than the early types at a given stellar mass. The absolute normalizations of the trends are similar between the ATLAS^{3D} sample and ours, with some small differences as discussed in the text.

(A color version of this figure is available in the online journal.)

4.3. Size and Rotation-velocity Scaling Relations

Before considering specific angular momenta and their correlations in the next section, we examine some trends among the raw ingredients that go into these analyses, a_e, v_s, and $M_\star$. Doing so provides a check that our results are consistent with the familiar size–mass and mass–rotation-velocity (Tully–Fisher) relations that have been established for nearby galaxies. We also introduce novel relations involving rotation, and explore some preliminary indications about angular momentum.

We first consider the standard scaling relation of galaxy size versus mass, or a_e versus $M_\star$ in our notation, showing the results in Figure 11, where we again compare our results to the volume-limited ATLAS^{3D} sample as a baseline check. We find that in both samples, late- and early-type galaxies have *roughly* the same sizes at a given mass (cf. Shen et al. 2003, 2007), but there is a clear systematic trend for the more bulge-dominated galaxies to be more compact (see also de Jong et al. 2004; Gadotti 2009; Maltby et al. 2010; McDonald et al. 2011; Dutton et al. 2011). Given the many different assumptions and data sources that went into our sizes and masses, these parameters match the ATLAS^{3D} results remarkably well overall (with some nuances discussed further in Appendix C). This suggests that our size and mass data are representative and reliable at the $\sim$0.1 dex level.

We can also consider separately the spiral *bulges*, plotting their sizes and masses for our sample in Figure 11. Although
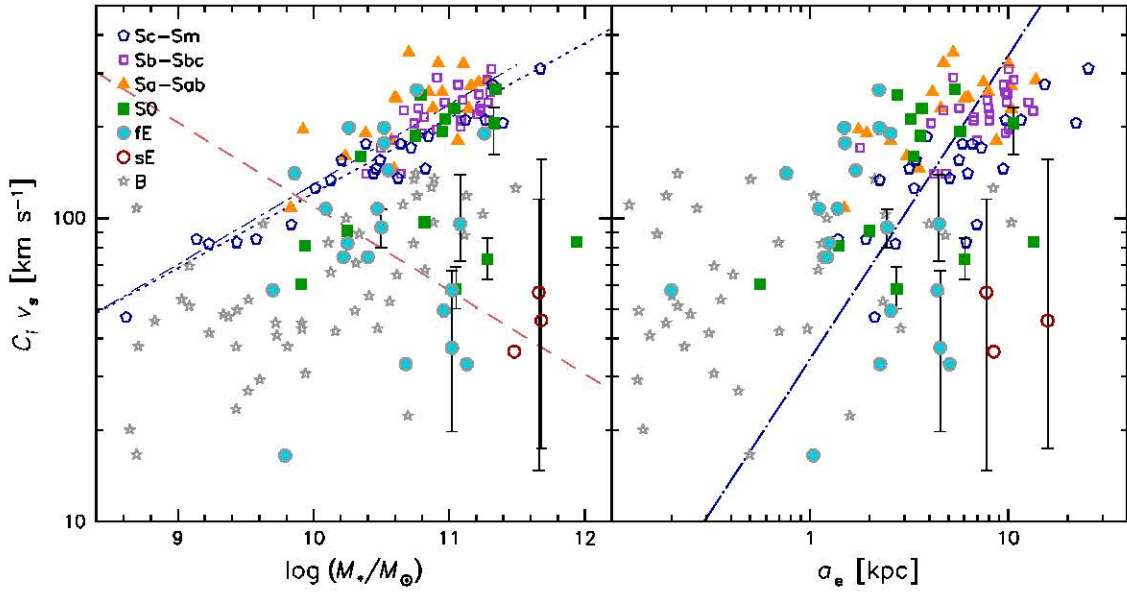
Figure 12. Relations between characteristic rotation velocity $C_i v_s$, stellar mass (left-hand panel) and size (right-hand panel) for our full galaxy sample, using the same data sources and symbols as in Figure 11. For the spiral disks, v_s is the outer gas-disk rotation velocity. For the lenticulars and ellipticals, v_s is the stellar rotation velocity measured along the semimajor axis at $2a_e$, except for the points with error bars, which are the eight cases studied in detail in Section 3, with v_s derived from full modeling of the rotation-velocity profiles. For the bulges, v_s is estimated indirectly using flattening and velocity dispersion observations (Section 4.1). In all cases, the rotation velocity has been deprojected for both inclination and "dilution" effects, using the factor C_i (see the text for details). In the left-hand panel, the dotted blue line shows a least-squares fit to the Sb–Sc disks, a dashed red line shows a proposed inverse trend for a subset of the E/S0s, and the blue dot-dashed line shows the baryonic Tully–Fisher relation for late-type galaxies from Trujillo-Gomez et al. (2011) for comparison. In the right-hand panel, the diagonal line shows a prediction for the spiral disks based on ΛCDM models (see Section 6.2). Overall, the spiral and elliptical galaxies follow mass–rotation-velocity and size–rotation-velocity trends that have remarkably opposite slopes. The trends for the lenticulars are between the spirals and ellipticals.

(A color version of this figure is available in the online journal.)

the full range of sizes is not visible in this plot, the bulges follow a roughly parallel size–mass relation to the elliptical galaxies, but smaller on average by a factor of $\sim$4 ($\sim$0.6 dex) and with a great deal of scatter (possibly because of the approximate nature of these size measurements). Other studies have also found that bulges are more compact than ellipticals (Graham & Worley 2008; Gadotti 2009; Laurikainen et al. 2010; Dutton et al. 2011), but the quantitative details vary considerably, and we therefore regard our bulge scaling relations as provisional.

The next scaling relation that we consider is rotation velocity versus mass. For spiral galaxies, this is the Tully–Fisher relation, but it has to our knowledge never been constructed previously for all galaxy types. We can already generate a broad expectation for what we will find, given the observed size–mass relations along with the assumption that $j_\star$ is independent of galaxy type. As mentioned in Section 2, we can then use Equation (6) to predict the ratio of characteristic rotation velocities for ellipticals and spirals:

$$\frac{v_{s,E}}{v_{s,Sp}} \sim \frac{k_1}{k_4} \frac{a_{e,Sp}}{a_{e,E}}, \qquad (10)$$

where we are approximating the spiral galaxy parameters as dominated by the disk component. With $k_1/k_4 = 0.5$, and $a_{e,Sp}/a_{e,E} \sim 2$ for our sample, we therefore predict $v_{s,E}/v_{s,Sp} \sim$ 1. Thus, *ellipticals should rotate at roughly the same velocity as spirals if they have the same specific angular momenta at a given mass.*

Without proceeding any further, this scaling analysis already suggests that ellipticals have lower $j_\star$ than spirals, or else they would be extremely flattened by rotation, similarly to the spiral disks which have near-maximal rotational support (modulo possible differences in dynamical mass between spiral and elliptical galaxies at the same stellar mass). The same argument

applies even more strongly to the spiral bulges, since they are far more compact than the disks at a given mass. If the bulges had the same $j_\star$ as the disks, then they would have to rotate much *faster*, which is impossible. Note also that these conclusions would be further strengthened if systematic variations in the stellar mass-to-light ratio $\Upsilon_\star$ were included (Section 3.4).

We now examine what our new collection of observations tells us directly about the rotation scaling relations. The left-hand panel of Figure 12 shows the characteristic rotation velocity v_s for the elliptical and lenticular galaxies, and the spiral disk and bulge subcomponents, in our sample. Here we are plotting the *intrinsic* rotation velocity, multiplying by the deprojection factor C_i, which is just $(\sin i)^{-1}$ for disks (see Appendix A.2), and Equation (A29) for bulges. For the early-type galaxies, the inclinations are unknown, and we have adopted median factors for C_i as discussed in Section 4.2.

We see that the disks follow a fairly tight relation of approximately $C_i v_s \propto M_\star^{0.25}$, with a residual trend for the later-type disks to rotate more slowly. This is equivalent to the familiar Tully–Fisher relation, and in the figure we include a recent result from the literature (Trujillo-Gomez et al. 2011), which matches our data very well (cf. the type dependence among spirals found by Masters et al. 2008). We also show in the right-hand panel of Figure 12 the relation between size and rotation velocity, which are strongly correlated parameters for disk galaxies.

The elliptical galaxies are completely different, showing an *anti-correlation* between rotation velocity and mass,[7] with $C_i v_s \propto M_\star^{-0.1}$. This result also contrasts markedly with standard

---

[7] This echoes a similar trend in the *central* rotation properties of early-type galaxies in general (shown in Figure 33). The eight galaxies studied in detail (points with error bars in Figure 12) are consistent with this trend but do not include enough lower-luminosity ellipticals to distinguish between v_s being constant or decreasing with mass.

relations for ellipticals involving the velocity dispersion σ_0 or the dynamical mass (e.g., $\sigma_0 \propto M_\star^{0.25}$; Faber & Jackson 1976; Trujillo-Gomez et al. 2011). In galaxy disks, the rotation velocity traces the dynamical mass, so the Tully–Fisher relation is a measure of both mass and angular momentum. In elliptical galaxies, on the other hand, the mass and angular momentum relations are decoupled. We also find an anti-correlation between rotation velocity and size (right-hand panel) that we will discuss later in this paper.

The behavior of the lenticulars in the mass–rotation-velocity diagram is difficult to discern in detail owing to the small sample size, but in general it appears intermediate to the other galaxy types. We also note an interesting pattern when considering the lenticulars and ellipticals together: there may be a *bimodal* mass–rotation-velocity relation,[8] with some galaxies following the trend for spirals, and others following a steep reverse relation, $C_i \, v_s \propto M_\star^{-0.3}$. The implication is that there may be two distinct populations of early-type galaxies, one of which is closely related to spirals, and which are not equivalent to standard E and S0 classifications.

The bulge rotation velocities appear to follow a similar trend to the spirals, at about half the amplitude. Here it should be remembered that the bulge "data" points are *indirect* estimates constructed in order to provide plausible adjustments to the total angular momenta of the spiral galaxies (Section 4.1). The results so far suggest that bulges are different from ellipticals in their mass–size–rotation-velocity relations, and we will see in the next section how their angular momenta compare.

Since both the sizes and the rotation velocities of elliptical galaxies are systematically lower than for spiral disks, we can already predict that the ellipticals will on average have much lower $j_\star$. Note that although this conclusion has already been widely adopted for decades, only now have the kinematic data reached large enough radii to confirm it with confidence.

To see that the low characteristic rotation velocities for ellipticals are not a mathematical sleight of hand, one may consider the specific cases of NGC 821 and NGC 3377 in Figure 6. The rotation-velocity profiles of these galaxies decline dramatically outside $x \sim (1–2) \, a_e$, which may be contrasted with the spiral galaxies in Figure 4. Preliminary analysis of additional *edge-on* cases, where the deprojection uncertainties are minimized, indicates that such declines are a *generic feature* of $\sim M_\star^*$ early-type galaxies (A. Romanowsky et al., in preparation).

This conclusion includes NGC 2768, which from the current data appears consistent with a constant or rising outer rotation velocity, but which with more extensive new PN data may have a declining outer profile. Even the cases of strongly rising rotation-velocity profiles out to $x \sim 2a_e$ found by Rix et al. (1999) appear upon closer inspection to turn over at larger radii. These results all contrast with early claims of high outer rotation in some early types, which were recently overturned with improved observations (e.g., Arnaboldi et al. 1994; Kissler-Patig & Gebhardt 1998; Romanowsky 2006; McNeil et al. 2010; Strader et al. 2011).

We can also begin making some interesting inferences about the relations among other galaxy types, based on both size and rotation-velocity trends (Figures 11 and 12). As discussed, the lenticulars share similar properties to spirals in some cases, and to ellipticals in others. The distinction between "fast" and "slow" rotator ellipticals based on their inner regions does not appear to hold up when considering their global rotation properties.

This overview of the observable scaling relations between mass, size, and rotation velocity gives us a preview of some of our overall conclusions about angular momentum, and provides more confidence in the solidity of those conclusions. We have constructed a novel mass–rotation-velocity relation for ellipticals, which is the analog of the Tully–Fisher relation for spirals, but with the remarkable difference of having a negative slope. The data also imply that both elliptical galaxies and spiral bulges must have lower specific angular momenta than spiral disks of the same mass. We address this issue more quantitatively in the next section, incorporating the additional mass-dependent factor k_n in calculating $j_\star$.

5. OBSERVATIONS: ANGULAR MOMENTA OF THE FULL SAMPLE

Having derived estimates of the $j_\star$ and $M_\star$ parameters for our full galaxy sample, we now examine the resulting observational trends, which constitute the key results of this paper. We begin by focusing on the late-type galaxies in Section 5.1, and combine these with the early types in Section 5.2. We discuss our proposed replacement for the Hubble sequence in Section 5.3, which we test by examining systematic residuals from the $j_\star$–$M_\star$ trends in Section 5.4. We further convert the $j_\star$–$M_\star$ data into one-dimensional histograms in Section 5.5.

5.1. Lessons from Spirals

Although the main novelty of this paper is our careful consideration of early-type galaxies, we also include the oft-studied category of spirals in order to provide an integrated analysis of bright galaxies of all types. Furthermore, the well-constrained angular momenta of the spirals also permit us to better understand systematic issues such as inclination corrections that are trickier to handle for early types.

We plot the total (disk+bulge) $j_\star$–$M_\star$ data for the spirals from Table 4 in Figure 13. In the top panel, we show the projected value, j_p, and in the bottom panel, the intrinsic value, j_t. These are related trivially by the disk inclination, but we wish to investigate how well the trends in projection reflect the intrinsic trends, since deprojection for the early-type galaxies will be more difficult.

Overall, the spiral galaxies appear to follow fairly tight $j_\star$–$M_\star$ trends, with similar slopes, regardless of Hubble sub-type. In more detail, we carry out least-squares fits to $j_\star$ as a function of $M_\star$ in log–log space:

$$\log j_{mod} = \log j_0 + \alpha [\log(M_\star/M_\odot) - 11], \qquad (11)$$

with a residual rms scatter that we parameterize as $\sigma_{\log j_\star}$. The uncertainties in the fit parameters j_0 and α are estimated by bootstrap resampling.

Our fitting results for various spiral subsamples are reported in Table 2. For total $j_\star$, the systematic uncertainties from the bulge rotation (see Section 4.1) turn out to be smaller than or equal to the statistical fitting uncertainties, even for the Sa–Sab galaxies, and in the table we have combined both uncertainties in quadrature.

---

[8] This pattern may be partially an artifact of inclination effects. In particular, some of the edge-on lenticulars were observed with long-slit spectroscopy directly along their embedded disks, which may not provide an accurate measurement of the overall rotation. However, for the ellipticals we find no correlation between apparent rotation velocity and ellipticity. An additional issue is that the occasional extremely low-inclination galaxy will not be treated well by our median-deprojection method (cf. the right-hand panel of Figure 24), so in any fits to the data, we will discard outliers with very low v_s or $j_\star$ (e.g., NGC 1419).

Figure 13. Total (disk plus bulge) stellar specific angular momentum of nearby spiral galaxies plotted against total stellar mass. The top and bottom panels show estimates of projected and intrinsic $j_\star$, respectively; the uncertainty in $j_\star$ for each galaxy is in almost all cases smaller than the plotted symbols. Different symbols denote galaxy sub-types as specified in the legends. The dotted lines show fits to the data in each panel, while the dashed lines show fits to the disk components alone (data not shown). The spiral galaxies follow a universal $j_\star$–$M_\star$ relation, with some dependence on Hubble type. The projected relation is very similar to the intrinsic relation, but with a small offset, and slightly increased scatter, in $j_\star$.

(A color version of this figure is available in the online journal.)

The data are basically consistent with a universal $j_\star$–$M_\star$ slope for spiral galaxies of all types, with $\alpha \sim 0.6$ and an rms scatter of $\sigma_{\log j} \sim 0.2$ dex. There is also a clear residual trend with Hubble type: the Sb–Sm galaxies have systematically higher $j_\star$ than the Sa–Sab galaxies at the same $M_\star$—an effect that would be stronger if variations in the stellar mass-to-light ratio $\Upsilon_\star$ were included. These conclusions hold for both j_p and j_t, although the uncertainties and the scatter are smaller for j_t, as expected if there are genuine, underlying physical correlations that become clearer after deprojection.

Table 2
Fits to Mass and Angular Momentum Data

Sample	$\log j_0$	α	$\sigma_{\log j_\star}$
All spirals, total, projected	3.11 ± 0.03	0.53 ± 0.05	0.22
All spirals, total, intrinsic	3.18 ± 0.03	0.52 ± 0.04	0.19
Sa–Sab, total, projected	2.93 ± 0.05	0.60 ± 0.06	0.17
Sa–Sab, total, intrinsic	3.02 ± 0.04	0.64 ± 0.07	0.12
Sb–Sbc, total, projected	3.15 ± 0.03	0.65 ± 0.14	0.16
Sb–Sbc, total, intrinsic	3.21 ± 0.03	0.68 ± 0.13	0.15
Sc–Sm, total, projected	3.25 ± 0.04	0.58 ± 0.06	0.20
Sc–Sm, total, intrinsic	3.29 ± 0.04	0.55 ± 0.05	0.18
All spirals, disks, projected	3.25 ± 0.02	0.62 ± 0.05	0.20
All spirals, disks, intrinsic	3.31 ± 0.02	0.61 ± 0.04	0.17
Sa–Sab, disks, projected	3.25 ± 0.05	0.76 ± 0.09	0.21
Sa–Sab, disks, intrinsic	3.34 ± 0.04	0.82 ± 0.08	0.17
Sb–Sbc, disks, projected	3.24 ± 0.03	0.71 ± 0.14	0.16
Sb–Sbc, disks, intrinsic	3.30 ± 0.03	0.75 ± 0.12	0.13
Sc–Sm, disks, projected	3.29 ± 0.05	0.61 ± 0.07	0.21
Sc–Sm, disks, intrinsic	3.33 ± 0.05	0.57 ± 0.05	0.19
All spirals, bulges, projected	2.20 ± 0.31	0.69 ± 0.11	0.58
All spirals, bulges, intrinsic	2.32 ± 0.31	0.69 ± 0.10	0.57
Sa–Sab, bulges, projected	2.30 ± 0.32	0.99 ± 0.15	0.47
Sa–Sab, bulges, intrinsic	2.44 ± 0.32	0.99 ± 0.15	0.46
Sb–Sbc, bulges, projected	1.89 ± 0.34	0.34 ± 0.20	0.58
Sb–Sbc, bulges, intrinsic	2.01 ± 0.33	0.34 ± 0.19	0.56
Sc–Sm, bulges, projected	2.21 ± 0.57	0.64 ± 0.27	0.60
Sc–Sm, bulges, intrinsic	2.30 ± 0.58	0.63 ± 0.28	0.60
Lenticulars, projected	2.97 ± 0.08	0.80 ± 0.14	0.29
Lenticulars, intrinsic	3.05 ± 0.08	0.80 ± 0.14	0.29
Ellipticals, projected	2.52 ± 0.05	0.60 ± 0.09	0.24
Ellipticals, intrinsic	2.73 ± 0.05	0.60 ± 0.09	0.24
Sb–Sm, intrinsic, fixed $\alpha = 2/3$	3.28 ± 0.03	0.67	0.19
Ellipticals, intrinsic, fixed $\alpha = 2/3$	2.75 ± 0.05	0.67	0.24
ΛCDM halos	*2.50*	*0.67*	*0.23*

The multi-component nature of our model galaxies allows us to look further at disk and bulge properties separately. We will take up this issue in Section 5.2, and for now provide the fits to the j_d–M_d and j_b–M_b relations in Table 2. It should be remembered that the bulge results depend on model assumptions, although as discussed, we have plausibly bracketed their upper and lower limits for $j_\star$.

As anticipated, the bulges turn out to have little impact on the total $j_\star$ trends for the Sb–Sm galaxies, which are dominated by the disk components. For the Sa–Sab galaxies, the bulges are responsible for the systematic offset with respect to the later types; this offset changes slightly but persists when adopting the upper or lower limits to the bulge rotation. The *disks* of all the galaxy types turn out to follow nearly the same $j_\star$–$M_\star$ relations.

This analysis demonstrates that inclination effects are not expected to have a major impact on our overall results, since for both disks and bulges, the intrinsic and projected $j_\star$–$M_\star$ trends as well as their scatter are very similar. There is an overall offset between disk j_t and j_p of $\sim$0.07 dex, which is comparable to the range of 0.04–0.06 dex that we would expect, given the median inclination $i = 67°$ of our sample, and depending on whether the $j_\star$–$M_\star$ trend represents a median or an average fit (see Appendix A.2 for further discussion).

For our ensuing study of early-type galaxies, we will therefore simply adopt median deprojection values for all of the galaxies, which we estimated in Section 4.2 to mean adding offsets of 0.08 dex and 0.22 dex to j_p to derive j_t, for lenticulars and ellipticals, respectively. We can also in general drop the usage
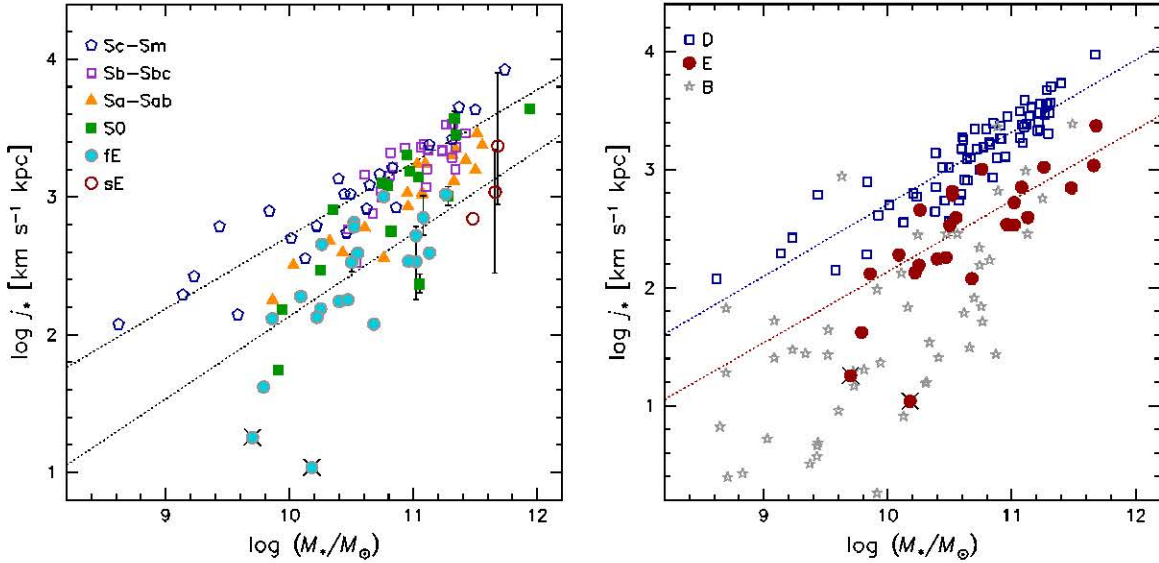
Figure 14. Left-hand panel: the total intrinsic specific angular momentum of galaxies plotted against their total stellar mass. Symbols show galaxy types according to the legend at the upper left. The points with error bars shown are based on the more detailed $j_\star$ estimator (Equation (3)); for the remainder of the galaxies, the approximate $j_\star$ estimator (Equation (6)) was used. The uncertainties are similar in both cases. The deprojection from observed j_p to intrinsic j_t was accomplished using individual inclinations for the spirals, and median deprojection factors for the lenticulars and ellipticals (see the main text). The least massive early-type galaxy in the sample is the compact elliptical NGC 4486B, which is probably in the process of being tidally stripped by the giant galaxy M87; the other low-$j_\star$ outlier is NGC 1419. Both are marked with black × symbols and excluded from all fits in this paper. Dotted lines show the best fits for the Sb–Sm and elliptical galaxies: these two galaxy types follow $j_\star$–$M_\star$ trends that are parallel but separated in $j_\star$ by ∼0.5 dex. Right-hand panel: as left-hand panel, but now plotting spiral disks and bulges alone, along with elliptical galaxies, as indicated by the legend. The upper line is now the fit to the disks (for all spiral types) rather than to the whole galaxies. Note that the slopes of the lines in this panel and the left-hand one should not be compared by eye, owing to the different axis ranges. The uncertainties in $j_\star$ for the disks are typically ∼0.04 dex, and for the bulges at least ∼0.2 dex; the $M_\star$ uncertainties are systematic (see the main text). Many of the most massive spiral bulges appear to a follow a similar $j_\star$–$M_\star$ relation to the ellipticals.

(A color version of this figure is available in the online journal.)

of j_p in the rest of this paper, in favor of the more physically meaningful j_t which we now adopt as our estimate for $j_\star$.

5.2. Combined Observational Results

We are now ready to include the early-type galaxies in our analysis, and thereby address most of the key science questions raised in Section 1. As a reminder, our starting point is the $j_\star$–$M_\star$ diagram from F83 that we have reproduced in Figure 1. Do we find the same $j_\star$–$M_\star$ trends with an updated and expanded data set, and more detailed analysis? Do ellipticals still appear to have systematically low $j_\star$ relative to spirals, or do we discover large reservoirs of additional $j_\star$ at large galactocentric radii, using modern data? Do Sa and S0 galaxies fill in any "gap" between spirals and ellipticals, and can we then connect the Hubble sequence to a sequence in $j_\star$? Can we characterize all galaxies as combinations of disks and bulges that follow universal scaling relations? (The main remaining question that connects to galaxy formation theory will be pursued in the next section.)

Taking our early-type galaxy $j_\star$ and $M_\star$ estimates from Table 5 (after statistically correcting projected to intrinsic quantities; see Table 1 for an error analysis), we plot them in Figure 14 (left), along with the spiral results discussed in Section 5.1. This new figure is the centerpiece of our paper. *Focusing first on the elliptical galaxies, our basic finding is that they follow a $j_\star$–$M_\star$ trend which is roughly parallel to the spirals but with a large systematic offset to lower $j_\star$.*

We thereby confirm the conclusions of F83, finding from a new synthesis of modern photometric and kinematic data that the "missing" angular momentum in ellipticals does *not* emerge at large radii, as had been expected from some theoretical studies. As discussed in Section 4.3, the new observations tend to show outer rotation profiles that *decline* rather than rise. Even the

nearby galaxy NGC 5128 (Cen A), which is often considered to be an elliptical formed through a recent major merger, shows a relatively low $j_\star$ when compared to spirals of the same stellar mass. Whether or not these observations pose a genuine problem to major-merger explanations for forming ellipticals will require renewed theoretical analysis, but as discussed in Section 4.3, there seems to be a pattern in the literature of misdiagnoses of high outer rotation from early, sparse data—which led to premature claims of evidence for major mergers.[9]

The specific angular momentum difference between spirals and ellipticals is also apparent from a simple, direct consideration of the data in Section 4.3, where the smaller sizes and rotation velocities for ellipticals suggested that they have lower $j_\star$. As an arbitrary benchmark, we use the median $j_\star$ at the L^* characteristic luminosity, which is $\log(L_K^*/L_{K,\odot}) \sim 11$, corresponding to $\log(M_\star/M_\odot) \sim 11$. For ellipticals and Sb–Sm spirals, we find projected values of $j_p \sim 330$ km s^{-1} kpc and ∼1600 km s^{-1} kpc, respectively, and true values of $j_\star = j_t \sim 540$ km s^{-1} kpc and ∼1800 km s^{-1} kpc.

In more detail, we report fits to the $j_\star$–$M_\star$ data toward the end of Table 2. The fitted slope for the ellipticals is consistent with that for the Sb–Sm spirals, but is significantly offset to lower $j_\star$ by a factor of ∼3.4 (∼0.5 dex). These findings are consistent with F83, except that the gap has narrowed from a factor of

---

[9] Norris et al. (2012) also recently noted an emerging trend for low rotation in elliptical-galaxy halos, at odds with major-merger expectations. One possible counter-example is the S0 galaxy NGC 1316, which is generally thought to be a major-merger remnant. Based on the new PN kinematics results from McNeil-Moylan et al. (2012), we confirm the finding of Arnaboldi et al. (1998) that the $j_\star$–$M_\star$ values for this galaxy are close to the mean trend for spirals. However, we caution that our photometric parameters and $\Upsilon_\star$ value are particularly insecure for this galaxy.

$\sim$6 ($\sim$0.8 dex).[10] Note, however, that if the stellar mass-to-light ratios for the ellipticals were systematically higher than for the spirals by a factor of $\sim$3 (cf. Section 3.4), then the $j_\star$ offset would increase to a factor of $\sim$7 ($\sim$0.85 dex)—very close to the F83 conclusion.

The scatter of $\sigma_{\log j_\star} = 0.24$ dex for the ellipticals is similar to the j_p scatter for the spirals. We also note that the general trends for the ellipticals are supported by the small sample of galaxies that we modeled in detail (see points with error bars in Figure 14, left). Although one might still have concerns that large formal uncertainties in $j_\star$ remain for most of the sample after extrapolating their rotation-velocity profiles beyond 2 R_e, in order to close the $j_\star$ gap between spirals and ellipticals, the rotation velocity would have to rise rapidly by a factor of $\sim$4 outside these radii, which seems implausible (cf. Figure 6).

The parallel nature of the spiral and elliptical trends is an interesting and non-trivial result, since Figure 12 showed that the slopes of the rotation-velocity scaling relations for these galaxies have opposite signs. Some mass-dependent conspiracy of size, rotation velocity, and Sérsic index must be at work in order for the $j_\star$–$M_\star$ slopes to turn out the same.

The few "slow-rotator" ellipticals in our sample show no indication of deviating systematically from the overall $j_\star$–$M_\star$ trend for ellipticals, which disagrees with earlier findings of much lower $j_\star$ for such galaxies (Bender & Nieto 1990). Although their outer regions, like their central parts, rotate slowly relative to most of the fast rotators (Figure 12), we find that this is compensated for by their larger scale radii and Sérsic indices (keeping in mind that the results for these galaxies are the most uncertain). Thus the global $j_\star$ measurements suggest that the slow and fast rotators may have more in common than was previously suspected.

Having confirmed the basic observational findings of F83, we now move on to fresh territory, beginning with the inclusion of Sa and S0 galaxies in Figure 14 (left). F83 suggested that these would fill the gap in $j_\star$–$M_\star$ space between ellipticals and late-type spirals, which is confirmed by our sample. Both of these galaxy types are on average offset to lower $j_\star$ from the Sb–Sm spirals trend by a factor of $\sim$1.8 ($\sim$0.25 dex; we will discuss variations about the average in Section 5.4).

One natural interpretation of this new finding is that the Hubble classifications are related to an underlying physical structure, where all galaxies are composed of some combination of two basic components: a disk and a spheroid (as illustrated schematically in Figure 2 of Section 1). These components would define two distinct sequences in the $j_\star$–$M_\star$ plane, which in combination would move the total values of galaxies to intermediate regions in this plane, depending on the bulge-to-total mass ratios, B/T.

To explore this idea, we plot the $j_\star$–$M_\star$ data separately for elliptical galaxies, and for spiral disk and bulge subcomponents, in the right-hand panel of Figure 14. The disks follow a similar relation to spiral galaxies overall, since these are dominated by their disks. More remarkably, the $j_\star$–$M_\star$ trend for bulges is fairly similar to the trend for ellipticals over the mass range where they overlap.[11] This is a surprising result, because as shown in Figure 11, the bulge sizes are systematically smaller than the ellipticals, and thus their rotation velocities (Figure 12) must be higher, in an apparent conspiracy to produce roughly the same $j_\star$.

A similar analysis could in principle be carried out for the fast-rotator ellipticals, since they are widely considered to host hidden, embedded disk-like components. Do the disk and bulge subcomponents of ellipticals follow the same $j_\star$–$M_\star$ relations as those of the spirals? We have investigated this question in Appendix D using decompositions from the literature, but the results are somewhat ambiguous. Thus, although we have been able to address all of the major questions raised initially about empirical $j_\star$–$M_\star$ trends, we flag the trends for the subcomponents in ellipticals (and lenticulars) as an important aspect remaining in need of clarification.

5.3. Replacing the Hubble Diagram

The foregoing discussion brings us to the diagram that we have already introduced schematically with Figure 2, which constitutes our own, physically motivated, substitute for the classic Hubble tuning fork, and which could provide the underlying explanation for the observational trends found in Figure 14. In this scheme, all galaxies are composed of a disk and a bulge, each adhering to a distinct and parallel $j_\star$–$M_\star$ scaling relation. If the disk and bulge relations are universal (which we will further test in Section 5.4), then the location of a galaxy in $j_\star$–$M_\star$ space can immediately be used to infer its B/T value uniquely and vice versa (i.e., there is a coordinate transformation between the two parameter spaces). Elliptical galaxies would then be the cases with $B/T \sim 1$, and bulges could be thought of as mini-ellipticals.

As with the original Hubble diagram, our $j_\star$–$M_\star$ diagram provides a simple *description* of galaxies, along with the temptation to interpret it as some kind of *evolutionary sequence*. However, our diagram differs, since the parameters used are physical quantities that may in principle be conserved, and thus it is actually justified to begin using the diagram directly as a tool to motivate and test some evolutionary scenarios for galaxies. This will be the objective of Section 6.

A key feature of our diagram is that it views galaxies as fundamentally populating a space of *two parameters*, angular momentum and mass, which are nearly equivalent to the more observationally accessible properties of bulge fraction and luminosity. In this framework, galaxies *cannot* be fruitfully reduced to a one-dimensional family controlled by a single parameter (e.g., Disney et al. 2008).

Our diagram may also be contrasted with another currently fashionable way to understand galaxies: as color–magnitude sequences that are generally related to star formation histories (e.g., Baldry et al. 2004; Faber et al. 2007). These properties are loosely related to $j_\star$–$M_\star$ space if star formation generally occurs in high-$j_\star$ disks. However, our framework is less astronomical and more astrophysical in nature, and we expect it to provide novel insights to galaxy formation that are complementary to other classifications, and perhaps more fundamental.

Another recently introduced classification for galaxies is also based loosely on specific angular momentum concepts:

---

[10] Our revised Sb–Sm relation is $\sim$0.1 dex lower than in F83, partly owing to the inclusion of bulges, and partly to new estimates for disk sizes and mass-to-light ratios. Our revised ellipticals relation is $\sim$0.2 dex higher than in F83; this difference appears to arise not so much from the rotation data (the extrapolations to large radius by F83 turn out very good on average), but from a refined treatment of the total angular momentum calculation for spheroids. Our slopes of $\alpha = 0.53 \pm 0.04$ and 0.60 ± 0.09 for the Sb–Sm and elliptical galaxies are shallower than the $\alpha = 0.75$ slope suggested by F83; for the Sb–Sm galaxies, this difference is driven mostly by our inclusion of bulges and of lower-mass galaxies ($\log (M_\star/M_\odot) \sim 9$); while for the ellipticals, a shallower slope was already apparent in F83.

[11] At lower bulge masses, the apparent tendency to relatively low $j_\star$ values should be viewed as speculative, since it is based on classical bulges rather than the pseudo-bulges that may predominate in this regime.
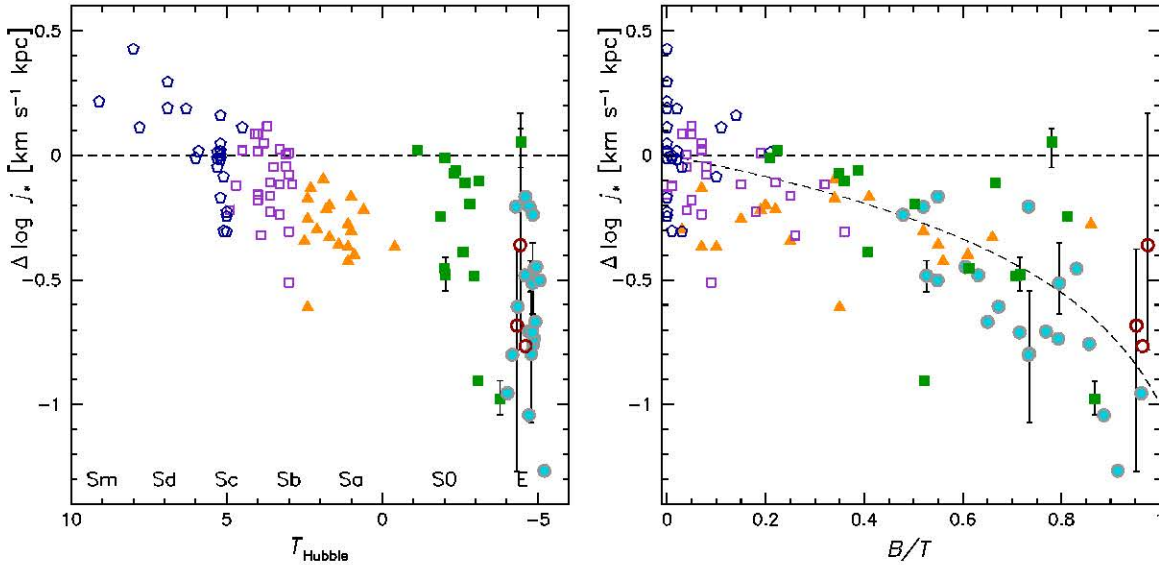
Figure 15. Specific angular momentum relative to the best-fitted trend for spiral disks. In the left-hand panel, these residuals are plotted vs. Hubble stage. For clarity, small random offsets have been added in the horizontal direction for the early-type galaxies. In the right-hand panel, the residuals are plotted vs. bulge-to-total mass ratio. The curved line shows a sample model prediction (not a fit to the data; see the text for details). There are strong systematic trends of the $j_\star$ residuals with respect to both Hubble type and bulge fraction, and the relative smoothness of this trend (particularly for the E/S0s) suggests that bulge fraction is the more fundamental driving parameter.

(A color version of this figure is available in the online journal.)

λ_R (Emsellem et al. 2007), which measures the rotational dominance in the central regions (typically inside $\sim R_e/2$) and is similar to a v/σ metric. Applied to early-type galaxies, a host of interesting patterns and correlations have emerged (Emsellem et al. 2011). However, this metric in practice is not only very scale dependent, but also misses exactly those scales that are most important for measuring true, physical angular momentum (recall Figure 3). In fact, we have seen evidence that $j_\star$ and the central λ_R are disjoint properties: the slow rotators (low-λ_R galaxies) do not appear to deviate from the $j_\star$–$M_\star$ trend for fast rotators.

A final related diagram to mention is $j_\star$–v_c, where v_c is the circular velocity, tracing the dynamical mass of a galaxy within some characteristic radius (e.g., Navarro & Steinmetz 2000; Kassin et al. 2012). There are complications with using this parameter space, since for spiral galaxies both $j_\star$ and v_c are normally based on the same rotation-velocity measurements, which causes a built-in correlation. Unlike $M_\star$, v_c is not a physical quantity subject to straightforward conservation laws. In addition, a critical point for our goal of analyzing all types of galaxies in a unified manner is that it is very hard to estimate v_c for a large sample of early types since they rarely host extended gas disks. Instead, extensive data are required from other tracers such as stellar kinematics (as needed for $j_\star$ estimation), as well as grueling dynamical modeling which even with the state-of-the art techniques can still leave considerable uncertainties (de Lorenzi et al. 2009). Similar problems apply to a $j_\star$–$M_{\rm vir}$ (virial mass) diagram, where the masses can be estimated only on a statistical rather than on an individual basis (e.g., Dutton & van den Bosch 2012).

5.4. Examining the Residuals

Our bulge–disk framework, although rather compelling, is not a unique explanation for the systematic trends in the left-hand panel of Figure 14. It is possible that the vertical displacements of $j_\star$ in this diagram are somehow more directly related to Hubble morphology than to B/T (although one should keep in

mind that B/T is one of the main factors in the morphological classifications, along with spiral arm winding and clumpiness).

To consider this point more clearly, and to better see the relative trends in the data, we flatten the $j_\star$–$M_\star$ relations into one dimension, dividing by the mean trend for the spiral disks and thus generating the quantity:

$$\Delta \log j_\star \equiv \log j_\star - \log j_{\rm mod}(M_\star), \qquad (12)$$

where $j_{\rm mod}$ is given by Equation (11). We plot $\Delta \log j_\star$ versus the Hubble stage parameter $T_{\rm Hubble}$ in Figure 15 (left-hand panel). There is clearly a strong positive correlation between $T_{\rm Hubble}$ and the $j_\star$–$M_\star$ residuals. Among the spirals, this trend is clearest when considering the Sa–Sab versus Sb–Sc galaxies. The Scd–Sm galaxies appear to continue the trend, but they inhabit the lowest-mass area of the $j_\star$–$M_\star$ diagram, where the mean relation is not defined well enough to be certain of the residuals.

The S0s break the smooth trend of $\Delta \log j_\star$ decreasing for smaller $T_{\rm Hubble}$. Many of them appear to have comparable specific angular momenta to typical Sb–Sc galaxies, which was foreshadowed by the rotation scaling relations of Figure 12. The implication is that lenticulars and spirals are overall dynamically similar, differing more in their finer morphological features which may be related to star formation activity. We can thus think of these lenticulars as faded spirals, or of the spirals as rejuvenated lenticulars, although they differ in average B/T values, and more nuanced comparisons will require analysis of $\Upsilon_\star$ (cf. Williams et al. 2010). As for the subset of lenticulars with low $\Delta \log j_\star$, they may either be very close to face-on, or else belong to a different family of objects that are related to the ellipticals.

Returning to our original hypothesis that B/T is the key parameter affecting the $j_\star$–$M_\star$ trends, we consider its correlation with the residuals $\Delta \log j_\star$. Since we do not actually have bulge–disk decompositions for the early-type galaxies in our sample, we introduce a novel technique that uses the degree of central rotational support as a rough proxy for B/T. The idea

here is that the bulge is to a first approximation non-rotating, so any observed rotation is from the disk: objects with higher (v/σ) imply higher disk fractions and lower B/T. Appendix D describes our methods for early-type B/T estimation in more detail. For the late types, we already have B/T estimates based on decompositions in the literature, as discussed earlier.

We show the results in the right-hand panel of Figure 15. The residuals *do* correlate clearly with B/T, in a fairly smooth trend that is followed equally well by all of the galaxy types, and which contrasts with the T_{Hubble} trend. We have marked a simple expectation for the B/T trend with the curved line, given the summation of Equation (9), along with an arbitrarily assumed $j_{\mathrm{b}} = 0.1 \times j_{\mathrm{d}}$. This model mimics the data remarkably well, although it should be remembered that the agreement is somewhat built-in already, since correlated rotational properties were used both to estimate B/T and to calculate $j_{\star}$.

Recalling that we also had to make strong modeling assumptions for the spiral bulges when calculating $j_{\star}$, the better connection of the residuals to B/T rather than T_{Hubble} should be considered preliminary. It is also difficult to tell how much of the scatter in $j_{\star}$ at fixed B/T is due to observational error, and how much is due to intrinsic variations, i.e., with bulges and/or disks not following perfectly standardized $j_{\star}$–$M_{\star}$ relations. Definitive resolution of these issues will require more detailed bulge–disk decompositions of all types of galaxies, including spectroscopic information (cf. Cortesi et al. 2011; Johnston et al. 2012; Dorman et al. 2012; Forbes et al. 2012), and allowances for $\Upsilon_{\star}$ variations.

We would, however, like to advance the proposition that bulge fraction is the fundamental driving parameter behind $j_{\star}$ variations, and is responsible for many of the observed variations in galaxy properties (see discussion in the previous subsection). This not only makes sense from a physical standpoint, but also the agreements between ellipticals and spiral bulges in Figure 14 (right), and between model and data in Figure 15 (right), provide provisional but strongly suggestive observational support. The radially declining rotation-velocity profiles of galaxies like NGC 821 and NGC 3377 in Figure 6 could also be naturally explained by central disk components embedded in non-rotating bulges. Furthermore, we will see from consideration of a cosmological context in Section 6.2 that the distribution of $j_{\star}$ is more naturally reconciled with distinct disk and spheroid subpopulations than with a simple continuum of galaxy $j_{\star}$.

5.5. Histograms of Stellar j Residuals

Before moving on to theoretical analyses, we construct one more representation of the data whose relevance will become particularly clear in the next section. We compress the preceding $j_{\star}$–$M_{\star}$ information into a histogram of residuals from the spiral disk relation, showing the results in Figure 16 (upper panel). Here it is apparent that the spiral galaxy data comprise a roughly lognormal distribution in $\Delta j_{\star}$, with an rms dispersion of $\sim$0.2 dex. The ellipticals have a less well-defined distribution that partially overlaps the spirals but is offset $\sim$0.5 dex lower, while the small sample of lenticulars spans almost the full range of residuals.

In the middle panel of Figure 16, we look instead at the disk and bulge subcomponents of the spiral galaxies, where we have also overplotted a Gaussian with a width of $\sigma_{\log j_{\star}} = 0.17$ dex for reference. Given the uncertainties and possible selection bias in our analysis, we consider the disks to be reasonably consistent with a lognormal distribution.
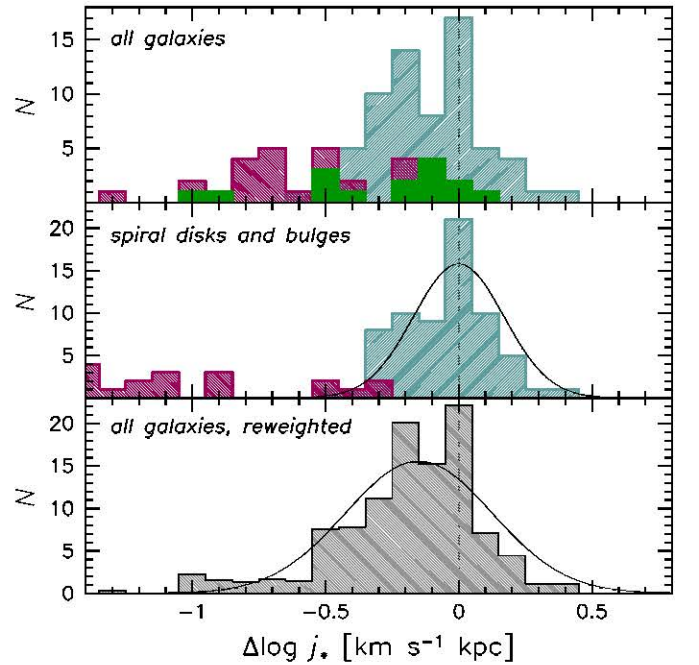
Figure 16. Histogram of specific angular momentum relative to the mean observed trend for spiral disks. In two of the panels, curves show example lognormal distributions for comparison to the data. In the upper panel, the red, green, and blue histograms show data from Figure 15 for spirals, lenticulars, and ellipticals, respectively. The middle panel shows the bulge and disk subcomponents of spiral galaxies, with red and blue histograms, respectively. The lower panel is a summation of the data from the upper panel, after renormalizing each galaxy sub-type by its frequency in the nearby universe (see the main text). The specific angular momentum does not appear to have a simple lognormal distribution, and may even be bimodal.

(A color version of this figure is available in the online journal.)

The $\Delta \log j_{\star}$ distribution for the spiral bulges resembles that of the ellipticals in the sense that both are systematically offset to lower values, as we have previously seen. The bulges apparently extend to much lower $\Delta \log j_{\star}$ than the ellipticals, but as discussed in Section 5.2, this is not a secure result, given the uncertainties in the bulge calculations.

Returning to the overall results, we would like to know whether or not galaxies follow a bimodal distribution in $\Delta \log j_{\star}$ as the top panel of Figure 16 suggests. The complication here is possible bias in the galaxy sample: if we were to study *all* bright galaxies in a volume-limited sample, the $\Delta \log j_{\star}$ distribution might look very different. To investigate this issue, we must re-weight the distribution of $j_{\star}$ in our sample by galaxy type.

The simplest approach is to renormalize by frequency or number density. We use the ATLAS$^{\mathrm{3D}}$ results that 70%, 22%, and 8% of the galaxies in the nearby universe are spirals, lenticulars, and ellipticals (over a stellar mass range similar to our observational sample; Cappellari et al. 2011a). The fractions in our sample are 63%, 14%, and 23%, demonstrating a strong bias toward ellipticals at the expense of lenticulars.

We plot the re-weighted results in the lower panel of Figure 16, showing also for reference a lognormal curve with $\sigma_{\log j_{\star}} = 0.27$ dex (a width that will be motivated in Section 6.2). The total distribution of $\log j_{\star}$ residuals appears slightly non-Gaussian, with a tail extending to low values. This feature may not be significant if one allows for systematic uncertainties in the selection effects, but the skewness will become clearer when compared to theory in Section 6.2.

An alternative scheme would be to re-weight by the stellar mass density of the different galaxy types. This would bring us

closer to a total distribution function for stellar j in the universe, rather than a distribution of galaxies with given $j_\star$. It is beyond the scope of this paper to carry out such an exercise in detail, but the basic outcome is clear. The high end of the mass distribution is dominated by early types (cf. lower panel of Figure 33), which means that the mass weighting would enhance the contributions of these galaxies relative to number weighting. The universal distribution of $j_\star$ would then appear *more non-Gaussian* than in the lower panel of Figure 16.

These distributions are also sensitive to assumptions about the stellar mass-to-light ratio $\Upsilon_\star$. If systematic variations in $\Upsilon_\star$ with galaxy type were adopted (cf. Section 3.4), then the main peak of the $\Delta \log j_\star$ distribution would become somewhat broader. The $\Delta \log j_\star$ values for the ellipticals would also decrease by ~ 0.3 dex, making them even stronger outliers from the main distribution.

We therefore find evidence that the residuals of the specific angular momenta of galaxies from the mean relation are not simply lognormal. The best match to a lognormal model is provided by the disk components of spirals, while the bulges and the ellipticals may comprise a distinct second population.[12] Again, a natural interpretation of this finding is that all galaxies are composed of some combination of high- and low-$j_\star$ material, which may be identified with disks and bulges, respectively.

Some implications of these results for galaxy formation in a modern cosmological context will be discussed in the next section. It should be remembered, however, that our empirical findings—of specific, strong correlations between galactic angular momentum, mass, morphology, and bulge fraction—stand on their own and must be explicable by any successful theory of galaxy formation, whether now or in the future.

6. CONNECTING TO THEORY

We are now ready to present a fresh theoretical way of looking at galaxies, using the $j_\star$–$M_\star$ diagram, which was introduced in F83, and which may now be reinvigorated by populating it with observational data for galaxies of all types. Our general approach is to take a step back from galactic *details*, whether these be spiral arms and dust lanes in observations, or unresolved gas physics and star formation recipes in simulations, and return to some simple physical parameters and conservation rules that may provide robust constraints and insights to galaxy formation.

We have shown in Sections 5.2 and 5.4 that the specific stellar angular momenta of observed galaxies follow remarkably tight correlations with their masses and bulge fractions. Such patterns in nature demand theoretical explanations, as they could be tracing fundamental physical processes. Indeed, the $j_\star$–$M_\star$ relation for spiral galaxies is well known in some circles, and provides a crucial benchmark for models of galaxy formation. However, the correlation for elliptical galaxies (already shown in a preliminary version by F83) is less well known and addressed with theoretical models. Our goal is to advance a general, physical framework for integrating these observational constraints into models of galaxy formation and evolution.

Our approach here is different from, and complementary to, the active field of hydrodynamical simulations of galaxy formation. Although such simulations have made notable progress toward the ultimate goal of reproducing realistic galaxies, they

still have a long way to go, with recent work highlighting large differences in the basic properties of simulated galaxies, depending on what code, resolution, and physical recipes are used (Scannapieco et al. 2012; Torrey et al. 2012).

Historically, such methods missed reproducing observed $j_\star$ trends by factors of up to ~ 30, and even the most recent work shows variations at the factor of ~ 2 level. The general concern is that many of the large-scale properties of galaxies could well depend strongly on transport processes at the scales of molecular clouds, which are not yet modeled satisfactorily in cosmological simulations. Therefore, some caution is still needed in assuming that the simulations are providing an adequate representation of reality.

In this context, simplified "toy" models continue to play a key role in defining the broad but solid outlines of the galaxy formation theory that is required to match the observational constraints. These models may also prove useful in physical understanding of the output of numerical hydrodynamical simulations.

We frame our analysis in the context of the current standard cosmological model for structure formation: cold dark matter with a cosmological constant (ΛCDM; Komatsu et al. 2011). This model makes specific, robust predictions for the angular momenta of DM halos. Because the visible galaxies, consisting of stars and gas, are presumed to reside in these DM halos, we may then ask whether or not the observed stellar angular momenta bear any resemblance to the predictions for DM halos.

We begin with the properties of ΛCDM halos as our "initial conditions" for galaxy formation, which we map to our observable space: $j_\star$–$M_\star$ for the stellar components of galaxies. We do this by parameterizing the retention of mass and angular momentum during galaxy formation, and then by introducing a menu of $j_\star$–$M_\star$ vectors of change that correspond to plausible physical processes (outflows, mergers, etc.).

We emphasize that the primary aim of this paper is *not* to concoct a new theory of galaxy formation, nor to weigh in on competing models by vetting specific simulation outputs against the $j_\star$–$M_\star$ diagram. Instead, we wish to lay out a generalized framework that can both constrain and explain the models. The methodology and merits of this approach should become clearer as we develop the ideas throughout this section, and as we eventually work through some practical examples.

We develop general theoretical predictions and make basic inferences about j retention in Section 6.1. In Section 6.2 we investigate two possible explanations for the observed $j_\star$ dichotomy between spirals and ellipticals. In Section 6.3 we consider coupling between changes in mass and angular momentum, and connect these to evolutionary scenarios for galaxies.

6.1. Basic Constraints

The overdense regions in an expanding universe are not spherically symmetric and exert tidal torques on each other, inducing a net angular momentum in each collapsing galaxy (Hoyle 1951). This rotational behavior is usually specified in terms of a dimensionless spin parameter that quantifies the dynamical importance of rotation, and is a combination of fundamental physical quantities:

$$\lambda \equiv \frac{J|E|^{1/2}}{GM^{5/2}}, \qquad (13)$$

where J is the angular momentum, E is the energy (kinetic and potential), G is the gravitational constant, and M is the mass
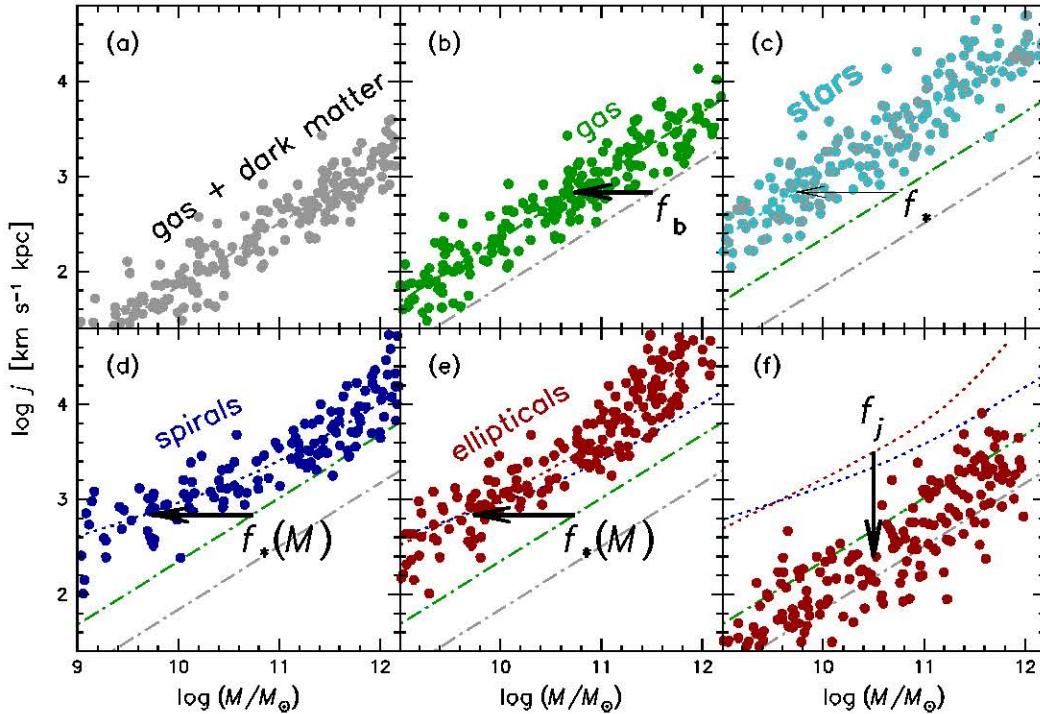
Figure 17. Schematic evolution of galaxies in the space of specific angular momentum and mass. Each point shows a galaxy randomly selected from a simple model (see the main text). Panel (a) shows the initial galactic halos of gas and DM. Panel (b) shows the gas component only, adopting a baryon fraction of $f_b = 0.17$, with an arrow illustrating the direction that a single galaxy takes in this diagram. Panel (c) shows the stellar component after forming from the gas with an average relative fraction of $\langle f_\star \rangle = 0.1$. Panels (d) and (e) show the stars of spiral and elliptical galaxies, respectively, after adopting more realistic variations of $\langle f_\star \rangle$ with mass. Panel (f) shows the effect of angular momentum loss, with a factor of $\langle f_j \rangle = 0.1$. Note that these are simple, idealized models, and not every aspect should be taken literally; e.g., spiral galaxies probably do not exist at masses of $M_\star \gtrsim 10^{12} M_\odot$.

(A color version of this figure is available in the online journal.)

(Peebles 1969).[13] Whether analyzed through linear tidal torque theory, or through N-body simulations of galaxy assembly, λ is predicted to follow an almost lognormal distribution that is relatively insensitive to cosmological parameters, time, galaxy mass, and environment (e.g., Barnes & Efstathiou 1987; Zurek et al. 1988; Steinmetz & Bartelmann 1995; Cole & Lacey 1996; Macciò et al. 2007; Bryan et al. 2012).

The spin parameter provides a convenient way to characterize DM halos, but it is not straightforward to connect λ to baryonic galaxies because it is not a physically conserved quantity (as energy is dissipated). We instead conduct our theoretical analysis in terms of the specific angular momentum parameter j, as we have done with the observations. Along with the mass M, j is a quantity that is potentially conserved at some approximate level during the evolutionary history of a galaxy.

To re-cast λ to j, we adopt a ΛCDM-based spherically symmetric halo profile from Navarro et al. (1996), truncated at the virial radius.[14] We then obtain

$$j_{\rm vir} = 4.23 \times 10^4 \lambda \left(\frac{M_{\rm vir}}{10^{12} M_\odot} \right)^{2/3} \ {\rm km \ s^{-1} \ kpc}. \quad (14)$$

We adopt a characteristic value[15] of $\langle \lambda \rangle = 0.035$, along with a 1σ log dispersion of 0.23 dex, based on a study of relaxed halos in a cosmological simulation with *WMAP*5 parameters, by Macciò et al. (2008). The log-averaged numerical coefficient in Equation (14) then becomes 1460 km s^{-1} kpc. Other recent studies are generally consistent with these results at the level of $\sim$10%. The $\alpha = 2/3$ exponent is also an explicit prediction of tidal torque theory (Shaya & Tully 1984; Heavens & Peacock 1988), and provides a reasonable approximation to the trends from *direct* calculations of $j_{\rm vir}$ and $M_{\rm vir}$ in N-body simulations (Antonuccio-Delogu et al. 2010).

Equation (14) can be considered as setting firm "initial conditions" for galaxies, characterizing their angular momenta near the time of virialization. This is shown schematically in panel (a) of Figure 17, which we have populated with toy-model "galaxies" consisting of primordial halos of gas and DM. Their masses are drawn from a uniform logarithmic distribution, and their angular momenta from a lognormal distribution using $\langle j_{\rm vir} \rangle$ and $\sigma_{\log j_{\rm vir}}$ as above.

We next consider a series of idealized evolutionary steps that allow us to parameterize evolution in the j–M diagram. We assume that the baryons consist initially of gas that is well mixed with the dark matter of its parent halo, and that does not collapse within the halo until after the linear and translinear regimes of tidal torque when most of the angular momentum is acquired. The gas may then be assumed to have the same value of j as the halo, which we show in panel (b) as a simple shift of the points to the left, according to a cosmological baryon fraction of $f_b = 0.17$ (Komatsu et al. 2011).

---

[13] Recall that the parameters (J, E, M) can be translated roughly into a more observationally oriented basis set of rotation velocity, effective radius, and luminosity ($v_{\rm rot}, R_e, L$), where in approximate terms: $M \propto L$, $E \propto L^2 R_e^{-1}$, and $J \propto v_{\rm rot} L R_e$.

[14] The virial radius is defined as bounding a region inside which the mean halo density is a factor of $\Delta_{\rm vir}$ times the critical density $\rho_{\rm crit} \equiv 3H^2/(8\pi G)$. We adopt a *WMAP*5 cosmology, with $H = 72$ km s^{-1} Mpc^{-1} and $\Delta_{\rm vir} = 95.3$ at $z = 0$ (Macciò et al. 2008). To calculate E for this halo, we use an expression from Mo et al. (1998) with a fixed concentration of $c_{\rm vir} = 9.7$; and we ignore variations due to concentration which affect λ at the $\sim$5% level. A related spin-proxy parameter, λ', is based on a singular isothermal sphere (Bullock et al. 2001), and is $\simeq$11% smaller than λ.

[15] This is based on the average value of log λ, but throughout this paper we use shorthand such as $\langle \lambda \rangle$ and $\langle j \rangle$ for log-averages.

In panel (c) we show what happens in a simple case where a fraction of the baryons form into stars, with a particular value of $\langle f_\star \rangle = 0.1$, and a dispersion of $\sigma_{\log f_\star} = 0.15$ dex. Again, j is assumed to be conserved, and the galaxies shift to the left. It is also usually assumed, though not required by the diagram, that this process involves the formation of a thin stellar disk whose collapse was halted by the balance between gravity and centrifugal force.

Our analysis does, however, assume that the baryon collapse extends all the way out to the halo virial radius. This conventional assumption is at some level implausible since DM collapse and gas cooling are governed by different physical scales in space and time. A more generalized approach where the baryon collapse radius is allowed to vary will be considered in Section 6.3.2.

Note that the $f_\star$ parameter can take on a more general meaning of *net* stellar mass fraction relative to initial gas mass, which allows for stars that are accreted by or ejected from the galaxy. We will shortly discuss a more refined model where $f_\star$ varies systematically with mass, but for now we continue with our very simplified constant-$f_\star$ model in order to consider its basic implications.

Our next model ingredient is an idealized process of angular momentum loss, with no concomitant change in mass, which we quantify by a fractional j net retention factor of f_j. An example of such a process would be internal j transfer from the stars to the DM halo. Given the parameters $f_\star$ and f_j, we may then translate the j–M relation (14) for DM halos to an equivalent one for the stellar components of galaxies:

$$j_\star = 2.92 \times 10^4 \, f_j \, f_\star^{-2/3} \, \lambda \left(\frac{M_\star}{10^{11} \, M_\odot} \right)^{2/3} \, \text{km s}^{-1} \, \text{kpc}, \quad (15)$$

where again using the prediction for $\langle \lambda \rangle$, the numerical coefficient for $\langle j_\star \rangle$ becomes 1010 km s^{-1} kpc.

This relation is identical to our parameterized fit to the observational data with Equation (11), modulo the numerical factors and the value for the exponent α. Since the observed $j_\star$–$M_\star$ relation can be approximated with $\alpha = 2/3$ and a normalization j_0, then we can express the difference between observation and theory through a combination of the parameters f_j and $f_\star$:

$$j_0 = 1010 \, \langle f_j \, f_\star^{-2/3} \rangle \, \text{km s}^{-1} \, \text{kpc}. \quad (16)$$

Equations (14)–(16) are simple but powerful, allowing us to connect the visible properties of galaxies to their invisible DM halos, using some basic parameters and assumptions. They also provide robust observational constraints on some essential characteristics of galaxy formation that are still far beyond the ability of raw theory to predict reliably. *The average value of $f_j \, f_\star^{-2/3}$ for a population of galaxies can be determined by observations as a strict constraint on theory.*

We can immediately use Equation (16) in combination with the observational results for j_0 from Table 2 for fixed $\alpha = 2/3$. We find that $\langle f_j \, f_\star^{-2/3} \rangle \simeq 1.9$ for Sb–Sm spirals and $\simeq 0.5$ for ellipticals. For example, if we assumed an arbitrary $\langle f_\star \rangle = 0.2$ for both types of galaxies, then we would infer $\langle f_j \rangle \simeq 0.65$ for spirals and $\simeq 0.1$ for ellipticals. This means a systematic difference in net angular momentum retention between the two galaxy types which, although there are many further details to work through below, will hold up as a basic result of this paper.

To derive firmer constraints on f_j, we need to break the $f_\star$–f_j degeneracy by introducing well-motivated values for $f_\star$, for both spirals and ellipticals. We also need to consider the complication that $f_\star$ cannot in reality have a simple, constant value, even on average. This is because the observed luminosity function of galaxies has a dramatically different shape from the predicted mass function of DM halos (e.g., White & Rees 1978; White & Frenk 1991; Marinoni & Hudson 2002; Yang et al. 2003; Moster et al. 2010). Below the characteristic "knee" luminosity L^*, the galaxies are observed to follow a shallower slope than the DM mass function $dN/dM \propto M^{-2}$, while at higher luminosities, the observations are *steeper* than the predictions. The implication is that the fraction of luminous-to-dark matter declines rapidly for galaxies fainter and brighter than L^*; i.e., assuming a constant f_b, the function $\langle f_\star \rangle (M_{\text{vir}})$ has a characteristic inverted U shape.

This empirical trend is thought to be caused physically by various feedback effects that inhibit star formation and become increasingly important in the low- and high-mass regimes (such as stellar and supermassive black hole feedback, respectively; e.g., Lacey et al. 1993; Cole et al. 1994; Somerville & Primack 1999; Bower et al. 2006; Croton et al. 2006). Regardless of the explanation, any self-consistent ΛCDM-based model must incorporate a strong, systematic mass dependence on star formation efficiency, $\langle f_\star \rangle (M_{\text{vir}})$.

One might be concerned that such a mass dependence would transform an underlying $j \propto M^{2/3}$ relation for DM halos into something very different for the stellar components of galaxies, and quite unlike our observational results. To check this, we will modify our simple model above to allow for a varying function $\langle f_* \rangle (M_{\text{vir}})$. Since this function is a tracer of undetermined baryonic physics during galaxy evolution, there is not yet any robust theoretical prediction for it, but fortunately it can be estimated empirically. This is done in an *average* sense through various techniques such as weak gravitational lensing, stacked satellite kinematics, and matching up the mass and luminosity functions mentioned above.

There have been many studies that estimated $\langle f_\star \rangle (M_{\text{vir}})$, but few that did so separately for different galaxy types, which is important for our analysis. We therefore adopt the relations for $\langle f_\star \rangle (M_\star)$ derived by Dutton et al. (2010). For the spiral galaxies, we use their relation for "late-type" galaxies:

$$\langle f_\star \rangle (M_\star) = \frac{f_0 \, (M_\star/M_0)^{1/2}}{[1 + (M_\star/M_0)]^{1/2}}. \quad (17)$$

Below a characteristic mass $\log(M_0/M_\odot) \simeq 10.8$, this relation has a dependence $\langle f_\star \rangle \propto M_\star^{1/2}$. At higher masses, it approaches a constant, $f_0 \simeq 0.33$. Here we have converted the Dutton et al. results to our definition of the virial mass and to our adopted stellar IMF, while using $h = 0.72$.

For elliptical galaxies, we adopt the Dutton et al. relation for "early-type" galaxies:[16]

$$\langle f_\star \rangle (M_\star) = \frac{f_0 \, (M_\star/M_0)^{0.15}}{\left[1 + (M_\star/M_0)^2\right]^{1/2}}, \quad (18)$$

where $\log(M_0/M_\odot) \simeq 11.2$, $f_0 \simeq 0.14$, and the asymptotic behaviors at low and high masses are $\langle f_\star \rangle \sim M_\star^{0.15}$ and $\langle f_\star \rangle \sim M_\star^{-0.85}$, respectively. One of the key features to note

---

[16] There has been very little work along these lines for elliptical and lenticular galaxies separately, but there is some recent evidence that the halo masses for these types are the same (Trujillo-Gomez et al. 2011). Note also that the Dutton et al. relations were derived for somewhat smaller mass ranges than covered by our data, and that their stellar mass determinations may not be fully consistent with our methods.

here is that an elliptical galaxy typically has a much lower value of $f_\star$ than a spiral with the same stellar mass: i.e., ellipticals inhabit systematically more massive DM halos, which in many cases extend up to "group" masses of $M_{\rm vir} \sim 10^{13}\ M_\odot$ and beyond (see also van Uitert et al. 2011).

These $\langle f_\star \rangle(M_\star)$ relations can be uniquely transformed to $\langle f_\star \rangle(M_{\rm vir})$, and taken together define an inverted U-shaped trend as discussed above. The relations were constructed using a compilation of different literature results, which showed an encouraging degree of mutual consistency, so we conclude that the average trends above are probably reliable at the $\sim$50% ($\sim$0.2 dex) level. There may also be non-zero galaxy-to-galaxy variations in $f_\star$ at a fixed mass and type; the value of this scatter is less well established, but recent analyses suggest that it may be $\sim$0.15 dex (Behroozi et al. 2010; More et al. 2011). We adopt this as our default value, which fortunately is smaller than the expected dispersion in halo spin of $\simeq$0.23 dex and so will not have much impact on our conclusions.

Using these variable $\langle f_\star \rangle(M_{\rm vir})$ relations to construct mock $j_\star$–$M_\star$ data sets as before, we plot the results in panels (d) and (e) of Figure 17. For both spirals and ellipticals, we can see that the curvature in $\langle f_\star \rangle(M_{\rm vir})$ translates to systematic deviations in the $j_\star$–$M_\star$ relation from a simple $\alpha = 2/3$ power law. We will investigate how these deviations compare to real observations in the next subsection.

Panels (d) and (e) of Figure 17 also demonstrate that at masses of $M_\star \gtrsim 10^{11}\ M_\odot$, the ellipticals are predicted to have *higher* $j_\star$ than the spirals of the same mass, owing to their differences in $f_\star$. The more massive DM halos of ellipticals ought to provide larger virial-radius lever arms that lead to larger $j_{\rm vir}$, and therefore larger $j_\star$—*if* they retain as much fractional angular momentum as spiral galaxies do. Therefore, the observed offset in $j_\star$–$M_\star$ between spirals and ellipticals implies an even larger difference in $\langle f_j \rangle$ than in the simple example above with fixed $\langle f_\star \rangle = 0.2$. We will examine this apparent f_j dichotomy further in the next subsection.

As a final illustrative exercise, we generate a mock data set for elliptical galaxies as in panel (e), then adopt $\langle f_j \rangle = 0.1$, with an assumed dispersion of $\sigma_{\log f_j} = 0.15$ dex. The results are plotted in panel (f), where we see that the galaxies have coincidentally returned to nearly the original j–M sequence for halos, modulo a little curvature and increased scatter.

Figure 17 thus shows how one could map the observed $j_\star$–$M_\star$ properties of a population of galaxies (panel (f)) to a theoretical prediction for their halos (panel (a)), and recover some basic parameters describing galaxy formation (see Equation (16)). This formulation is closely related to a classic theoretical framework for the formation of spiral galaxy disks, whose observed sizes and rotation velocities are generally consistent with the approximate conservation of primordial specific angular momentum ($f_j \sim 1$; e.g., Fall & Efstathiou 1980; Dalcanton et al. 1997; Mo et al. 1998). However, our formulation is more general by including also the early-type galaxies, as well as the bulge components within spiral galaxies (which we will discuss below).

6.2. Investigating the Spread in $j_\star$

As just discussed, the observed dichotomy between the $j_\star$–$M_\star$ relations of spirals and ellipticals may imply differences in their specific angular momentum retention, expressed here by the factor f_j. This interpretation is based on an implicit assumption that the parent halos of both galaxy types had the same average λ. However, a natural halo-to-halo scatter in λ is expected, and one could instead imagine the other extreme case, in which f_j

is the same for the two galaxy types, while their halo λ values are systematically different (e.g., Kashlinsky 1982; Blumenthal et al. 1984; Catelan & Theuns 1996). In other words, spirals and ellipticals are drawn from the high- and low-spin tails of the λ distribution, respectively.

We call these two alternatives the "variable f_j" and "spin-bias" scenarios. In reality, a mixture of both scenarios may be present, which would be difficult to disentangle, but we can begin by investigating these two limiting cases in detail. Thus the aim of this section is to test how consistent each of these cases is with the data.

The reason we can make headway on this issue is that there are predictions from ΛCDM not only for the average value of λ, but also for its probability distribution, i.e., a lognormal with a characteristic dispersion as discussed in Section 6.1. We continue to focus on the spirals and ellipticals as the two interesting extremes of the observed $j_\star$ range (at fixed $M_\star$), and consider the lenticulars as intermediate either in f_j or in λ.

We begin with the spin-bias scenario. If correct, adopting a constant f_j value for a complete, unbiased galaxy sample would allow us to work backward to infer the underlying λ distribution, which could then be compared to the theoretical prediction. One might think that we have already implicitly carried out this test by examining the residuals from the observed $j_\star$–$M_\star$ relation in Section 5.5 and Figure 16. However, that analysis did not account for the differences in $f_\star$ between different galaxy types.

We therefore proceed with a more direct comparison to theory by generating $j_\star$–$M_\star$ model predictions for each galaxy type, and calculating the observed residuals with respect to these models. We use Equation (15) with $\lambda = \langle \lambda \rangle = 0.035$, along with the empirical $\langle f_\star \rangle(M_\star)$ relations (17) and (18), and an ad hoc $\langle f_j \rangle = 0.55$, to predict a mean $j_\star$–$M_\star$ relation for each galaxy type. We then derive the residuals $\Delta \log j_\star$ by subtracting the model from the observations as in Equation (12). If the spin-bias scenario is correct, then the properly re-weighted distribution of these residuals ought to follow a lognormal with dispersion $\sigma_{\log j_\star} \simeq 0.27$ (which accounts for observational errors and the intrinsic scatter in $f_\star$).

Figure 18 presents histograms of these residuals, both by separate galaxy types (top panel), and in combination (bottom panel), which uses a renormalization by frequency of galaxy types from the ATLAS$^{\rm 3D}$ survey, as in Section 5.5. We find that overall, the total distribution of $\Delta j_\star$ has approximately the predicted width. However, the distribution in detail appears significantly different from a lognormal: there is an excess of low-$\Delta j_\star$ galaxies, and a missing tail at high-$\Delta j_\star$. In particular, there are too many elliptical galaxies in the nearby universe to be explained by the tail of low-spin halos.[17]

This histogram analysis appears to exclude a simple spin-bias scenario, but there are some caveats, such as small sample sizes and the assumption of perfect lognormality for the distribution of halo spins. We can make further progress by recognizing that the scenario makes predictions for the $j_\star$ residuals not only for all galaxies combined, but also as a function of mass. This is because λ is not predicted to depend on halo mass, while the relative frequencies of different galaxy types are observed to vary strongly. One can then immediately see a serious problem with the spin-bias scenario: at high masses, almost all of the galaxies are ellipticals, which should thus be

---

[17] Hernandez et al. (2007) also found in attempting to infer halo λ values for spirals and ellipticals that an ad hoc rescaling of the elliptical values was required in order to avoid a double-peaked λ distribution.
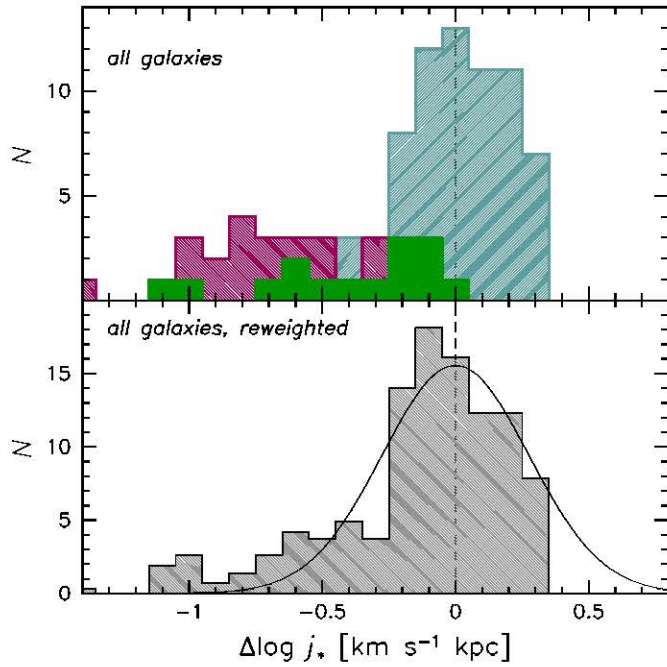
Figure 18. Distributions of residuals in the observed stellar specific angular momentum, with respect to the mean theoretical prediction for ΛCDM halos, after assuming a fixed j-retention parameter, $f_j = 0.55$. As in Figure 16, red, green, and blue histograms in the top panels show the residuals for elliptical, lenticular, and spiral galaxies, respectively. The bottom panel shows the same distribution, renormalized for the relative frequencies of galaxies in the nearby universe. The curve shows a predicted lognormal distribution for comparison. The distribution of residuals for spiral galaxies is narrower than expected from the distribution of halo spins, while the overall galaxy distribution shows clear departures from the lognormal model (with an excess at low $j_\star$ and a deficit at high $j_\star$).

(A color version of this figure is available in the online journal.)

an unbiased population representing the full range of halo spins (Dutton & van den Bosch 2012 made a similar point for low-mass disk galaxies).

We investigate this issue in more detail by constructing a mock data set as in Figure 17, while this time incorporating a schematic model for spin bias. We now assume that all galaxies have $f_j = 0.45$, with the late types inhabiting the high-spin halos, and the early types the low-spin ones. Using the number densities of early and late types as a function of $M_\star$ from ATLAS[3D], we use the $\langle f_\star \rangle(M_\star)$ relations to translate this to the relative fractions at fixed halo mass (which can be quite different from the fractions at fixed $M_\star$). We then randomly draw a distribution of biased spin parameters for each galaxy type; e.g., if spirals comprise 25% of galaxies at a given mass, we draw mock spirals from the top quarter of the spin distribution. We also adopt a similar mass range and total number of galaxies as in our real data sets.

We show the resulting $j_\star$–$M_\star$ mock data set in the left-hand panel of Figure 19, which can be compared to the real data in the middle panel. We see that the low-mass ellipticals could indeed be drawn from only the low-spin tail because of their rarity. However, at high masses the ellipticals are common and their predicted $j_\star$ values are similar to the spirals. To salvage the spin-bias scenario would thus seem to require a mass-dependent bias, which seems epicyclic and therefore not appealing.[18]

The biasing idea can also be discredited by environmental considerations: there are strong observational correlations between environmental density and galaxy morphology, but as mentioned earlier, halo spins in theory depend only weakly on environment (which has some observational support in the case of disk galaxies; Cervantes-Sodi et al. 2008; Berta et al. 2008). In addition, if we consider disks and bulges to be manifestations of the same $j_\star$–$M_\star$ trends as spiral and elliptical galaxies, then the coexistence of these subcomponents within the same galaxies provides a clear argument against halo spin bias.

We next turn to the variable-f_j scenario, where spirals and ellipticals are drawn from the same underlying distribution of halo spins, but their baryonic components have systematic differences in retaining j. Given that we know $\langle f_\star \rangle$ for each galaxy type, Equation (16) suggests that we can immediately use the observed j_0 normalization to infer $\langle f_j \rangle$. However, the situation is more complicated since $\langle f_\star \rangle$ varies with mass and therefore one does not expect an exact $\alpha = 2/3$ for fixed f_j (recall Figures 17(d) and (e)).

As we did for the spin-bias scenario, we again construct mean $j_\star$–$M_\star$ relations for each galaxy type, while now leaving f_j as a free parameter. Carrying out least-squares fits to the data, we find values of $\langle f_j \rangle = 0.56 \pm 0.03$ and $\langle f_j \rangle = 0.12 \pm 0.01$ for the spiral and elliptical galaxies, respectively. The difference in $\langle f_j \rangle$ of a factor of 4.7 ± 0.8 is slightly larger than the observed $j_\star$–$M_\star$ relative offset, as anticipated in the previous section because of the differences in $\langle f_\star \rangle$ (e.g., Equation (16)).

These $\langle f_j \rangle$ values would be revised if systematic variations in the stellar mass-to-light ratio were included when estimating the masses of galaxies (Section 3.4). The general trend would be for the spirals to have higher values, perhaps approaching $\langle f_j \rangle \sim 1$, but it is difficult to be precise without carefully accounting for similar details in the $\langle f_\star \rangle$ estimates. Alternatively, given the degeneracy between f_j and $f_\star$, the inferred f_j dichotomy could in principle be an artifact of errors in our adopted values for $\langle f_\star \rangle$. However, these errors would have to amount to a combined factor of $\sim$5: e.g., with true $\langle f_\star \rangle \sim 0.1$ for the spirals along with $\sim$0.2 for the ellipticals, rather than $\sim$0.25 and $\sim$0.1.

The next step is to verify that these best-fit models provide reasonable representations of the data. We again construct mock data sets, using the new f_j models (with 0.15 dex of scatter in $f_\star$), and show the results in the right-hand panel of Figure 19. Here we see that, unlike the spin-bias model, these variable-f_j models provide a remarkably good match to the data. The curvature of the predicted $j_\star$–$M_\star$ relation turns out to be imperceptible, once we account for observational errors, small-number statistics, and a limited mass range.[19] Furthermore, the observed slope for the spirals is shallower than $\alpha = 2/3$, which is predicted by the model.

This comparison does not entirely succeed in accounting for the *scatter* about the $j_\star$–$M_\star$ relations. As can be seen in Figure 19, the real observations appear to follow *tighter* trends than predicted by our simple model, for both spirals and ellipticals. The model fits give rms scatters of $\sigma_{\log f_j} = 0.18$ dex and 0.25 dex for the spirals and ellipticals, which is already *less* than the expected scatter of 0.27 dex from λ and $f_\star$, even without allowing for measurement errors, and scatter in f_j (see also the

---

[18] There may be reasons of stability for ellipticals to be dominant at high masses (e.g., Dalcanton et al. 1997; van den Bosch 1998; Dutton & van den Bosch 2012), but this ostensibly changes the *morphology* and not $j_\star$.

[19] Future empirical estimates of $j_\star$ and $M_\star$ over a larger dynamic range could provide a strong test of constant-f_j scenarios. Given the observational difficulty of measuring $j_\star$ at high masses where the underlying halos pertain to entire galaxy groups and clusters, the best prospect for improvement would be to study lower-mass galaxies, with $\log (M_\star/M_\odot) \lesssim 9$.
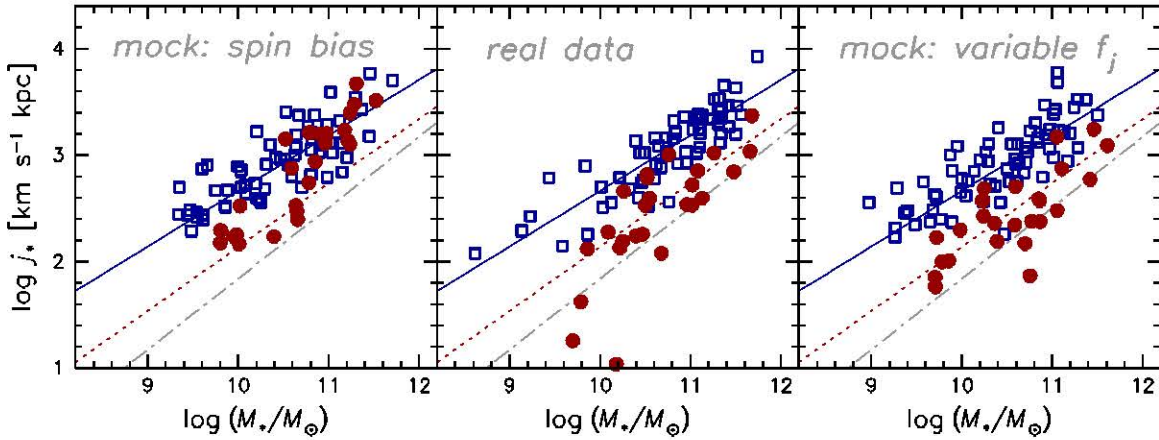
Figure 19. Stellar specific angular momentum vs. stellar mass, comparing mock data generated from ΛCDM-based models (left- and right-hand panels) to real data (middle panel). The model on the left includes halo spin bias, while the model on the right assumes systematic differences in angular momentum retention between spirals and ellipticals. Blue open squares and red filled circles show spirals and ellipticals, respectively, with the solid blue and dotted red lines showing the best-fit power laws for the real data. The relation for halos is also shown for reference as a gray dot-dashed line. The mock data sets include intrinsic scatter in the parameters λ and $f_\star$ at a given mass, but *not* observational errors. The simple variable-f_j mock data on the right resemble the real data, while the spin-biased model does not.

(A color version of this figure is available in the online journal.)

histogram of spirals in the top panel of Figure 18, compared to the curve in the lower panel).

One possible explanation for this reduced scatter is that the baryonic processes responsible for j loss could act as some kind of "attractor" to specific values of f_j (cf. de Jong & Lacey 2000). Alternatively, halo spin bias could be at work in a secondary role, even while f_j variation is the primary effect.[20]

Our overall conclusion is that the variable-f_j model reproduces the $j_\star$–$M_\star$ observations well in general, is fairly insensitive to the exact trend of $\langle f_\star \rangle$ with mass, and does not require any additional variation of $\langle f_j \rangle$ with mass. The spirals appear to have been fairly efficient in preserving the specific angular momentum imprints of their parent halos, while ellipticals have lost the vast majority of theirs.

This is a plausible scenario from a physical standpoint if we return to our proposed framework where all galaxies are composed of bulges and disks (Figure 2 and Section 5.3). Unfortunately, we do not have $\langle f_\star \rangle (M_\star)$ relations for the bulges and disks themselves in order to directly derive their $\langle f_j \rangle$ trends. However, given the similarities in $j_\star$–$M_\star$ that we found between these subcomponents and the galaxies overall, it seems reasonable to suppose that bulges and disks have $\langle f_j \rangle \sim 0.1$ and ∼0.6, respectively, and that these values are characteristic of two distinct modes of galaxy evolution.[21] We will return to this topic in the next section.

Our conclusions about *spiral* galaxies echo similar findings in the literature, which have typically inferred $\langle f_j \rangle \sim 0.5$–0.6 overall (e.g., Navarro & Steinmetz 2000; Dutton et al. 2007; Burkert 2009; Dutton & van den Bosch 2012; Kassin et al. 2012). In particular, Dutton & van den Bosch (2012) used a model parameterization similar to our ($f_\star$, f_j), and found that $\langle f_j \rangle$ is fairly constant over a wide mass range. Note that these authors used a parameterized mass model to fit the Tully–Fisher relation, which was then converted to an average $j_{\rm vir}$–$M_{\rm vir}$ relation. Our

approach works instead in the space of observables, $j_\star$–$M_\star$, which is more direct and transparent while also allowing us to analyze galaxy-to-galaxy variations.[22]

Our finding for the *ellipticals* is novel, as neither the predictions for $j_\star$–$M_\star$ of ellipticals nor their subsequent f_j inferences have been well studied before now. We have not carried out a comparable analysis on *lenticulars* since the constraints on them are less certain. Qualitatively speaking, their observed log $j_\star$ normalization is between the other two galaxy types, which for plausible values of $\langle f_\star \rangle$ implies $\langle f_j \rangle$ values that are intermediate to those for the spirals and ellipticals. In addition, there may be two subpopulations of lenticulars as discussed in Section 5.4, with low and high $\langle f_j \rangle$.

There are two interesting implications about these findings. One is that that we now have a remarkably simple and successful framework for describing and connecting some of the most fundamental properties of galaxies. The observable galaxies may be connected to their unobservable host halos using $j_\star$ and $M_\star$ along with some relatively basic parameters f_j and $f_\star$. Such a model may appear implausibly oversimplified in the light of our ever-expanding awareness of the complexities of galaxy formation physics, but for some reason it seems to work.

The other implication is that these parameters may give us insight into the formation of disks and bulges, and into the origins of the Hubble sequence. To illustrate this point, we use our modeling procedures as described above to work backward and estimate $f_\star$ and f_j values for *individual* galaxies. The outcome is shown in Figure 20, where one should focus on the *average* results for each galaxy type, since no attempt was made to model the scatter in $f_\star$ and λ.

The general picture that we obtain is that spiral and elliptical galaxies are clumped around two regions of parameter space: ($f_\star$, f_j) ∼ (0.25, 0.55), and ∼(0.1, 0.1), respectively. *Whatever processes formed and shaped these galaxies were efficient*

---

[20] It has been suggested that later-type galaxies are biased to *lower* spin halos (D'Onghia & Burkert 2004). If correct, the net impact on the $j_\star$ scatter is unclear, but one implication is that the f_j dichotomy between spirals and ellipticals would be even larger than in our no-bias scenario.

[21] One concern here is that for more bulge-dominated galaxies, one might expect the disk-only $\langle f_\star \rangle$ to be relatively low, and thus the disk $j_\star$ to appear relatively high. However, the observations are somewhat suggestive of the *opposite* trend, i.e., disk $j_\star$ anti-correlating with B/T.

[22] As a consistency check, we also take a slightly different approach and make a model prediction for the mean relation between size and rotation velocity for spirals (cf. Mo et al. 1998; Burkert & D'Onghia 2004). We adopt a value of $\langle f_\star \rangle = 0.56$, and rather than assuming some function $\langle f_\star \rangle (M_\star)$, we relate disk rotation and the virial circular velocity by $v_s \simeq 1.2 v_{\rm vir}$. Given $\langle \lambda \rangle = 0.035$, there is a linear relation predicted between v_s and a_e, which we show in the right-hand panel of Figure 12. To zeroth order, this prediction agrees well with the spiral data.
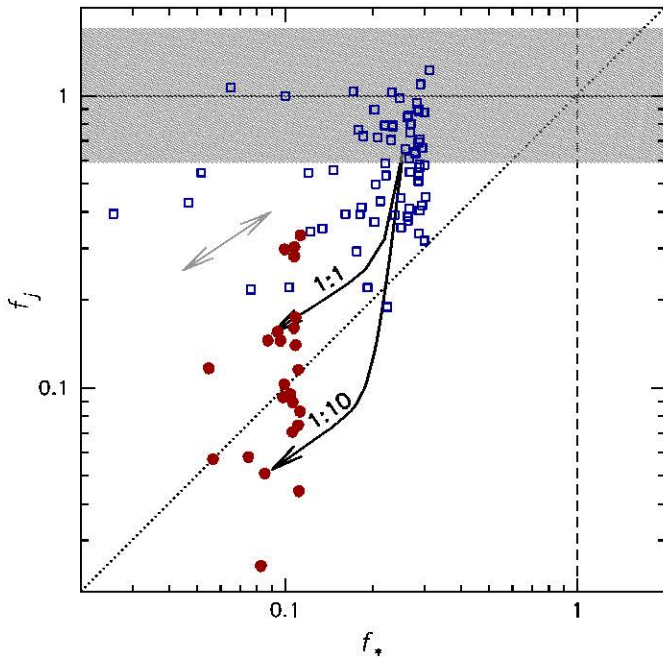
Figure 20. Specific angular momentum retention fraction plotted against stellar mass fraction, as inferred for individual galaxies, with symbols as in Figure 19. The dotted diagonal line is the one-to-one relation, and the gray double arrow shows the direction of the uncertainties as driven by the $f_j \propto f_\star^{2/3}$ degeneracy. The width of the shaded region around $f_j = 1$ corresponds to the scatter in spin expected for ΛCDM halos. The black arrows show schematic vectors from 1:1 and 1:10 mergers, as discussed in Section 6.3. The spiral and elliptical galaxies occupy distinct regions of the diagram, while a simple model implies that converting spirals into ellipticals would require a very large amount of growth through $\sim$1:3 mergers.

(A color version of this figure is available in the online journal.)

at both forming stars and retaining total specific angular momentum for the spirals, and inefficient for the ellipticals.

As discussed in Section 1, early cosmologically based simulations struggled to reproduce such high f_j values for spirals, finding typically $f_j \sim 0.01$–0.1, which was later realized to be due in part to numerical artifacts, and in part to inadequate feedback recipes. Feedback could be particularly important for slowing down gas collapse and star formation so that the baryons are not affected by torque-driven j transfer during early mergers (Weil et al. 1998; Sommer-Larsen et al. 2003; Hummels & Bryan 2012; Scannapieco et al. 2012). However, whatever physical processes are now invoked to explain the f_j values of spirals must simultaneously allow for much lower f_j in ellipticals (e.g., by having less efficient feedback; Zavala et al. 2008; Scannapieco et al. 2008).

6.3. Physically Motivated Models for Galaxy Evolution

Now that we have derived a comprehensive framework for connecting $j_\star$–$M_\star$ observations with simulated ΛCDM halos, and thereby derived generic constraints on specific angular momentum retention, f_j (Figure 20), we will work through some case studies of plausible physical processes in galaxy formation and evolution. These cases are not meant to be exhaustive, nor to provide immediate ammunition for current debates about galaxy formation, but to serve as practical examples of how the j–M diagram can be used as a tool to furnish physical insight. The models involved will treat f_j and $f_\star$ as covariant parameters, unlike in the previous sections where for simplicity they were independent.

A general constraint to keep in mind is that for each galaxy type, f_j is approximately constant as a function of mass, including little additional scatter, which accounts for the observed j–M relations appearing so similar to those for theoretical DM halos. *Any model for angular momentum evolution should explain why galaxies appear to remember so faithfully the overall initial conditions of their parent halos.*

The challenge of this f_j constancy has been recognized previously for disk galaxies. There are a variety of physical mechanisms during galaxy evolution that could involve j transfer (e.g., gas cooling and feedback), but unlike gravitational clustering, these baryonic processes (and the resulting f_j values) are expected to depend strongly on mass, which appears to require some degree of fine tuning to reconcile with the observations (e.g., Dutton & van den Bosch 2012). Our inclusion of early-type galaxies in this framework, with near-constant f_j, deepens the mystery: there are now *two* fine-tuning conspiracies to explain.

Here we emphasize again a distinction from comparisons between *internal* distributions with radius of j for stars and DM halos (e.g., Bullock et al. 2001; van den Bosch et al. 2001; Maller et al. 2002; Sharma & Steinmetz 2005). As mentioned in Section 1, there is ample reason to expect redistribution of $j_\star$ to occur within the baryonic component of a galaxy and thereby violate strong j conservation. However, this does not affect our examination of weak conservation, where the overall value of j may remain roughly the same (assuming negligible transfer of j between baryons and DM).

We may reduce the potential explanations for the systematic difference in f_j between spirals and ellipticals into two basic scenarios, which we will examine before summarizing the overall picture. One general scenario is an *internal* angular momentum bias, where high- and low-$j_\star$ galaxies were formed from parts of their available gas supply that had preferentially high or low j. The other is that these galaxies experienced systematic differences in angular momentum transport *after* star formation, and during subsequent galaxy assembly phases.

Below, Section 6.3.1 discusses outflow and stripping scenarios, Section 6.3.2 considers biased collapse, and Section 6.3.3 examines mergers. Section 6.3.4 surveys the plausibility of these evolutionary modes in the light of the $j_\star$–$M_\star$ observations.

6.3.1. Outflows and Stripping

One example of the first scenario involves *gas outflows*, whether caused by galactic winds or by some other mechanism. Let us assume that the baryons in a galaxy collapse into a thin disk while preserving the total specific angular momentum, i.e., $f_j = 1$ (recall Figure 17(b)). The local specific angular momentum within the disk, $j_g(R) \propto R\,v_{\rm rot}(R)$, is assumed to increase monotonically with galactocentric radius, which is unavoidable if the gas follows corotating circular orbits (the rotation-velocity profile cannot decrease any more rapidly than Keplerian, while the lever arm R in the j calculation increases linearly).

Before many stars form, an outflow begins which we parameterize by a mass loss that is proportional to the gas surface density to some unknown power β:

$$\Delta M_g \propto \Sigma_g^\beta. \qquad (19)$$

Because the gas is presumed to settle into a configuration where the density increases toward the center (e.g., an exponential profile), the parameter β translates into a biased removal of gas from different disk *radii*, which in turn means depletion of gas parcels with systematically different j_g.
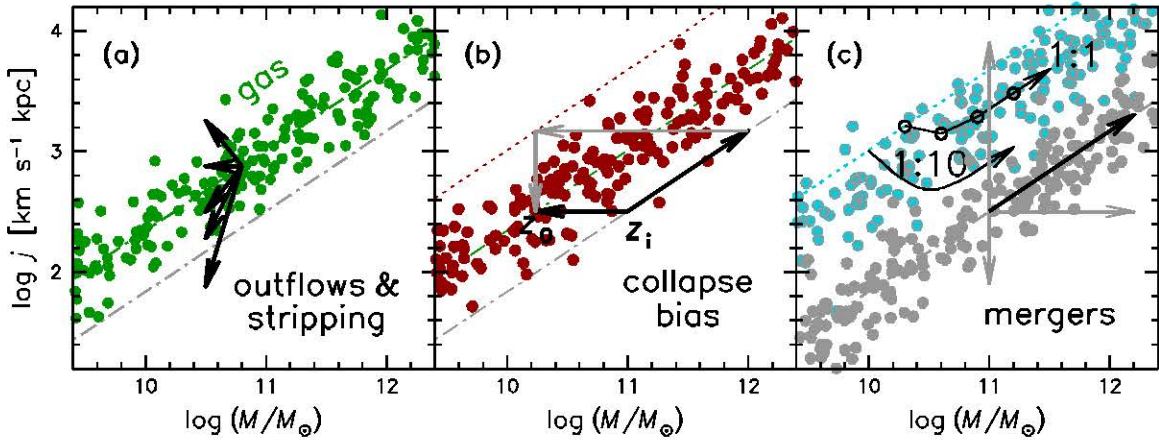
Figure 21. Schematic evolution of galaxies in specific angular momentum and mass, as in Figure 17, but now considering evolution through gas outflows, stripping, and biased baryon collapse, and galaxy mergers. Panel (a) shows initial conditions for pre-collapse gas (dots), and possible evolutionary vectors from outflows and stripping (arrows; see the text for details). Panel (b) shows the collapse of gas and formation of stars at some initial redshift z_i, preserving the $j_\star$–$M_\star$ values until a final redshift z_0 (black arrow to the left, with dots illustrating a population of galaxies). The halo grows until redshift z_0 with no further star formation (black arrow to upper right). At z_0, the expected trend with perfect j conservation is the dotted line, and net values for $f_\star$ and f_j would be inferred using the leftward and downward gray arrows, respectively. Panel (c) shows initial conditions for DM halos as gray dots, and schematic vectors of evolution through mergers (gray arrows): mass growth (to the right), specific angular momentum decrease through cancellation of the spin components (downward), and increase through the orbital component (upward). The net evolution is a black diagonal arrow to the upper right. The upper dotted track marks the initial conditions for stellar disks, and the blue dots show disks after having undergone four 1:1 mergers each. The upper black curved vector illustrates the typical evolution of a galaxy, with each black dot marking the beginning of a discrete merger event. The lower black curved vector shows the same for a series of 1:10 mergers (note that for clarity, the curved vectors are arbitrarily shifted relative to the $f_j = 1$ starting point for the DM vector). In both cases, after the mass has grown by a factor of ∼2, the orbital $j_\star$ dominates the evolution, moving merger remnants along a $j_\star$–$M_\star$ track parallel to, but lower than, the initial disk trend.

(A color version of this figure is available in the online journal.)

To analyze this scenario further, we now introduce Figure 21, which like Figure 17 illustrates schematic vectors of mass and angular momentum evolution, but now extends to more specific, physically motivated processes. In Figure 21(a), the horizontal arrow to the left illustrates an outflow with $\beta = 0$: the gas everywhere in the disk is depleted by an equal fraction, and its initial specific angular momentum is preserved, while its mass decreases. If $\beta > 0$, then the outflows occur preferentially in the high-density, central regions that have relatively low j_g, and so the overall j_g for the galaxy increases (diagonal arrow toward the upper left; cf. Binney et al. 2001; Maller & Dekel 2002; Sharma et al. 2012). If $\beta < 0$, then the mass loss is preferentially from the outer regions, and the overall j_g decreases (diagonal arrows toward the lower left). Thus, outflows could in principle produce either a net increase or decrease in f_j.

It should be kept in mind that these outflows represent only material that is launched completely out of the galaxy, never to return. Other types of outflows may also occur, where gas is expelled outward but remains bound and falls inward again, as in a galactic fountain (e.g., Brook et al. 2012). However, such internal processes might alter only the detailed distribution with radius of j, and not affect the overall value which concerns us here (see the discussion above of weak and strong j conservation). More complex scenarios could also be considered, where fountain material interacts with halo gas and exchanges angular momentum (e.g., Melioli et al. 2009; Marinacci et al. 2011), leading to shifts in $j_\star$ for the stellar disk that eventually forms.

A mechanism related to gas outflows is galaxy *stripping* through gravitational interactions with other galaxies in a dense environment. Here the effects on $j_\star$ and $M_\star$ depend on whether the tidal stripping occurs before or after the gas collapses. If a galactic halo is tidally stripped *before* the gas collapses (e.g., Larson et al. 1980), then the reservoir of M_g and j_g available for collapse is depleted in a manner that depends on the internal

distribution of these quantities. F83 adopted some plausible distributions and worked out the resulting j–M changes: we will not repeat the analysis here, but merely show the equivalent evolutionary vectors as the three arrows in Figure 21(a) pointing downward to the left.

There are two key features to note with the gaseous stripping arrows. One is that unlike outflows, this stripping can only *decrease* f_j ($\beta < 0$) since it acts solely on the outer regions. The second is that plausible j-loss vectors are accompanied by substantial mass loss, which means that it is fairly difficult to move galaxies away from the initial j–M sequence. This conclusion is supported by N-body simulations of ΛCDM halos, which find that the environmental dependencies of halo λ are fairly weak (Zurek et al. 1988; Lemson & Kauffmann 1999; Reed et al. 2005).

If instead the stripping occurs *after* the gas collapse, then j and M decrease for the DM but not for the baryons. This leads to elevated values of f_j and $f_\star$, which could be investigated through observational constraints on M_{vir} for field galaxies in comparison to satellite galaxies in massive groups.

6.3.2. Biased Collapse

There is another scenario that is functionally equivalent in the j–M diagram to outflow or stripping, but which merits special attention. Here we consider a *spatially biased* subcomponent of the initial gas which collapses and forms stars. Rather than our default assumption of uniform efficiencies $f_\star$ and f_j throughout the virial region, we assume that stars form preferentially in the *inner regions* of the halo, while the outer regions remain largely gaseous and form relatively few stars.

This scenario was introduced by Fall (2002) and is motivated by the higher densities, and thus overall gas dissipation rates (through cooling and cloud collisions), in the inner regions. The consequent spatial bias in star formation can also be understood as a *temporal* bias, if one considers an idealized

onion-shell model wherein galaxies form by inside-out collapse, with virialization and star formation occurring first in the central regions (cf. van den Bosch 1998; Kepner 1999). Even in more realistic, hierarchical galaxy models, it is uncontroversial that a large fraction of the baryons within a galaxy halo at any given time will not yet have formed stars, and are located preferentially at larger radii. The stars observed in a galaxy at $z = 0$ will have formed on average at higher redshifts, and from gas that was more centrally confined than the $z = 0$ virial volume.

Because j for a ΛCDM halo is expected to increase systematically with both internal radius and time, the above biasing scenario implies that $j_\star$ for a galaxy will be lower than its total j (including DM). Such a biasing framework was used by Kassin et al. (2012) to connect observed disk galaxies with simulated ΛCDM halos, and thereby infer a radius of baryonic collapse. Here we outline a generic toy model of collapse bias, to understand its implications in the context of j–M evolution vectors.

For simplicity, we adopt a step-function model where at an initial redshift z_i, all of the gas within the virial radius instantaneously collapses and forms stars with perfect efficiency and angular momentum conservation ($f_\star = f_j = 1$), and subsequently no star formation occurs ($f_\star = 0$). This scenario is illustrated by Figure 21(b), where z_i marks the initial halo parameters. The leftward arrow shows the formation of the stars, with $j_\star$–$M_\star$ parameters that are preserved until $z_0 = 0$. The diagonal arrow to the upper right shows the subsequent evolution of the halo. Because the halo continues to grow in M and j, the net values of $f_\star$ and f_j for the stars will decrease with time, which is illustrated by the gray arrows which are the inferences made by connecting the final conditions of the halo and stars.

This biasing scenario might seem to provide a tidy alternative for understanding galaxies that have *apparently* experienced baryonic angular momentum loss. However, it is important to realize that such biasing cannot explain just any arbitrary set of $j_\star$–$M_\star$ observations. For example, the vectors in Figure 21(b) were constructed to represent a typical early-type galaxy with a net $f_\star = 0.1$ at $z = 0$, which turns out to have a net $f_j = 0.22$, i.e., not reproducing the apparent $\langle f_j \rangle \sim 0.1$ from observations. Note that this model had an initial $f_\star = 1$, but in reality, we expect an initial $f_\star < 1$, which would increase the discrepancy. We will discuss this scenario further in Section 6.3.4; for now, it serves as an important illustration of how constructing physically motivated vectors in the $j_\star$–$M_\star$ diagram can provide tight constraints on possible evolutionary scenarios.

6.3.3. Mergers

We next consider galaxy *merging* following star formation, which is likely to be more important for ellipticals than for spirals. The mass of a galaxy increases through a merger, while its final j is determined by the vector sum of three initial j components (the internal j for the two progenitor galaxies, and their relative orbital j), as well as by any exchange of j with the environment (e.g., between the stars and their surrounding DM halos). The random relative orientations of the first two components will cause them to partially cancel out, which contributes a net *decrease* to j. That is, after N equal-mass mergers, there will be average trends for the remnant of $J \propto N^{1/2}$ and $M \propto N$, and therefore $j \propto N^{-1/2}$ (Fall 1979; Aarseth & Fall 1980). The orbital j and the j exchange processes are more difficult to model a priori.

The effects of mergers on DM halos have been studied extensively through numerical simulations, resulting in a general picture where major mergers tend to "spin up" the halos, while minor mergers and smooth accretion tend to spin them down (e.g., Gardner 2001; Maller et al. 2002; Vitvitska et al. 2002; Peirani et al. 2004; D'Onghia & Burkert 2004; Hetznecker & Burkert 2006). Given that the $j_{\rm vir}$–$M_{\rm vir}$ relation is scale free and has a normalization that is expected to change only gradually, if at all, with time (e.g., Navarro & Steinmetz 1997), we conclude that for individual halos, the co-addition of the above processes must amount to a random walk that takes them on average *along* the $j_{\rm vir}$–$M_{\rm vir}$ sequence.

We illustrate this process in Figure 21(c) with a schematic evolutionary vector for galaxy halos, broken down into sub-components of $j_{\rm vir}$ and $M_{\rm vir}$ changes.[23] Doubling the mass should typically increase $j_{\rm vir}$ by a factor of $2^{2/3} = 1.6$.

The effects of mergers on the stellar components of galaxies, which have collapsed by large factors within their DM halos, are somewhat different. Qualitatively speaking, it is a generic dynamical requirement that the stars shed some of their orbital angular momentum, via tidal torques or dynamical friction, in order to coalesce into a bound merger remnant (e.g., Frenk et al. 1985; Zurek et al. 1988; Barnes 1988; D'Onghia et al. 2006).

More quantitatively, we may make an initial, plausible guess that the "final pass" of the merger before coalescence involves an impact parameter and relative velocity that are similar to the stellar scale length and circular velocity of the larger progenitor. This would mean that the smaller progenitor would bring in an orbital $j_{\star,2}$ of a similar magnitude to internal $j_{\star,1}$ of the larger progenitor (i.e., $\Delta J_\star = j_{\star,2} M_{\star,2} \sim j_{\star,1} M_{\star,2}$).

We sketch out some implications of this kind of merger evolution in Figure 21(c). Starting with galaxy disks randomly selected along the median $j_\star$–$M_\star$ trend as in Figure 17(c) (adopting a simple $f_\star = 0.1$ model with scatter included for halo λ), we apply a sequence of four mergers to each disk. Each merger has a 1:1 mass ratio, and the relative vectors of internal $j_\star$ and orbital $j_\star$ are selected randomly (this is similar in spirit to the orbital-merger model of Maller et al. 2002). The blue dots show the end result after the merger sequence, and the upper arrow shows the median trend for a single galaxy, with black dots marking the discrete merger events. Note that at this point, the series of four 1:1 events is meant as a thought experiment and not necessarily as a likely merger history.

After an initial decrease of $j_\star$ in the first merger from cancellation of the internal spin vectors, the orbital $j_\star$ dominates the evolution of the merger remnant (e.g., Aarseth & Fall 1980; Hetznecker & Burkert 2006; this also means that the results hardly change if the "accreted" galaxies are low-$j_\star$ spheroids rather than disks as we have assumed here). Because the orbital $j_\star$ term is assumed to be similar to the disk $j_\star$–$M_\star$ trend, the final trend for the merger remnants parallels the disk trend, while being offset to lower $j_\star$ by a factor of ~ 2 (~ -0.3 dex). Referring back to Figure 17, this corresponds to an effective angular momentum loss term of $f_j \sim 0.5$. The distribution of the offset is also shown by a histogram in Figure 22.

We have carried out the same exercise for a series of 1:10 mergers, with a median trend shown by the lower vector in Figure 21(c). The result is similar to the 1:1 case, with orbital $j_\star$ dominating the evolution after the galaxy grows in mass by a

---

[23] In the merging of DM halos, the resulting angular momentum and mass are *not* the simple sum of those properties from the progenitors. The combination of the two virial regions in a merger increases the *density* within a fixed physical radius, but also increases the *volume* of the virial region, so that more of the surrounding material falls under the gravitational sway of the two galaxies together. A 1:1 merger typically increases $M_{\rm vir}$ by a factor of ~ 2.3; similar effects apply to $j_{\rm vir}$.
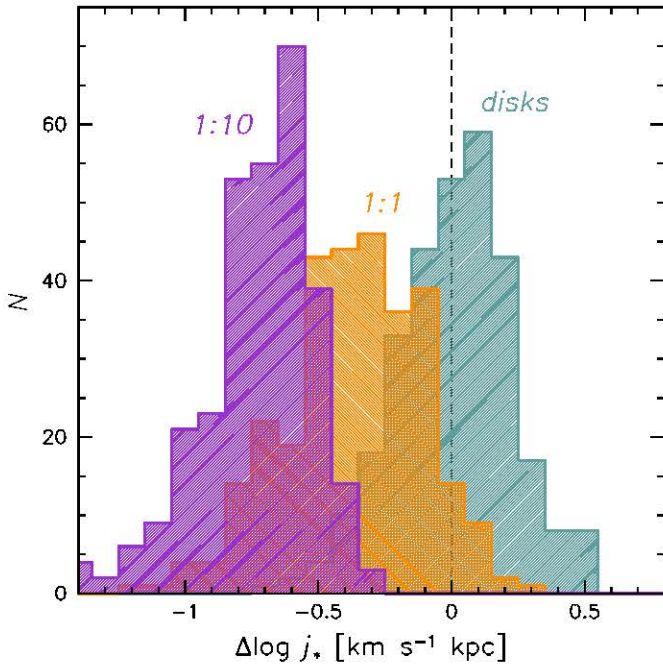
Figure 22. Distributions of specific angular momentum residuals, relative to the mean trend for spiral disks, using the same analysis as in Figure 21(c). The right histogram shows the disk initial conditions. The middle and left histograms show merger remnants after having grown by a factor of 16 in mass, for 1:1 and 1:10 mergers, respectively. The $j_\star$ distribution has a smaller mean and dispersion for the 1:10 mergers than for the 1:1 mergers.

(A color version of this figure is available in the online journal.)

factor of $\sim$2. However, the final $j_\star$ trend is now lower than the disks by a factor of $\sim$6 ($\sim$−0.8 dex; $f_j \sim 0.15$), with less scatter than in the 1:1 case (see Figure 22 again). These differences arise because there is less stochasticity with the 1:10 mergers, where random-walk effects tend both to wash out variations and to dilute the orbital contributions to $j_\star$.[24] A more realistic mixture of multiple mergers with varying mass ratios would presumably produce a $j_\star$ distribution with a peak intermediate to our 1:1 and 1:10 scenarios, and with a larger scatter.

These calculations are laden with simplifying assumptions and could easily be wrong by a factor of two in $j_\star$. However, they are meant to illustrate some possible implications of merger activity in a hierarchical context. First of all, it is plausible that spheroids with a merger origin would follow a $j_\star$–$M_\star$ relation that is parallel to that of spiral disks, but offset to lower $j_\star$ by a factor of a few.[25] Second, the scatter in $j_\star$ introduced by random merging may be relatively small.

These two results in our toy model are both driven by the dominant contributions of orbital $j_\star$. Similar points were made by Fall (1979) and by Zurek et al. (1988), in the latter case based on the prediction that λ would be fairly constant with radius inside DM halos. The stars that condense at the center of a halo, and then participate collisionlessly in its merger history,

would naturally follow the same j–M scaling relations as the overall halos, modulo a smaller scale length in converting from λ to j (in Equation (13), $|E|$ is inversely proportional to the radius).

6.3.4. Evaluating the Possibilities

We now step back and consider how well the preceding evolutionary scenarios (outflows, stripping, collapse bias, and mergers) mesh with the observational constraints (Figures 14 and 20). The idea is to find a vector (or combination of vectors) that connects up the well-established endpoints in the j–M diagram: the ΛCDM halo initial conditions and the $z = 0$ galaxy observations. It should however be remembered that the focus of this paper is not to solve long-standing questions about galaxy evolution which may require a detailed understanding of the physics involved. Instead, our more modest goals are to illustrate how the j–M diagram can be used in practical terms as a constraint on theory, while looking for any hints as to the viability of various scenarios.

Recent work in numerical simulations of *disk* galaxy formation has emphasized how outflows might remove low-j_g material, which counteracts j loss through tidal torques during galaxy collapse, and maintains a high net level of f_j (e.g., Brook et al. 2011; Guedes et al. 2011). We could then imagine that the differences between spiral and elliptical galaxies originate from the spirals having much stronger outflows at early times.

This outflow scenario implies more mass loss in spirals and so would initially seem to work the wrong way in explaining the $f_\star$ differences—but there could be other factors besides gas depletion that affect $f_\star$. It is beyond the scope of this paper to explore this scenario in detail, but we emphasize that the focus on reproducing f_j and $f_\star$ for spirals needs to expand to include simultaneously the constraints from ellipticals, beyond these being nuisance factors that represent failed disks.

We have already discussed how stripping before baryonic collapse is not expected to produce large changes in the observable $j_\star$–$M_\star$ relations, which may indeed be part of the reason that there is not more scatter in these relations.[26] There is also a more obvious constraint that both spirals and ellipticals exist in the field and in clusters, so present-day environment cannot be the unique driver of morphology and j evolution.

Collapse bias is an appealing possibility because it would provide a natural explanation for the positive correlation between $f_\star$ and f_j as in Figure 20. In this scenario, elliptical galaxies would cease to build up both $M_\star$ and $j_\star$ at relatively early times, with the remaining baryonic M and j at late times either residing in a hot gas halo or having been blown out into intergalactic space. Spiral galaxies would have more protracted star formation histories that increase $M_\star$ and $j_\star$ monotonically with time.

Besides explaining the relative positions of ellipticals and spirals in the $j_\star$–$M_\star$ diagram, this scenario also fits in naturally with the observation that the stars in spirals are on average much younger than those in ellipticals. There may be additional implications if one connects the *baryon* collapse to the *overall halo* collapse, which has a well-understood theoretical underpinning. At a given $z = 0$ mass, some halos should have collapsed earlier than others, leading to their DM distributions being more centrally concentrated. Given a fixed λ, the central DM and associated stars would then have relatively low j

---

[24] This scenario has some parallels to discussions in the literature about the systematic relations between angular momentum and merger histories, and the implications for the observed properties of galaxies (e.g., D'Onghia & Burkert 2004; Vitvitska et al. 2002; Primack 2005; D'Onghia & Navarro 2007; Sharma et al. 2012). However, those studies did not always make a clear distinction between the differing merger dynamics of DM halos and of their embedded stellar components.

[25] More generally, a similar slope would presumably be driven by any merger history that involves a scale-free mass spectrum of progenitors. This is a basic property of ΛCDM halos, but is incorrect at some level for stellar galaxies, owing to the strong break in their luminosity function.

[26] There is one case where severe stripping has apparently led to a large reduction in $j_\star$: NGC 4486B, which is a low-$j_\star$ outlier in Figure 14, and is discussed in Romanowsky et al. (2012). This "compact elliptical" is a fairly rare type of galaxy.

values. Since halo collapse time is correlated strongly with environmental density, one would then expect the low-$j_\star$ galaxies to reside preferentially in high-density environments—which is indeed what is found observationally (through the traditional morphology–density relation).

A potential problem with this scenario is that it does not appear by itself to be capable of explaining the apparent deficit of $j_\star$ in ellipticals, as discussed in Section 6.3.2. More detailed analysis would be needed to see if halo concentration makes a difference, and to understand the baryonic physics of why early-collapsing galaxies would also shut down their star formation more drastically than late collapsers. In addition to collapse bias, other effects may also need to be involved, such as a bias to low spin for their halos, or a component of real j loss.

The merger scenario is a common explanation for ellipticals, since it accounts for spheroidal morphologies through violent relaxation (Toomre 1977), and because there is strong observational evidence for some elliptical galaxies actively forming through mergers (e.g., Rothberg & Joseph 2006). Our toy-model analysis suggests that the overall effect of mergers is to *reduce* the $j_\star$ of the remnant relative to an initial $j_\star$–$M_\star$ trend for disks, while the combination of *multiple* mergers may move the remnants parallel to that trend (Figure 21(c)). This might provide a natural explanation for the observed $j_\star$–$M_\star$ trend for ellipticals: the slope, scatter, and offset relative to disks. Note that it is not entirely clear in this context why the spiral bulges and the ellipticals would follow the same $j_\star$–$M_\star$ trends.

A more quantitative comparison of our model to the observations allows us not only to constrain the typical mass ratios in mergers (as Figure 22), but also to infer the amount of mass growth in ellipticals since their assumed primordial disk phase. We do so by mapping our toy-model vectors for mergers in the key f_j–$f_\star$ diagram (Figure 20), starting from initial conditions similar to present-day spirals ($f_\star = 0.25$, $f_j = 0.6$), and requiring that they terminate at ($f_\star = 0.1$, $f_j = 0.1$).

Recalling that $M_{\rm vir}$ growth slightly outpaces $M_\star$ growth we find that reducing $f_\star$ by a factor of 2.5 requires a very long series of mergers, with a final growth factor of $\sim$100 in $M_\star$ and $\sim$300 in $M_{\rm vir}$. Consideration of the f_j constraint then suggests a typical merger mass ratio of $\sim$1:3. Such "major mergers" seem like a reasonable pathway to forming elliptical galaxies, although recent work suggests a more dominant role for *minor* mergers (e.g., $\sim$1:10; Naab et al. 2009; Bezanson et al. 2009; Khochfar et al. 2011; Oser et al. 2012; Johansson et al. 2012; Lackner et al. 2012), which is motivated in part by explaining trends in size evolution, and is also supported by the observed *shapes* of rotation-velocity profiles (see Section 5.2 and Arnold et al. 2011).[27]

This apparent tension is not of great concern since our current results involve significant observational uncertainties and a crude model for the merging vectors in Figure 21(c), while not taking proper account of the redshift dependence of virial quantities. Our analysis of the observed $j_\star$–$M_\star$ relations may also have underestimated the importance of systematic variations in the stellar mass-to-light ratio (Sections 3.4 and 5.2), which might imply better agreement with a minor-merger

scenario. In any case, these exercises are intended to illustrate conceptually the kinds of constraints that are possible with more careful modeling.

A merger scenario may successfully explain the $j_\star$–$M_\star$ properties of ellipticals, but it should be remembered that in a cosmological context, all galaxies including spirals should experience a continuous rain of accreting objects. Even if spiral galaxies have systematically avoided the most extreme merger events, they will have still experienced events in the $\sim$1:10 range (e.g., Kauffmann & White 1993; Stewart et al. 2008; Fakhouri et al. 2010), which as shown in our toy models could significantly reduce $j_\star$. A more detailed analysis of $j_\star$–$M_\star$ evolution within a cosmological framework is needed in order to investigate the quantitative differences that might arise between spirals and ellipticals owing to varying merger histories. In particular, an explanation for the observed bulge–disk $j_\star$ bimodality is needed, since a spectrum of merger histories is more suggestive of a smooth distribution of $j_\star$. It should also be kept in mind that $\langle f_\star(M_\star) \rangle$ is observationally constrained not only for present-day galaxies, but also at earlier times (e.g., Conroy & Wechsler 2009; Moster et al. 2012), which introduces additional "boundary conditions" to j–M evolution.

Synthesizing the scenarios above, it seems plausible that ellipticals might be explained through a combination of collapse bias and multiple mergers—which bears a notable resemblance to recent discussions of two-phase galaxy formation (Oser et al. 2010). In this context, an early burst of star formation would both imprint a relatively low initial $j_\star$ and allow more opportunity for subsequent mergers to reduce $j_\star$ further. Spirals would be those systems where late gas infall both brings in higher j, and avoids the most active merging period.

There are of course other considerations besides angular momentum when constructing models of galaxy evolution, which are beyond the scope of this paper to evaluate. We have also been able to cover only a subset of possible scenarios.

One significant omission is the disk-instability pathway for bulge formation (e.g., Toomre 1964; Dalcanton et al. 1997; van den Bosch 1998; Parry et al. 2009), which is an internal process where the bulge and disk either form from high- and low-j material, or else exchange j through gravitational torques. While this pathway is usually considered in connection with pseudo-bulges, there are recent proposals that the special conditions in high-redshift galaxy disks can lead to the massive, classical bulges of present-day spirals, lenticulars, and ellipticals (e.g., Noguchi 1999; Immeli et al. 2004; Elmegreen et al. 2008; Dekel et al. 2009a, 2009b; Ceverino et al. 2010). The filamentary nature of mass and j inflows at high redshift may also require significant revisions to standard spherical models (Danovich et al. 2012; Sales et al. 2012; Dubois et al. 2012; Kimm et al. 2011).

Our overarching emphasis here is that whatever the mechanisms for galaxy formation, they must reproduce the basic $j_\star$–$M_\star$ scaling relations *observed for both spiral and elliptical galaxies*. A combination of all the processes mentioned above, and more, could be operational in real galaxies, where each process must be associated with a vector of $j_\star$–$M_\star$ evolution that is not arbitrary but physically motivated, as we have sketched in Figures 20 and 17. The sum of these vectors over the lifetime of the galaxy must preserve the halo-like scaling relations, *along with a relatively small scatter*. These may be very challenging constraints to match in practice, particularly if one includes boundary conditions on $f_\star(M_\star)$ evolution with redshift, and requires that the $j_\star$–$M_\star$ relations hold for both bulge and disk components simultaneously within the same galaxies.

---

[27] In more detail, the fast- and slow-rotator subcategories of ellipticals (Section 4.2) are often thought to originate in different merger histories, such as binary versus multiple mergers (e.g., Burkert et al. 2008; Bois et al. 2011). Our discussion concerns primarily the fast rotators, since these represent the vast majority of ellipticals, and in addition, our $j_\star$ constraints for the slow rotators are less certain. However, as discussed in Sections 5.2 and 5.3, we detect no systematic difference in $j_\star$–$M_\star$ space between the two galaxy types, suggesting that they may have relatively similar merger histories after all.

Thus, a fresh approach to j–M analysis appears to hold promise for providing new, powerful constraints on galaxy evolution. We would encourage numerical simulators to keep this approach in mind as part of their toolkit, tracking the evolution of their simulated galaxies in the j–M diagram, while refining our schematic estimates of Δj–ΔM vectors, and thereby gaining more insights into the underlying physical processes in the simulations.

7. SUMMARY AND CONCLUSIONS

We have revisited the pioneering study of F83 which derived observational estimates for the fundamental quantities $M_\star$ and $j_\star$ (stellar mass and specific angular momentum) of spiral and elliptical galaxies, and compared these to theoretical expectations based on hierarchical assembly. Although the amount and distribution of $j_\star$ in late-type galaxies has been an intensively studied topic in the intervening years, even the most basic trends for early types have not been satisfactorily established. We have capitalized on the advent of radially extended kinematic data for a large sample of early-type galaxies, to update and extend the analyses of F83.

We focus first on detailed analysis of a small sample of galaxies with data extending to typically five effective radii, which is the distance one must reach for a high degree of confidence in the $j_\star$ estimates. We derive various formulae for use in quantifying $j_\star$ for pressure supported systems, including deprojection effects. In order to estimate $j_\star$ for a larger sample of galaxies without requiring detailed modeling and data to very large radii, we test a simple, heuristic $j_\star$-estimator.

Based on the shapes of observed rotation-velocity profiles for the detailed sample of galaxies, we find that a convenient metric for the characteristic rotation velocity v_s of a galaxy is provided by the observed rotation at a semimajor-axis distance of two effective radii. This approximation is accurate at the level of ~ 0.1 dex, which is suitable for studying galaxy-to-galaxy variations in $j_\star$.

We next assemble a large sample of galaxies in the nearby universe with adequate photometric and kinematic data for estimating $j_\star$ and $M_\star$. This sample covers the full spectrum of bright galaxy types from bulgeless-spiral to diskless elliptical, as well as a wide range in $M_\star$, centered approximately at the characteristic mass $M_\star^*$. We use our simple formula for estimating $j_\star$, while adopting simple bulge+disk models for the spiral galaxies.

Along the way, we also introduce an important new observational scaling relation for galaxies of all types: v_s versus $M_\star$. This relation is analogous to the well-known Tully–Fisher relation for disk galaxies, but is more closely related to angular momentum than to dynamical mass. Unlike the generalized Tully–Fisher relation, the mass–rotation-velocity relation shows *near-perpendicular* rather than parallel trends for spiral and elliptical galaxies. These rotation-velocity trends combine with size–mass trends to trace the more fundamental $j_\star$–$M_\star$ trends.

Our combined $j_\star$–$M_\star$ estimates confirm the basic result of F83 that late-type spiral and elliptical galaxies follow parallel sequences of roughly $\alpha \sim 2/3$ log-slope, but with a large zero-point difference (in our analysis, the ellipticals have a factor of ~ 3–4 lower $j_\star$ at a fixed $M_\star$, which would increase to a factor of ~ 7 with possible variations in the stellar mass-to-light ratio $\Upsilon_\star$). Although this conclusion has already been used in some theoretical analyses, now it has a much firmer observational

basis. In particular, the data do not support previous suggestions that major mergers have transported large amounts of angular momentum into the outer regions of ellipticals.

We confirm for the first time that lenticular galaxies on average lie intermediate to ellipticals and late-type spirals in the $j_\star$–$M_\star$ plane, with tentative indications for two families of lenticulars characterized by low and high $j_\star$. We see no indication of systematic, overall differences between centrally fast- and slow-rotator ellipticals. We also find that spiral bulges are consistent with following the $j_\star$–$M_\star$ sequence for ellipticals, despite having very different relations between mass, size, and rotation. Thus, as far as the fundamental parameters $j_\star$ and $M_\star$ are concerned, spiral bulges are essentially like mini-ellipticals.

We examine the residuals of the combined galaxy $j_\star$–$M_\star$ data with respect to the disk-only trend, and find that these correlate better with disk-to-bulge ratio than with Hubble type. They also deviate from a lognormal distribution, possibly suggesting instead a bimodality in $j_\star$. Considering all of these results together, we propose an alternative framework to the Hubble sequence, based on more physically motivated parameters. In this picture, all galaxies are a combination of a bulge and a disk, which are distinct subcomponents with different characteristic amounts of $j_\star$. Galaxy morphology may then be seen as a secondary manifestation of the mix of high- and low-j material, or equivalently, the position of a galaxy in $j_\star$–$M_\star$ parameter space is a reflection of its bulge-to-disk ratio.

We next connect our observational results to a theoretical framework based on the hierarchical assembly of galaxy halos in a ΛCDM cosmology. We use numerically informed analytic methods that are much simpler than hydrodynamical simulations, but less susceptible to the large, lingering uncertainties about baryonic recipes, resolution effects, and other numerical issues. We find that the predictions for universal mean values of halo spin translate into j_{vir}–M_{vir} relations with an $\alpha = 2/3$ log-slope, which is remarkably similar to the observed $j_\star$–$M_\star$ relations. The zero-point differences among these relations provide valuable clues to the formation processes of different galaxy types.

Mapping between halo and stellar quantities involves two basic parameters: the net fraction of baryons turned into stars, $f_\star$, and the fraction of specific j retained, f_j. We find that realistic variations of $f_\star$ with mass produce surprisingly mild deviations of the $j_\star$–$M_\star$ relation from a simple $\alpha = 2/3$ power law. The most noticeable correction is a slightly shallower predicted slope for the spirals, which turns out to agree well with the observations.

We explore two simplified alternative scenarios for explaining the spiral-elliptical dichotomy in the $j_\star$–$M_\star$ plane: the formation of spiral and elliptical galaxies in low- and high-spin halos, respectively (spin-bias scenario); and a difference in j retention (variable-f_j scenario). We find that spin bias does not explain the tails of the observed $j_\star$ distribution, nor does it agree with the observed trend as a function of mass for the elliptical galaxies. The variable-f_j scenario, on the other hand, matches the data well and suggests universal values of $f_j \sim 0.55$ and $f_j \sim 0.1$ for spirals and ellipticals, or for disks and bulges, respectively. The near-constancy of these values is intriguing, and means that all the complexities of galaxy evolution somehow effectively reduce to a simple model, where galactic stars have preserved the "initial" conditions of their host halos, including the j_{vir}–M_{vir} slope and scatter. This interpretation may be useful for semi-analytically populating DM halos with both spiral and elliptical galaxies (cf. Mo et al. 1998).